NACA RM A51E03

NACA

RESEARCH MEMORANDUM

SUBSONIC MACH AND REYNOLDS NUMBER EFFECTS ON THE SURFACE PRESSURES, GAP FLOW, PRESSURE RECOVERY, AND DRAG OF A NONROTATING NACA 1-SERIES E-TYPE COWLING AT AN ANGLE OF ATTACK OF 0°

By Robert M. Reynolds and Robert I. Sammonds

Ames Aeronautical Laboratory
Moffett Field, Calif.

NATIONAL ADVISORY COMMITTEE
FOR AERONAUTICS

WASHINGTON
July 17, 1951

NATIONAL ADVISORY COMMITTEE FOR AERONAUTICS

RESEARCH MEMORANDUM

SUBSONIC MACH AND REYNOLDS NUMBER EFFECTS ON THE SURFACE PRESSURES, GAP FLOW, PRESSURE RECOVERY, AND DRAG OF A NONROTATING NACA 1-SERIES E-TYPE COWLING AT AN ANGLE OF ATTACK OF 0°

By Robert M. Reynolds and Robert I. Sammonds

SUMMARY

A wind-tunnel investigation has been made to evaluate the effects of Mach number and Reynolds number on the characteristics of the internal and external flow about an E-type cowling suitable for a turbine-propeller power-plant installation. Surface-pressure distributions, cowl-gap flow, total-pressure recoveries, and momentum losses in the cowl wake were measured for the model at an angle of attack of 0° with the cowling stationary, that is, not rotating. With the inlet-velocity ratio varied between 0.06 and 0.78, data were obtained for a Reynolds number of 1.80 million through a Mach number range of 0.23 to 0.88 and for Reynolds numbers of 5.20 and 8.10 million at a Mach number of 0.23.

For a given inlet-velocity ratio, increasing either the Mach number or the Reynolds number resulted in only small changes in the pressure recoveries in the duct and in the external-drag coefficient of the cowl. The measured critical Mach number of the cowl was 0.83 for inlet-velocity ratios of 0.3 or greater.

For inlet-velocity ratios less than about 0.15, negative pressure-coefficient peaks occurred near the leading edge of the cowl. Generally, increasing the inlet-velocity ratio resulted in more positive pressure coefficients on the external surface of the cowl, lower ram-recovery ratios in the duct, and decreasing external-drag coefficients for the cowl.

The cowl-gap leakage air flow had little effect on the external pressure distributions. The total-pressure losses through the cowl gap were small.

Average ram-recovery ratios at the compressor inlet were 0.98 or higher throughout the Mach number range for inlet-velocity ratios of 0.4 or less.

INTRODUCTION

A growing need for data concerning the high-speed characteristics of air inlets suitable for the turbine-propeller type of power-plant installation has recently led to increased emphasis on research in this field. One of the principal problems encountered in the design of a power-plant installation utilizing a turbine engine is the efficient handling of the large quantities of air required by the engine. The NACA E-type cowling is one of the inlet types under consideration for obtaining efficient air induction for the turbine-propeller power plant.

The E-type cowling, as described in reference 1, is a cowling designed to rotate with a propeller and consists of an external cowling and an internal spinner which are interconnected by streamline fairings for the propeller blade shanks. Specific information regarding the aerodynamic characteristics and design of the E-type cowling is rather limited. The most recent investigation for which published data are available is an experimental and analytical study of the pressure-rise and leakage-loss characteristics of a rotating cowling (reference 1). Also available are the results of tests to determine the effect of the cowling gap on the pressures available for cooling in the E-type cowling (reference 2). Both of these reports present data only for low speeds. Information regarding the characteristics of open-nose inlet configurations, applicable in the design of E-type cowlings, is more complete. Reference 3 is a report of an investigation at low test speeds of a group of NACA 1-series cowlings with and without spinners, and includes design charts and the procedure for the selection of cowlings for specific high-speed requirements. References 4 and 5 report on investigations of open-nose inlets at high speeds.

The present tests were conducted in the Ames 12-foot pressure wind tunnel to ascertain the subsonic Mach and Reynolds number effects on the characteristics of the internal and external flow about a representative turbine-propeller installation utilizing an NACA E-type cowling. The tests were made with the cowling stationary, that is, nonrotating, and at an angle of attack of 0°.

SYMBOLS

A	cross-sectional area in a plane perpendicular to the model center line, square feet
a	speed of sound, feet per second
C	orifice coefficient for the cowl gap
C_{D_e}	external-drag coefficient $\left(\frac{D_e}{q_o A_5}\right)$
c_d'	point-drag coefficient
D	maximum diameter of cowl, feet
D_e	external drag, pounds
H	total pressure, pounds per square foot
$\frac{H-p_o}{H_o-p_o}$	ram-recovery ratio
M	Mach number $\left(\frac{V}{a}\right)$
M_{cr}	critical Mach number, the free-stream Mach number at which sonic velocity is first attained on the external surface of the cowl
m	mass rate of internal flow (ρAV), slugs per second
$\frac{m_1}{m_o}$	mass-flow ratio $\left(\frac{\rho_1 A_1 V_1}{\rho_o A_1 V_o}\right)$
P	pressure coefficient $\left(\frac{p-p_o}{q_o}\right)$
P_{cr}	critical pressure coefficient, corresponding to local Mach number of 1.0
p	static pressure, pounds per square foot
q	dynamic pressure $\left(\frac{\rho V^2}{2}\right)$, pounds per square foot
R	Reynolds number $\left(\frac{\rho V_o D}{\mu}\right)$
r	radius from cowling center line, inches

V velocity, feet per second

W_a weight rate of flow, pounds per second

X total length of any component of the model, such as the cowl, spinner, or propeller-blade-shank fairing, inches

x distance from any reference, such as the leading edge of the cowl, spinner, or propeller-blade-shank fairing, measured along the longitudinal axis, inches

ρ mass density of air, slugs per cubic foot

μ viscosity of air, slugs per foot-second

ω angular station, clockwise from top center when viewed looking downstream, degrees

Subscripts

The numerical subscripts refer to stations shown in figure 1.

o free stream

1 cowling inlet

2 cowl-gap exit

3 ram-recovery rake location

4 compressor-inlet rake location

5 drag-survey rake location

b propeller-blade-shank fairing

c cowl

s spinner

MODEL

The principal model dimensions and the variation of the duct area with longitudinal station are shown in figure 1. A photograph of the model installed in the 12-foot pressure wind tunnel is shown in figure 2.

Coordinates for the internal and external contours are listed in table I.

Design of the Model

The model investigated was a 1/5-scale representation of pertinent portions of a turbine-propeller installation utilizing an NACA E-type cowling.

The following conditions were assumed for the full-scale design: an operating altitude of 35,000 feet, a flight Mach number of 0.80 (critical Mach number of the cowl to be 0.83), and a turbine engine of the 5,000 to 6,000 horsepower class at design altitude and speed, requiring air at the rate of 40 pounds per second and a cowling diameter of 70 inches.

The main features of the full-scale design between the cowling inlet and the compressor inlet of the turbine engine were represented in the model. The first step in the full-scale design was the selection of the smallest NACA 1-series spinner which would enclose a representative propeller hub. The spinner chosen, following the designation of reference 3, was the NACA 1-41.43-042.86 spinner. Then, with an allowance for air flow through the cowl gap at a rate equal to 17 percent of the flow through the inlet, an NACA 1-series open-nose cowling was selected for the flight Mach number of 0.80, the critical Mach number of 0.83, and a design inlet-velocity ratio of 0.3. From the design charts of reference 3, the cowling chosen, with an NACA 1-series inner-lip fairing, was the NACA 1-51-117 cowl. Propeller-blade-shank fairings having NACA 0030-34.5 sections (reference 6), an angle of attack of 0°, no twist, and no fillets at the spinner or cowling junctures were selected for representative propeller-shank clearance requirements. The design of the cowl gap was based upon the recommendations of reference 2, with an assumed full-scale clearance gap of 0.375 inches between the rotating and stationary portions of the cowl. Six struts, equally spaced at angular intervals of 60° starting from top center, were included for accessory-drive housings and structural support of the spinner. These struts spanned the duct radially at a station upstream of the compressor inlet and were faired into the duct contours with generous fillets. The midspan portions of the struts had NACA 0020-64 sections. The relatively long duct between the cowl gap and the compressor inlet was included in the original design to permit the adaptation of the model to an E-type cowling for a dual-rotation propeller.

Instrumentation of the Model

Flush orifices were installed in the model at the locations listed in table II. In addition to these, nine flush orifices, equally spaced at angular intervals of 40° starting 15° from top center, were installed in the inner surface of the cowl gap 9.85 inches from the leading edge of the cowl (station 2, fig. 1).

Three total-pressure tubes were located at station 2. These were 0.040 inch in diameter, equally spaced at angular intervals of 120° starting 75° from top center, and approximately alined with the mean line of the cowl gap.

Survey rakes were located at stations 3, 4, and 5 (fig. 1).

The ram-recovery rake at station 3 contained a total of 42 total-pressure tubes. A group of 21 tubes (seven tubes spaced at angular intervals of 6.75° at each of three radii) was centered behind the propeller-blade-shank fairing 315° from the top center. Also, seven tubes were distributed radially across the duct at each of three locations, 0°, 90°, and 180° from the top center.

The rake at the compressor inlet, station 4, was made up of 15 static- and 35 total-pressure tubes. The 35 total-pressure tubes were distributed in the duct in a pattern such that each was located at the center of an area equal to 1/35 of the total duct area in order to permit the use of an integrating manometer in setting the mass rate of flow in the duct. A drawing of the rake pattern at station 4 is shown in figure 3.

A drag-survey rake containing 11 static- and 42 total-pressure tubes was located at station 5 on the uppermost surface of the model.

TESTS

Surface-pressure distributions, cowl-gap flow, total-pressure recoveries, and momentum losses in the cowl wake were measured for the model at an angle of attack of 0° with the cowling stationary. The cowl was positioned so that the four propeller-blade-shank fairings were 45°, 135°, 225°, and 315° from top center, respectively. All pressure measurements were indicated on multitube manometers and recorded simultaneously by photographic means.

With the inlet-velocity ratio varied over the maximum range attainable by means of the throttle near the duct exit (fig. 1), data were

obtained for the following conditions: (1) for a Reynolds number (based on the maximum diameter of the cowl) of 1.80 million through a Mach number range of 0.23 to 0.88, and (2) for Reynolds numbers of 5.20 and 8.10 million and a Mach number of 0.23. The tests were conducted in two parts: (1) with the rakes installed at stations 2, 4, and 5, and (2) with the rakes installed at stations 2, 3, and 4.

CORRECTIONS

The method presented in reference 7 was used to estimate the tunnel constriction effects on the flow at the model. The magnitude of the corrections applied to the Mach number and to the dynamic pressure is indicated in the following tabulation:

Corrected Mach number	Uncorrected Mach number	Corrected q_o / Uncorrected q_o
[1]0.88	0.866	1.018
.86	.848	1.015
.84	.830	1.014
.82	.812	1.012
.80	.793	1.011
.75	.745	1.009
.70	.696	1.007
.60	.598	1.006
.23	.230	1.004

Prior to the installation of the model in the tunnel, the rake at station 4 was calibrated against a standard A.S.M.E. orifice meter through the range of mass rate of flow anticipated for the model tests. A correction to the mass rate of flow indicated by the rake at station 4 was made on the basis of this calibration.

RESULTS AND DISCUSSION

Pressure-Coefficient Distributions

Pressure coefficients on the cowl.- The distributions of the pressure coefficient on the external surface of the cowl are shown in figure 4 for the range of Mach numbers and inlet-velocity ratios of the tests. The minimum inlet-velocity ratio was attained when the movable

[1]The measured choking Mach number of the wind tunnel with the model installed was 0.92.

throttle was in a closed position (fig. 1). Since the throttle made an imperfect seal with the afterbody of the model, permitting some leakage through the throttle, the minimum inlet-velocity ratio resulted from the sum of the flow through the throttle and the flow through the cowl gap. The maximum inlet-velocity ratio was attained when the ratio of the pressure at the inlet to the pressure at the exit of the duct was a maximum or when choking occurred at the compressor inlet where the duct area was a minimum.

The compressibility effects on the distribution of pressure coefficient on the cowl, for various inlet-velocity ratios, may be seen in figure 4. In general, increasing the Mach number resulted in more positive pressure coefficients over approximately the forward 10 percent of the cowl and more negative pressure coefficients on the rear 80 percent of its length. For inlet-velocity ratios less than about 0.15, negative pressure-coefficient peaks occurred on the forward portion of the cowl. At and above the design inlet-velocity ratio of 0.3 the pressure distributions over the forward portion of the cowl were generally favorable.

Figure 4 also shows a negative pressure-coefficient peak on the aft portion of the cowl between 0.7 and 0.8 of the cowl length behind the nose, which is in general agreement with the data presented for the NACA 1-50-100 inlet in references 4 and 5, figures 7 and 6(e) respectively. The similarity in both shape and magnitude of the pressure-coefficient distributions reported herein to the pressure-coefficient distributions reported in references 4 and 5 for the NACA 1-50-100 inlet (no gap) for comparable Mach numbers and inlet-velocity ratios indicates that the leakage air flow through the cowl gap had little effect on the external pressure-coefficient distributions.

For the range of inlet-velocity ratios of the test, the data of figures 4(i), 5(a), and 5(b) show no significant effects of Reynolds number on the pressure-coefficient distributions on the external surface of the cowl for the range of Reynolds numbers between 1.8 and 8.1 million.

Pressure coefficients on the inner lip of the cowl.- The pressure-coefficient distributions on the inner lip of the cowl are shown in figures 6 and 7. In general, increasing Mach number resulted in more positive pressure coefficients for the lower inlet-velocity ratios. Increasing the inlet-velocity ratio above about 0.35 resulted in the formation of pressure-coefficient peaks near 0.025 of the cowl length. Except at a Mach number of 0.23 and excluding the data for longitudinal station 0, the inlet-velocity ratios of these tests were not large enough to produce static pressures inside the cowl less than the free-stream static pressure.

Figures 6(i), 7(a), and 7(b) show little change in the pressure-coefficient distributions due to increasing the Reynolds number from 1.8 to 8.1 million.

Pressure coefficients on the spinner.- The pressure-coefficient distributions on the spinner are presented in figures 8 and 9. For inlet-velocity ratios greater than about 0.3, the distributions show favorable pressure gradients up to about 0.7 of the spinner length with pressure recovery occurring behind this station. For the test conditions covered, the minimum static pressure on the spinner was always greater than the free-stream static pressure. Comparison of the data of figure 8 for equal inlet-velocity ratios indicates little effect of compressibility on the distributions of the pressure coefficient, and similarly, figures 8(i), 9(a), and 9(b) show little change in the pressure-coefficient distributions due to an increase of the Reynolds number from 1.8 to 8.1 million.

Pressure coefficients on the propeller-blade-shank fairings.- Figures 10 and 11 show the pressure-coefficient distributions at radii of 3 and 4 inches on the propeller-blade-shank fairings. For inlet-velocity ratios greater than about 0.3, the fairing pressure gradients were favorable up to about 0.3 of the fairing chord length, with pressure recovery occurring behind this station. It is of interest to note that the favorable pressure gradients on the spinner and propeller-blade-shank fairing terminated at approximately the same longitudinal position, since 0.3 of the propeller-blade-shank fairing length and 0.7 of the spinner length corresponded to distances of 4.9 and 4.7 inches, respectively, from the leading edge of the cowl. The static pressure on the fairing was nowhere less than the free-stream static pressure. The pressure-coefficient distributions on the fairings were little affected by either increasing Mach number or increasing Reynolds number.

Critical Mach Number

The variation with Mach number of the minimum pressure coefficients on the cowl, from cross plots of the data of figure 4, is shown in figure 12 for constant inlet-velocity ratios from 0.10 to 0.50, and the resulting variation of the critical Mach number with inlet-velocity ratio is shown in figure 13. The critical Mach number of 0.83 at an inlet-velocity ratio of 0.3 is the value predicted for the cowl from the design chart (fig. 53) of reference 3. The critical Mach number was little affected by increasing the inlet-velocity ratio above 0.25.

Cowl-Gap Flow

The E-type cowling requires that more air be taken in through the inlet than is needed for the engine in order to make up for the leak flow through the clearance gap between the rotating and stationary parts of the cowl. The present tests provide information regarding the magnitude of the gap flow and its effects on the external and internal flows for this specific gap design.

The variation with inlet-velocity ratio of the average pressure coefficients measured in the cowl-gap exit, station 2, is shown in figure 14 for the range of Mach numbers of the tests. Figure 15 shows the variation with inlet-velocity ratio of the ratio of the average total pressure in the cowl-gap exit to the average total pressure inside the cowl at station 3. As shown in figure 15, the maximum total-pressure loss through the cowl gap for high Mach numbers and inlet-velocity ratios was only of the order of 7 percent, and for the design condition (a Mach number of 0.8 and an inlet-velocity ratio of 0.3) the cowl-gap total-pressure loss was less than 3 percent. Since the total-pressure losses through the cowl gap were small and the leakage air flow through the cowl gap had little effect on the external pressure-coefficient distributions, as previously discussed, the gap design is considered satisfactory.

An orifice coefficient for the cowl gap may be expressed by the relationship

$$C = \frac{W_{a_2}}{gA_2\sqrt{2\bar{\rho}(H_3-p_c)}}$$

which is derived from the method discussed in reference 1. In this expression, the quantities represented by the symbols are as follows:

W_{a_2} weight rate of flow through the cowl gap measured at station 2

g standard acceleration of gravity

A_2 cross-sectional area of the cowl gap at station 2

$\bar{\rho}$ average of the mass density of the air on the cowling surface at the gap exit and the mass density of the air inside the cowl just upstream of the cowl gap

H_3 average total pressure at station 3

p_c local static pressure on the cowling surface at the gap exit (As used herein, p_c is obtained from figure 4 as the average of the pressures measured at the orifices just upstream and downstream of the gap exit.)

The variation of the measured cowl-gap weight flow with the computed function $gA_2\sqrt{2\rho(H_3-p_c)}$ is shown in figure 16 for the range of Mach numbers of the tests. The numerical average of the orifice coefficients for the cowl gap, obtained from the data of figure 16 and shown therein as a dashed line, is 0.68. This value is in good agreement with the value presented in reference 1.

The ratio of the weight rate of flow through the cowl gap (W_{a_2}) to the weight rate of flow through the inlet (W_{a_1}) is shown in figure 17 as a function of the inlet-velocity ratio for the range of Mach numbers of the tests. In general, the portion of the inlet flow discharged through the cowl gap steadily increased with decreasing inlet-velocity ratio until, at an inlet-velocity ratio of about 0.06, there was no flow through the compressor inlet and all the air entering the inlet was discharged through the cowl gap. For inlet-velocity ratios less than about 0.7, increasing the Mach number resulted in a reduction in this weight-flow ratio. For the design Mach number of 0.80 and an inlet-velocity ratio of 0.3, the weight-flow ratio was about 0.19 which compares favorably with the estimated weight-flow ratio allowed for in the selection of the cowling.

Ram Recovery

As used throughout this report, the average recovery at a given radius of the duct is the numerical average of the recoveries at the tubes of the survey rake at that radius, and the average recovery at a given station in the duct is the numerical average of the recoveries at all the tubes of the rake. Because of the particular spacing of the total-pressure tubes in the compressor-inlet rake, the numerical averages of the recoveries at all the tubes of the rake were weighted averages based on area.

Ram recovery at station 3.- Figure 18 shows the effects of the variation of Mach number and inlet-velocity ratio on the radial distribution of the pressure recovery at station 3, which is downstream of the propeller-blade-shank fairings and the cowl gap. In general, the ram-recovery ratio decreased with increasing inlet-velocity ratio and was highest near the outer portion of the duct, possibly due to the diversion of a portion of the flow through the cowl gap upstream of the survey station. For a given Mach number and inlet-velocity ratio, the ram-recovery ratio distributions between radii of 3.3 and 4.2 inches were

nearly the same at the top, bottom, and side of the duct. However, differences in the distribution at top, side, and bottom were evident near the inner surface of the duct and possibly may be attributed to local surface discontinuities at adjoining parts of the spinner just upstream of the rake. Figures 19 and 20 show the circumferential variation of the ram-recovery ratio at three radii (fig. 19) and an average of the three (fig. 20) for Mach numbers of 0.23, 0.80, and 0.88. The ram-recovery ratios shown in figures 19 and 20 for angular stations of 270° and 360° are the averages of the ram-recovery ratios at the top, side, and bottom of the duct obtained from the data of figure 18 for the three radii noted in figures 19 and 20. The large losses in the central region of the quadrant occurred in the wake of the propeller-blade-shank fairing, but these losses would be more evenly distributed around the duct for a rotating cowling at the design condition.

The separate effects of variation of the inlet-velocity ratio and Mach number on the ram recovery at station 3 are summarized in figures 21 and 22, respectively. The changes in the ram-recovery ratios resulted almost entirely from variation of the inlet-velocity ratio. For inlet-velocity ratios up to 0.6, the ram-recovery ratios at station 3 were about 0.98.

Ram recovery at the compressor inlet.- Figure 23 shows the typical circumferential variation of the ram-recovery ratio for one radius at the compressor inlet. The lower ram-recovery ratios occurred in the wakes from the propeller-blade-shank fairings and the strut fairings. The effects of variation of the inlet-velocity ratio on the average ram-recovery ratios at three radii at the compressor inlet are summarized in figure 24. The low pressure recovery evident near the central body surface was apparently due to the boundary-layer flow in the duct. Figure 25 further summarizes the combined effects of variation of the inlet-velocity ratio and Mach number on the pressure recoveries at the compressor inlet. For all three radii (figs. 25(a), 25(b), and 25(c)), variation of the inlet-velocity ratio again had a greater effect on the average ram-recovery ratios than did an increase in Mach number.

Figure 25(d) presents the average ram-recovery ratios at the compressor inlet. In general, for inlet-velocity ratios of 0.4 or less the average ram-recovery ratio at the compressor inlet exceeded 0.98 for the range of Mach numbers of the test. For the design condition, an inlet-velocity ratio of 0.3 at a Mach number of 0.8, the average ram-recovery ratio at the compressor inlet was 0.99.

Figure 26 shows the effects of Reynolds number in the range between 1.8 and 8.1 million on the average ram-recovery ratios at the compressor inlet. Increasing the Reynolds number resulted in higher ram-recovery ratios throughout the test range of inlet-velocity ratios.

Contours of the total pressure at the compressor inlet of the model are shown in figure 27 for the design Mach number and inlet-velocity ratio. Additional values of the deviation of total pressure from average values at three radii at the compressor inlet are tabulated in table III for various inlet-velocity ratios at the three Mach numbers compared throughout this report.

Summary.- Trend lines connecting the average ram-recovery ratios at the inlet (where an average ram-recovery ratio of 1.00 is assumed), station 3, and the compressor inlet are shown in figure 28 for Mach numbers of 0.88, 0.80, and 0.23. These lines merely provide an indication of the variation of the average ram-recovery ratio with increasing distance along the duct and are not meant to represent the absolute distribution of recovery along the duct. The average ram recovery decreased with increasing distance from the inlet, as would be expected, except for inlet-velocity ratios less than about 0.25 at a Mach number of 0.23 where the indicated change in recovery between stations 3 and 4 is within the experimental accuracy of the measurements at this Mach number.

Wake-Survey Drag

Figure 29 presents a typical radial variation of the point-drag coefficient calculated by the method discussed in reference 8 from the local momentum defect in the flow at the tubes of the drag-survey rake at station 5 (fig. 1). The variation with inlet-velocity ratio of the external-drag coefficient is shown in figure 30, and the compressibility effects on the external-drag coefficients are summarized in figure 31 for constant values of inlet-velocity ratio.

The increase in drag with decreasing inlet-velocity ratio throughout the Mach number range is believed to result from the formation of negative pressure-coefficient peaks on the cowl and from the discharge of low-energy air from the cowl gap.

The variation of the external-drag coefficient with inlet-velocity ratio at Reynolds numbers of 5,200,000 and 8,100,000 is shown in figure 32, and the effect of the Reynolds number on the drag for a constant Mach number is shown in figure 33. These data show only small changes in external drag with variation of the inlet-velocity ratio as the Reynolds number was increased above 1.8 million. The gradual decrease of drag with increasing Reynolds number may be attributed to a reduction of the skin-friction-drag coefficient with increasing Reynolds number.

CONCLUDING REMARKS

The following remarks may be made regarding an investigation of the effects of Mach number and Reynolds number on the characteristics of the internal and external flow about an E-type cowling at an angle of attack of 0° and with the cowl stationary.

For a given inlet-velocity ratio, increasing either the Mach number or the Reynolds number in the ranges reported herein resulted in only small changes in the pressure recoveries in the duct and in the external-drag coefficient of the cowl.

For inlet-velocity ratios greater than about 0.30, increasing the Mach number resulted in a slight decrease in the minimum pressure coefficient on the cowl for Mach numbers up to about 0.7, with a rather rapid decrease as the Mach number was further increased to 0.88. The measured critical Mach number of the cowl increased from 0.72 for an inlet-velocity ratio of 0.1 to 0.83 for inlet-velocity ratios of 0.3 and above.

Significant changes in the characteristics of the flow about the cowl occurred with variation of the inlet-velocity ratio. Generally, increasing the inlet-velocity ratio resulted in more positive pressure coefficients on the external surface of the cowl, lower ram-recovery ratios in the duct, and decreasing external-drag coefficients for the cowl. For inlet-velocity ratios less than about 0.15, negative pressure-coefficient peaks occurred near the leading edge of the cowl. For an inlet velocity ratio of about 0.06, no flow entered the compressor inlet and all the air entering the cowl inlet was discharged through the cowl gap.

The cowl-gap leakage air flow had little effect on the external pressure-coefficient distributions. The total-pressure losses through the cowl gap were small.

Average ram-recovery ratios at the compressor inlet were 0.98 or higher throughout the Mach number range for inlet-velocity ratios of 0.4 or less.

Ames Aeronautical Laboratory,
National Advisory Committee for Aeronautics,
Moffett Field, Calif.

REFERENCES

1. Runckel, Jack F., and Hieser, Gerald: Pressure-Rise and Leakage-Loss Characteristics of a Rotating Cowling. NACA RM L50D07, 1950.

2. Becker, John V., and Mattson, Axel T.: The Effect of Spinner-Body Gap on the Pressures Available for Cooling in the NACA E-Type Cowling. NACA CB, March 1943.

3. Nichols, Mark R., and Keith, Arvid L., Jr.: Investigation of a Systematic Group of NACA 1-Series Cowlings with and without Spinners. NACA Rep. 950, 1949.

4. Pendley, Robert E., and Smith, Norman F.: An Investigation of the Characteristics of Three NACA 1-Series Nose Inlets at Subcritical and Supercritical Mach Numbers. NACA RM L8L06, 1949.

5. Pendley, Robert E., and Robinson, Harold L.: An Investigation of Several NACA 1-Series Nose Inlets with and without Protruding Central Bodies at High-Subsonic Mach Numbers and at a Mach Number of 1.2. NACA RM L9L23a, 1950.

6. Stack, John, and von Doenhoff, Albert E.: Tests of 16 Related Airfoils at High Speeds. NACA Rep. 492, 1934.

7. Herriot, John G.: Blockage Corrections for Three-Dimensional-Flow Closed-Throat Wind Tunnels, with Consideration of the Effect of Compressibility. NACA Rep. 995, 1950. (Formerly NACA RM A7B28)

8. Baals, Donald D., and Mourhess, Mary J.: Numerical Evaluation of the Wake-Survey Equations for Subsonic Flow Including the Effect of Energy Addition. NACA ARR L5H27, 1945.

TABLE I.- E-TYPE COWLING COORDINATES

[Coordinates in inches]

Distance from leading edge of cowl	NACA 1-51-117 cowl, radius	Outer duct, radius	NACA 1-41.43-042.86 spinner, radius	Inner duct, radius	NACA 0030-34.5 propeller-blade-shank fairing, half thickness
0	3.654	3.654	- - -	- - -	- - -
.25	4.083	3.530	- - -	- - -	- - -
.50	4.271	3.514	0	- - -	- - -
.75	4.429	3.571	.633	- - -	- - -
1.00	4.567	3.639	.945	- - -	- - -
1.50	4.804	3.779	1.390	- - -	- - -
2.00	5.007	3.910	1.715	- - -	- - -
2.50	5.184	4.054	1.983	- - -	- - -
3.00	5.339	4.239	2.210	- - -	- - -
3.25	5.412	4.343	2.309	- - -	0
3.50	5.480	4.452	2.399	- - -	.301
4.00	5.610	4.678	2.559	- - -	.553
4.50	5.731	4.837	2.683	- - -	.701
5.00	5.844	4.943	2.779	- - -	.791
5.50	5.951	5.004	2.849	- - -	.833
6.00	6.051	5.023	2.887	- - -	.835
6.50	6.145	5.004	2.900	- - -	.799
7.00	6.233	4.952	- - -	2.900	.720
7.50	6.316	4.874	- - -	2.900	.596
8.00	6.392	4.773	- - -	2.900	.424
8.50	6.465	4.654	- - -	2.900	.202
8.75	6.501	4.590	- - -	2.900	.071
9.75	6.627	4.360	- - -	2.900	- - -
10.00	[1]6.568	4.360	- - -	2.900	- - -
10.50	[1]6.665	4.360	- - -	2.900	- - -
11.00	[1]6.744	4.360	- - -	2.900	- - -
11.50	6.801	4.360	- - -	2.900	- - -
12.00	6.841	4.360	- - -	2.900	- - -
12.50	6.876	4.360	- - -	2.900	- - -
13.00	6.906	4.360	- - -	2.900	- - -
13.50	6.932	4.360	- - -	2.900	- - -
14.00	6.954	4.360	- - -	2.900	- - -
14.50	6.973	4.360	- - -	2.900	- - -
15.00	6.987	4.360	- - -	2.900	- - -
15.50	6.996	4.360	- - -	2.900	- - -
16.00	7.000	4.360	- - -	2.900	- - -
16.38	7.000	4.360	- - -	2.900	- - -
18.80	- - -	4.360	- - -	2.900	- - -
19.00	- - -	4.360	- - -	2.890	- - -
19.40	- - -	4.310	- - -	2.830	- - -
19.80	- - -	4.200	- - -	2.720	- - -
20.80	- - -	3.790	- - -	2.290	- - -
21.20	- - -	3.660	- - -	2.070	- - -
21.60	- - -	3.530	- - -	1.850	- - -
22.00	- - -	3.420	- - -	1.640	- - -
23.00	- - -	3.260	- - -	1.280	- - -
23.35	- - -	3.240	- - -	1.250	- - -
24.35	- - -	3.240	- - -	1.250	- - -

[1]These radii which form the cowl-gap exit are smaller than the corresponding NACA 1-series radii.

TABLE II.- STATIC ORIFICE LOCATIONS FOR THE E-TYPE COWLING

[In inches from leading edge of cowl]

Orifices in NACA 1-51-117 cowl surface, in vertical plane of symmetry on uppermost surface	Orifices in surface of cowl inner lip, in vertical plane of symmetry on uppermost surface	Orifices in spinner surface, in vertical plane of symmetry on uppermost surface	Orifices in propeller-blade-shank fairing surface, on uppermost surface of the fairing at 315° from the top center[1]
0	0.16	0.50	3.25
.16	.32	.80	3.39
.32	.64	1.10	3.53
.64	.96	1.70	3.81
.96	1.28	2.30	4.09
1.28	1.60	2.80	4.37
1.60	2.40	3.70	4.93
2.40	- - -	4.10	5.49
3.20	- - -	4.70	6.05
4.80	- - -	5.30	6.61
6.40	- - -	5.90	7.17
8.00	- - -	6.50	7.73
11.20	- - -	7.10	8.29
12.80	- - -	7.70	8.57
14.40	- - -	8.30	- - -
16.38	- - -	8.90	- - -

[1]Fourteen orifices at each of two radii, 3 and 4 inches.

TABLE III.– THE VARIATION OF TOTAL PRESSURE IN THE DUCT AT THE COMPRESSOR INLET (STATION 4). R, 1,800,000

Tube number	Radius (in.)	Angular station (deg)	M_o, 0.88											
			V_1/V_o, 0.55		0.52		0.43		0.33		0.19		0.08	
			H, 835		845		861		871		882		887	
			Numerical average (lb/sq ft)	Deviation from average (lb/sq ft)	Numerical average (lb/sq ft)	Deviation from average (lb/sq ft)	Numerical average (lb/sq ft)	Deviation from average (lb/sq ft)	Numerical average (lb/sq ft)	Deviation from average (lb/sq ft)	Numerical average (lb/sq ft)	Deviation from average (lb/sq ft)	Numerical average (lb/sq ft)	Deviation from average (lb/sq ft)
1	1.468	0	775	18	797	7	833	−2	855	−7	877	−1	887	0
2	↓	72	↓	−51	↓	−37	↓	−22	↓	−10	↓	−3	↓	0
3	↓	144	↓	17	↓	17	↓	8	↓	6	↓	1	↓	0
4	↓	216	↓	13	↓	17	↓	17	↓	8	↓	1	↓	0
5	↓	288	↓	3	↓	−4	↓	−2	↓	5	↓	1	↓	0
6	2.004	18	844	−17	852	−17	863	−15	872	−8	882	−1	887	0
7	↓	54	↓	1	↓	0	↓	1	↓	1	↓	1	↓	0
8	↓	90	↓	7	↓	6	↓	5	↓	4	↓	−1	↓	0
9	↓	126	↓	−6	↓	−4	↓	0	↓	1	↓	2	↓	1
10	↓	162	↓	7	↓	6	↓	4	↓	−2	↓	−1	↓	0
11	↓	198	↓	6	↓	6	↓	4	↓	−4	↓	−1	↓	1
12	↓	234	↓	−6	↓	−8	↓	−6	↓	−2	↓	1	↓	1
13	↓	270	↓	8	↓	8	↓	5	↓	4	↓	1	↓	0
14	↓	306	↓	−10	↓	−8	↓	−6	↓	−1	↓	1	↓	0
15	↓	342	↓	7	↓	6	↓	5	↓	4	↓	2	↓	0
16	2.781	0	846	−5	855	−5	866	−2	875	−2	884	−1	887	0
17	↓	18	↓	5	↓	3	↓	2	↓	1	↓	0	↓	0
18	↓	36	↓	1	↓	2	↓	2	↓	1	↓	0	↓	0
19	↓	54	↓	−5	↓	−5	↓	−6	↓	−4	↓	0	↓	1
20	↓	72	↓	4	↓	3	↓	2	↓	1	↓	0	↓	0
21	↓	90	↓	5	↓	3	↓	2	↓	−1	↓	0	↓	0
22	↓	108	↓	4	↓	3	↓	2	↓	1	↓	0	↓	1
23	↓	126	↓	−2	↓	−1	↓	1	↓	−1	↓	0	↓	1
24	↓	144	↓	−8	↓	−5	↓	1	↓	1	↓	0	↓	1
25	↓	162	↓	4	↓	3	↓	2	↓	1	↓	0	↓	0
26	↓	180	↓	−8	↓	−7	↓	−3	↓	−2	↓	0	↓	0
27	↓	198	↓	5	↓	3	↓	2	↓	1	↓	0	↓	0
28	↓	216	↓	−8	↓	−7	↓	−6	↓	−1	↓	0	↓	1
29	↓	234	↓	−9	↓	−8	↓	1	↓	1	↓	0	↓	1
30	↓	252	↓	5	↓	3	↓	2	↓	1	↓	0	↓	0
31	↓	270	↓	5	↓	3	↓	2	↓	1	↓	0	↓	0
32	↓	288	↓	6	↓	5	↓	2	↓	1	↓	0	↓	0
33	↓	306	↓	−1	↓	0	↓	1	↓	−1	↓	0	↓	1
34	↓	324	↓	−4	↓	−4	↓	−2	↓	−2	↓	−1	↓	0
35	↓	342	↓	5	↓	3	↓	2	↓	1	↓	0	↓	0

Tube number	Radius (in.)	Angular station (deg)	M_o, 0.80											
			V_1/V_o, 0.60		0.54		0.42		0.29		0.17		0.07	
			H, 878		895		909		917		922		924	
			Numerical average (lb/sq ft)	Deviation from average (lb/sq ft)	Numerical average (lb/sq ft)	Deviation from average (lb/sq ft)	Numerical average (lb/sq ft)	Deviation from average (lb/sq ft)	Numerical average (lb/sq ft)	Deviation from average (lb/sq ft)	Numerical average (lb/sq ft)	Deviation from average (lb/sq ft)	Numerical average (lb/sq ft)	Deviation from average (lb/sq ft)
1	1.468	0	818	43	855	15	888	−2	908	−5	919	0	923	0
2	↓	72	↓	46	↓	−39	↓	−17	↓	−7	↓	−2	↓	0
3	↓	144	↓	13	↓	8	↓	9	↓	4	↓	1	↓	0
4	↓	216	↓	11	↓	6	↓	11	↓	6	↓	1	↓	0
5	↓	288	↓	−22	↓	8	↓	0	↓	1	↓	0	↓	0
6	2.004	18	888	5	901	−1	910	−11	918	−4	922	0	924	−1
7	↓	54	↓	−1	↓	0	↓	2	↓	2	↓	0	↓	0
8	↓	90	↓	5	↓	5	↓	4	↓	2	↓	0	↓	−1
9	↓	126	↓	−11	↓	−4	↓	0	↓	2	↓	1	↓	0
10	↓	162	↓	5	↓	5	↓	4	↓	2	↓	0	↓	−1
11	↓	198	↓	5	↓	0	↓	2	↓	−1	↓	0	↓	0
12	↓	234	↓	−10	↓	−8	↓	−4	↓	−2	↓	0	↓	0
13	↓	270	↓	5	↓	5	↓	4	↓	1	↓	0	↓	−1
14	↓	306	↓	−11	↓	−10	↓	−4	↓	−1	↓	1	↓	0
15	↓	342	↓	5	↓	5	↓	4	↓	2	↓	1	↓	−1
16	2.781	0	887	−6	902	−3	913	−3	919	0	923	0	924	−1
17	↓	18	↓	4	↓	4	↓	1	↓	1	↓	0	↓	0
18	↓	36	↓	−14	↓	−9	↓	1	↓	1	↓	0	↓	0
19	↓	54	↓	−1	↓	−1	↓	−3	↓	−2	↓	0	↓	0
20	↓	72	↓	6	↓	4	↓	1	↓	1	↓	0	↓	0
21	↓	90	↓	6	↓	4	↓	1	↓	1	↓	0	↓	0
22	↓	108	↓	4	↓	4	↓	1	↓	1	↓	0	↓	0
23	↓	126	↓	1	↓	1	↓	0	↓	1	↓	0	↓	0
24	↓	144	↓	−6	↓	−3	↓	1	↓	1	↓	0	↓	0
25	↓	162	↓	6	↓	4	↓	0	↓	1	↓	−4	↓	0
26	↓	180	↓	−7	↓	−5	↓	−1	↓	0	↓	0	↓	0
27	↓	198	↓	6	↓	4	↓	1	↓	1	↓	0	↓	0
28	↓	216	↓	−6	↓	−3	↓	−3	↓	0	↓	0	↓	0
29	↓	234	↓	−7	↓	−6	↓	0	↓	1	↓	0	↓	0
30	↓	252	↓	6	↓	4	↓	1	↓	1	↓	0	↓	0
31	↓	270	↓	6	↓	4	↓	1	↓	1	↓	0	↓	0
32	↓	288	↓	6	↓	4	↓	1	↓	1	↓	0	↓	0
33	↓	306	↓	0	↓	−1	↓	−4	↓	−3	↓	−4	↓	−4
34	↓	324	↓	−3	↓	−2	↓	−1	↓	0	↓	0	↓	0
35	↓	342	↓	6	↓	4	↓	1	↓	1	↓	0	↓	0

NACA

TABLE III.- CONCLUDED

Tube number	Radius (in.)	Angular station (deg)	M_o, 0.23															
			V_1/V_o, 0.77		0.76		0.67		0.57		0.47		0.37		0.25		0.18		0.11	
			H, 2107		2107		2104		2103		2103		2103		2101		2098		2098	
			Numerical average (lb/sq ft)	Deviation from average (lb/sq ft)	Numerical average (lb/sq ft)	Deviation from average (lb/sq ft)	Numerical average (lb/sq ft)	Deviation from average (lb/sq ft)	Numerical average (lb/sq ft)	Deviation from average (lb/sq ft)	Numerical average (lb/sq ft)	Deviation from average (lb/sq ft)	Numerical average (lb/sq ft)	Deviation from average (lb/sq ft)	Numerical average (lb/sq ft)	Deviation from average (lb/sq ft)	Numerical average (lb/sq ft)	Deviation from average (lb/sq ft)	Numerical average (lb/sq ft)	Deviation from average (lb/sq ft)
1	1.468	0	2087	15	2089	16	2091	10	2095	2	2097	-2	2099	-2	2099	-1	2098	0	2097	0
2	↓	72	↓	-2	↓	-2	↓	-9	↓	-7	↓	-3	↓	-2	↓	-1	↓	0	↓	0
3		144		1		0		0		2		1		2		1		0		0
4		216		1		0		7		5		4		3		1		0		1
5		288		-13		-14		-9		-1		1		1		1		0		1
6	2.004	18	2110	2	2110	2	2106	1	2104	-3	2103	-3	2103	-2	2101	-1	2098	0	2098	0
7	↓	54	↓	1	↓	1	↓	1	↓	1	↓	1	↓	-1	↓	0	↓	0	↓	0
8		90		2		2		1		1		-1		-1		-1		0		0
9		126		1		2		-1		-2		-1		-1		0		0		0
10		162		-9		-8		-4		1		1		1		0		0		0
11		198		2		2		1		0		-1		-1		-1		0		0
12		234		-2		-2		-4		-3		-2		-1		-1		0		0
13		270		2		2		1		1		1		-1		0		0		0
14		306		-2		0		-2		-2		-1		-1		0		0		0
15		342		2		2		1		1		1		1		0		0		0
16	2.781	0	2110	0	2110	1	2106	-1	2105	-1	2104	-2	2104	-2	2101	0	2098	0	2098	0
17	↓	18	↓	2	↓	2	↓	1	↓	0	↓	0	↓	0	↓	0	↓	0	↓	0
18		36		-5		-3		-4		0		0		0		0		0		0
19		54		0		0		-1		-1		-2		0		0		0		0
20		72		2		2		1		0		0		0		0		0		0
21		90		2		2		1		0		0		0		0		0		0
22		108		2		2		1		0		0		0		0		0		0
23		126		-3		-3		-2		-1		0		0		0		0		0
24		144		-3		-3		-1		0		0		0		0		0		0
25		162		2		2		1		0		0		0		0		0		0
26		180		0		1		1		-1		0		0		0		0		0
27		198		0		2		1		0		0		0		0		0		0
28		216		-2		-2		-2		-1		0		0		0		0		0
29		234		0		0		-2		-1		0		0		0		0		0
30		252		2		2		1		0		0		0		0		0		0
31		270		2		2		1		0		0		0		0		0		0
32		288		2		2		1		0		0		0		0		0		0
33		306		-5		-3		-1		0		0		0		0		0		0
34		324		0		0		-1		-1		0		-2		0		0		0
35		342		2		2		1		0		0		0		0		0		0

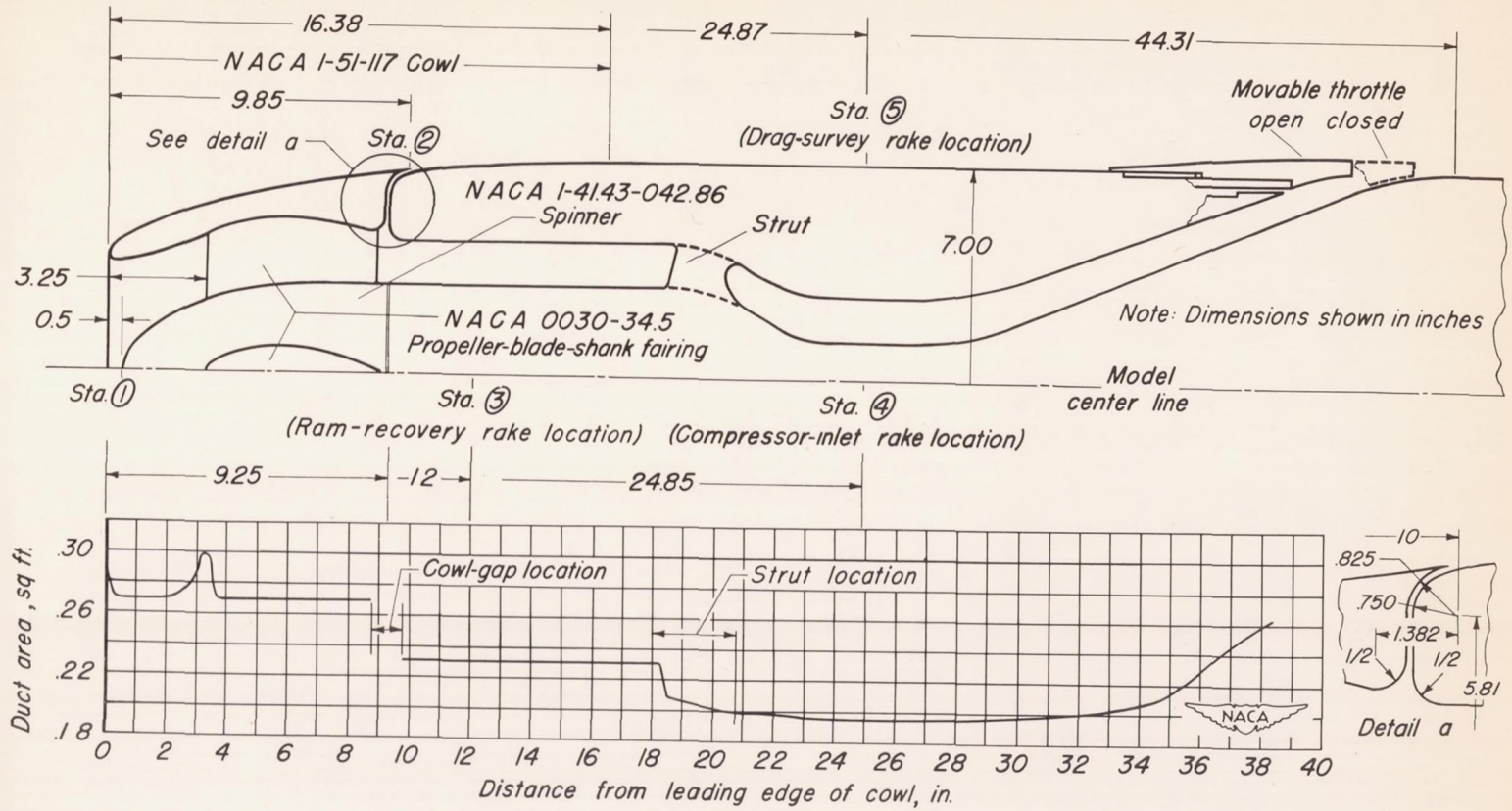

Figure 1.–Model arrangement and duct area distribution.

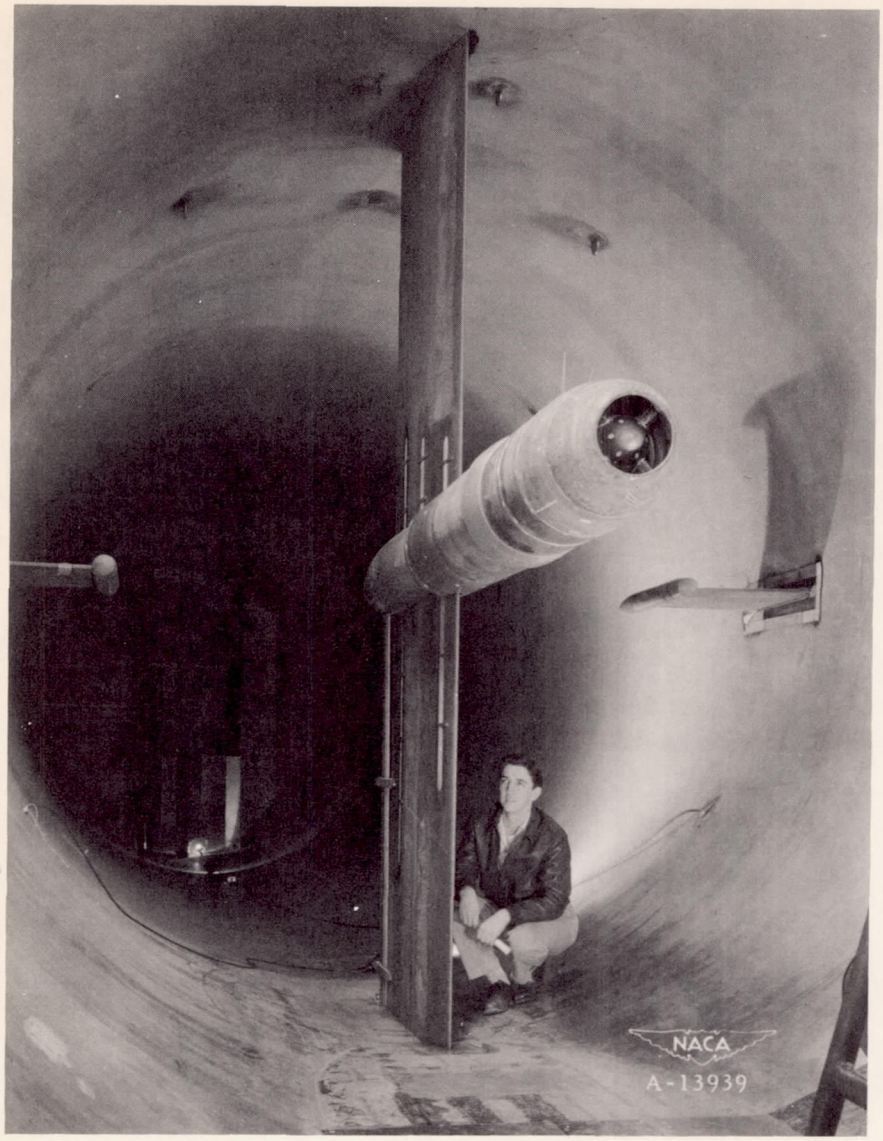

Figure 2.– The model NACA 1–series E–type cowling mounted in the 12–foot pressure wind tunnel.

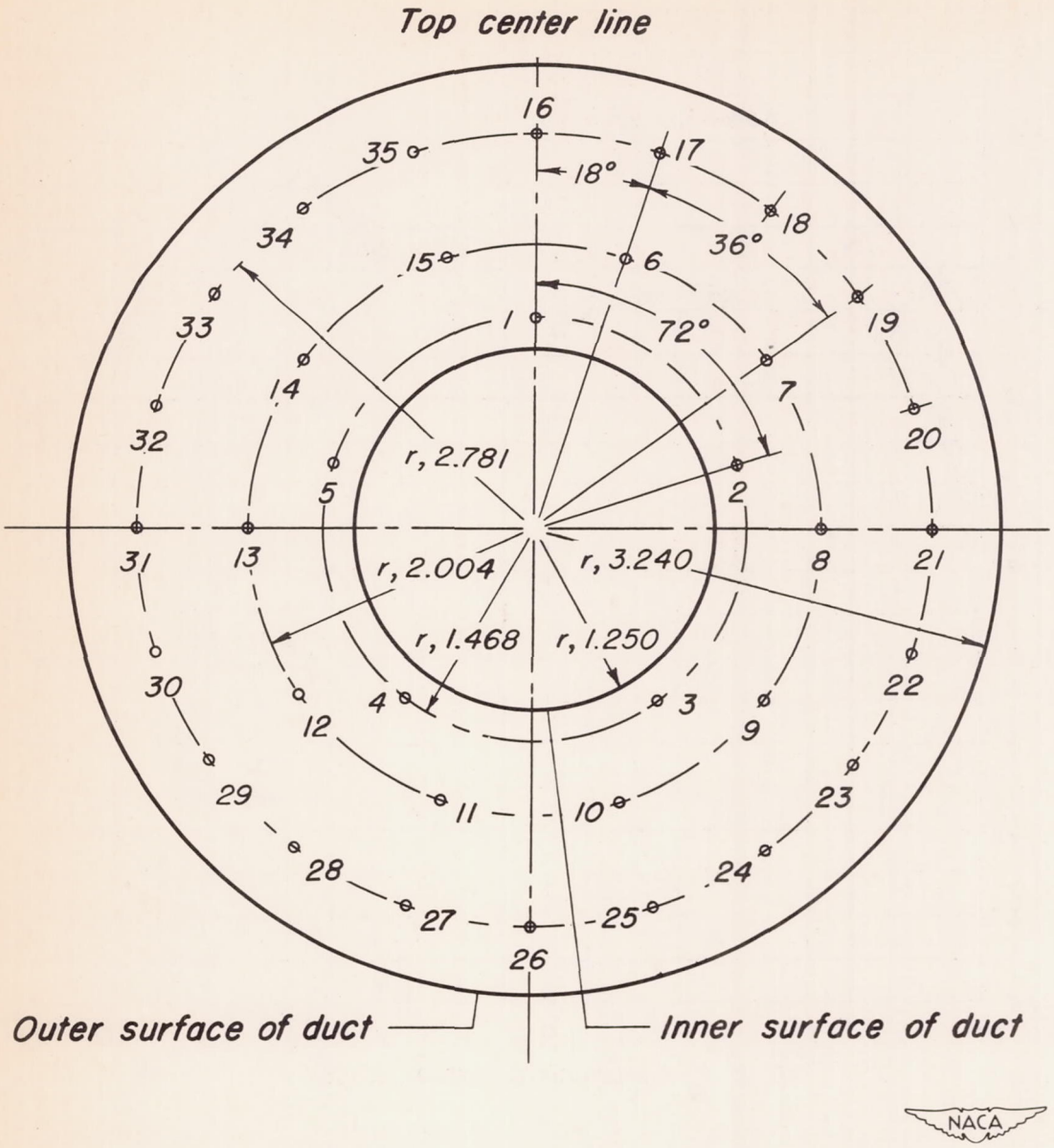

Figure 3.– The location and designation of the total-pressure tubes at the compressor inlet (station 4).

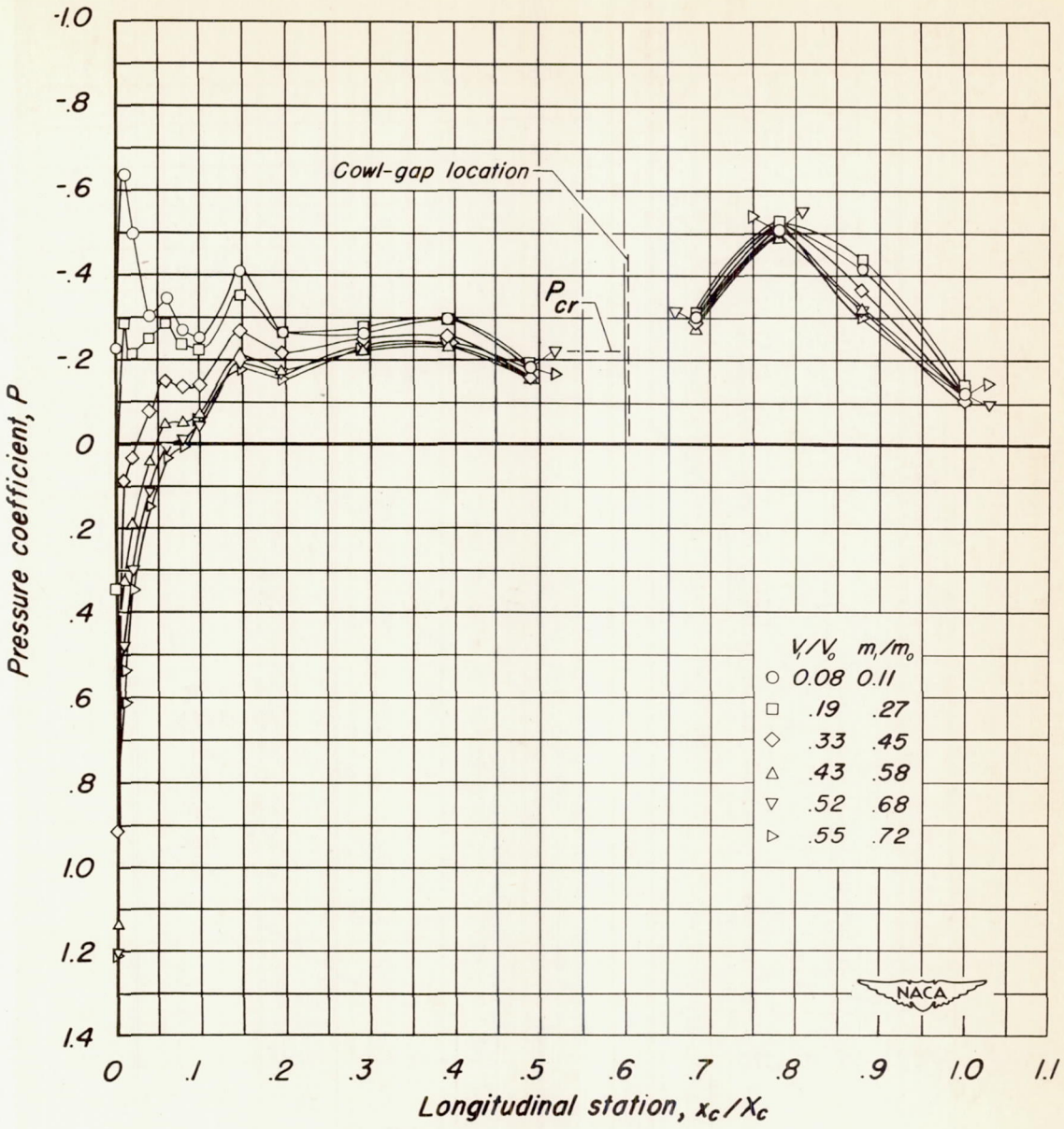

(a) M_o, 0.88

Figure 4.- Distribution of the pressure coefficient over the external surface of the cowl for various Mach numbers. R, 1,800,000.

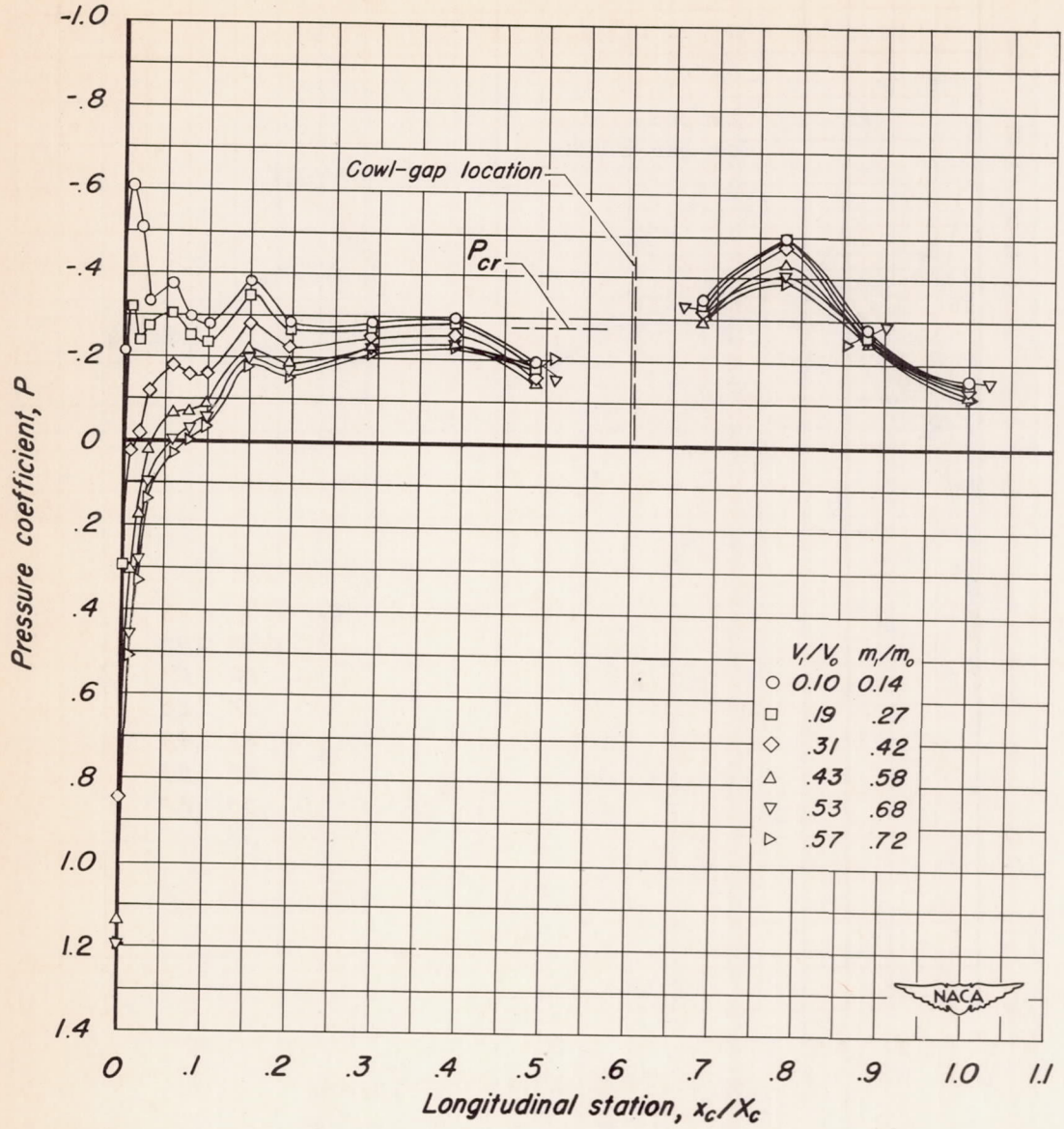

(b) M_o, 0.86

Figure 4.- Continued.

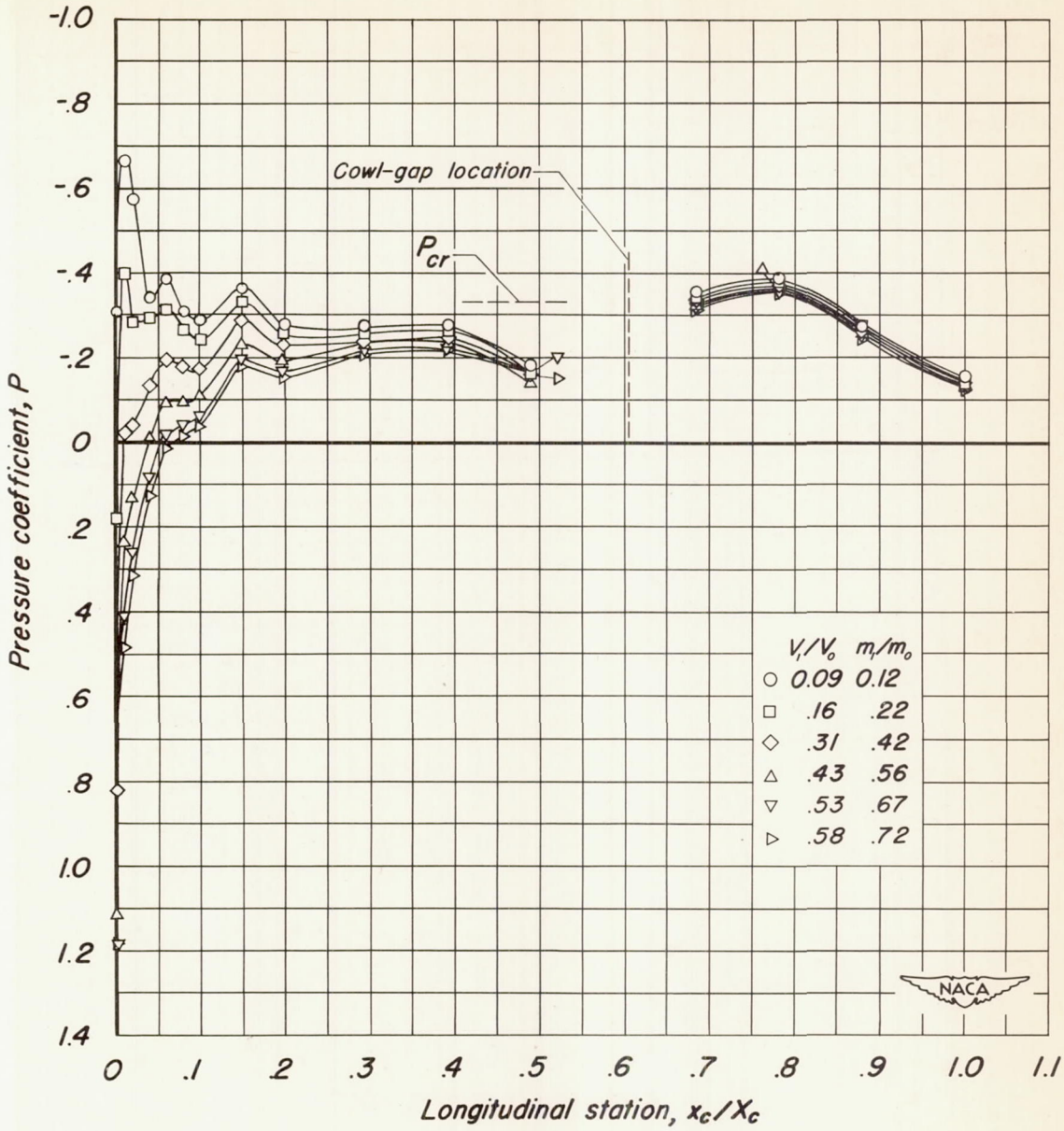

(c) M_o, 0.84

Figure 4.- Continued.

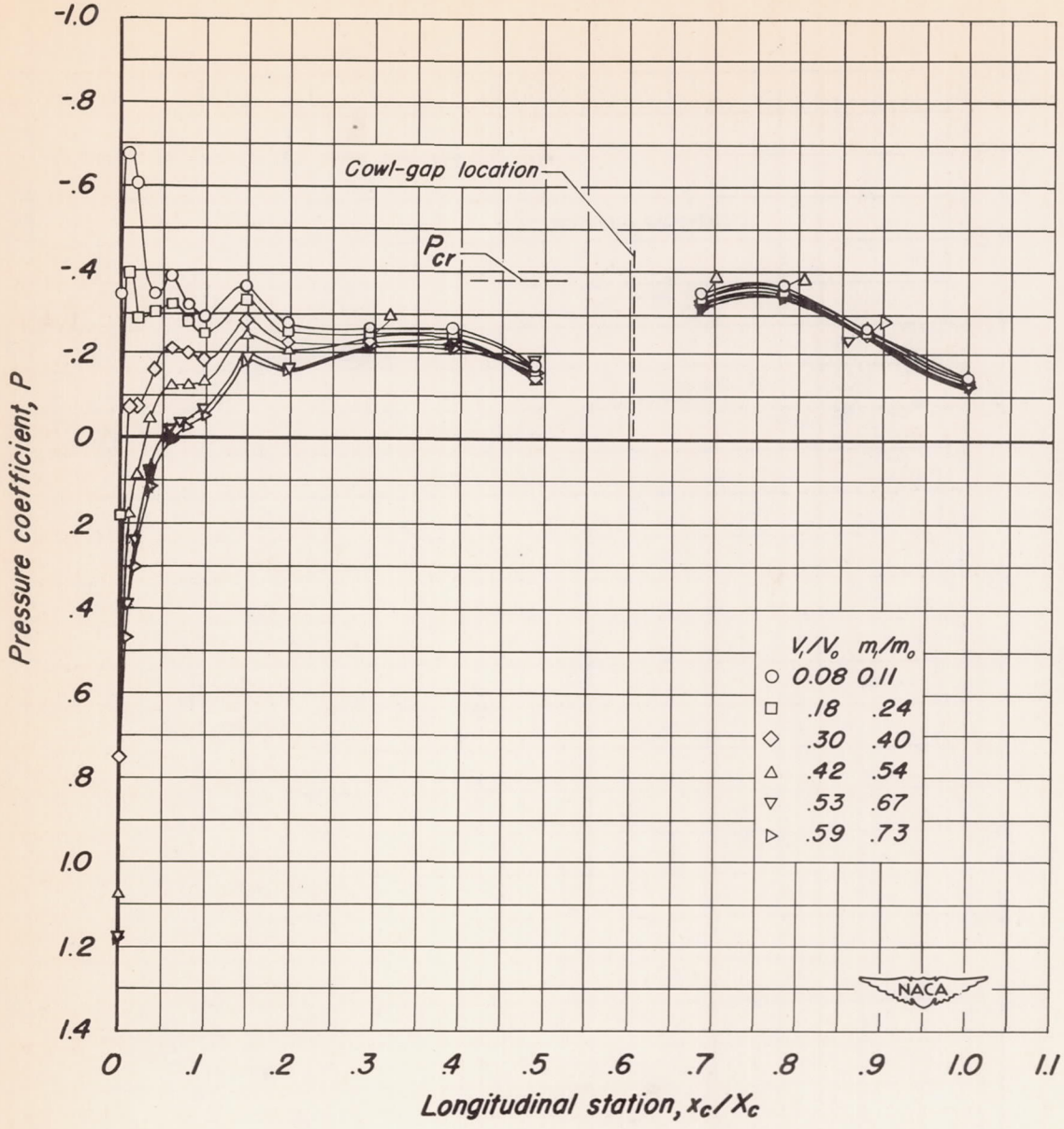

(d) M_o, 0.82

Figure 4.- Continued.

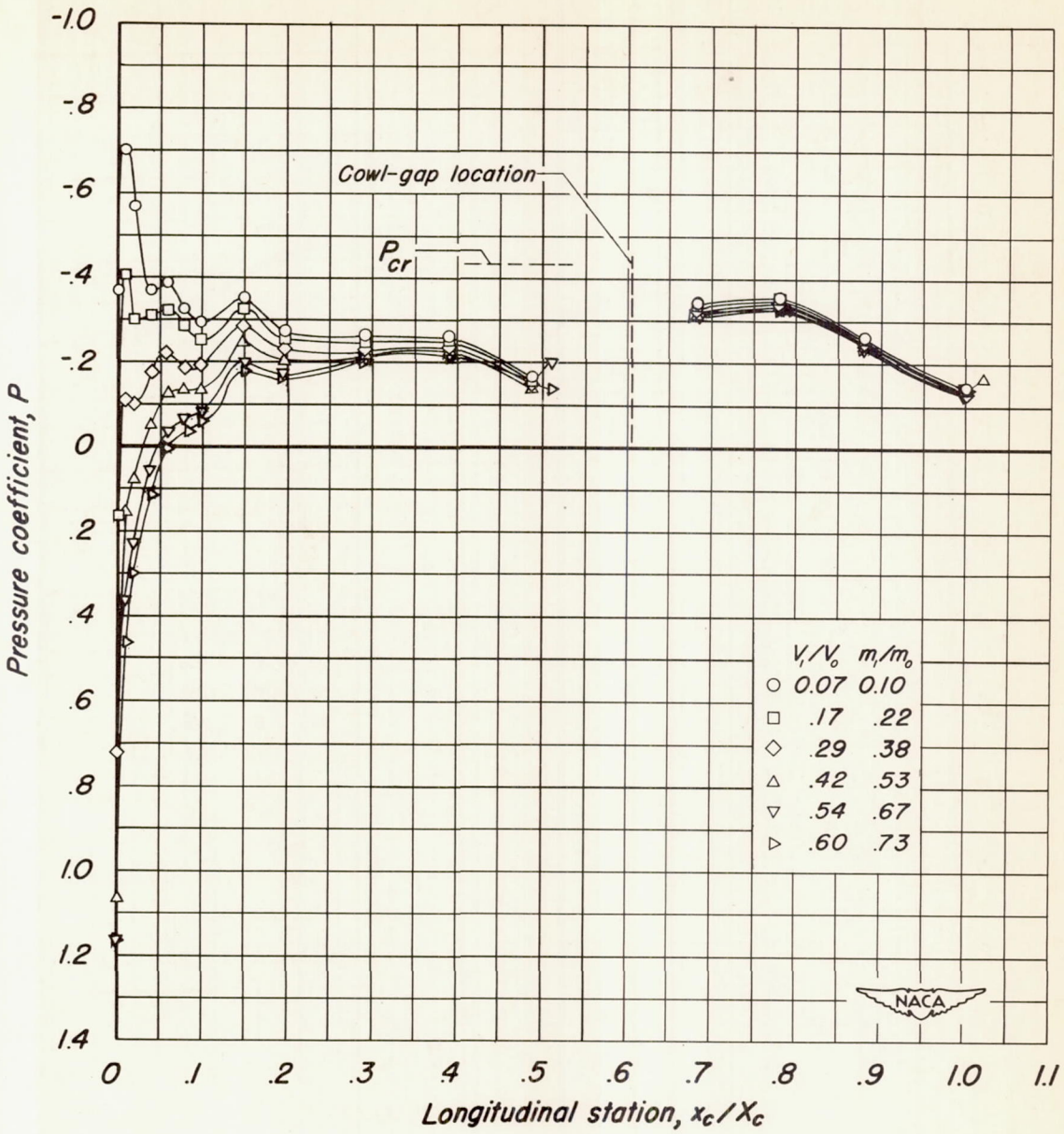

(e) M_o, 0.80

Figure 4.- Continued.

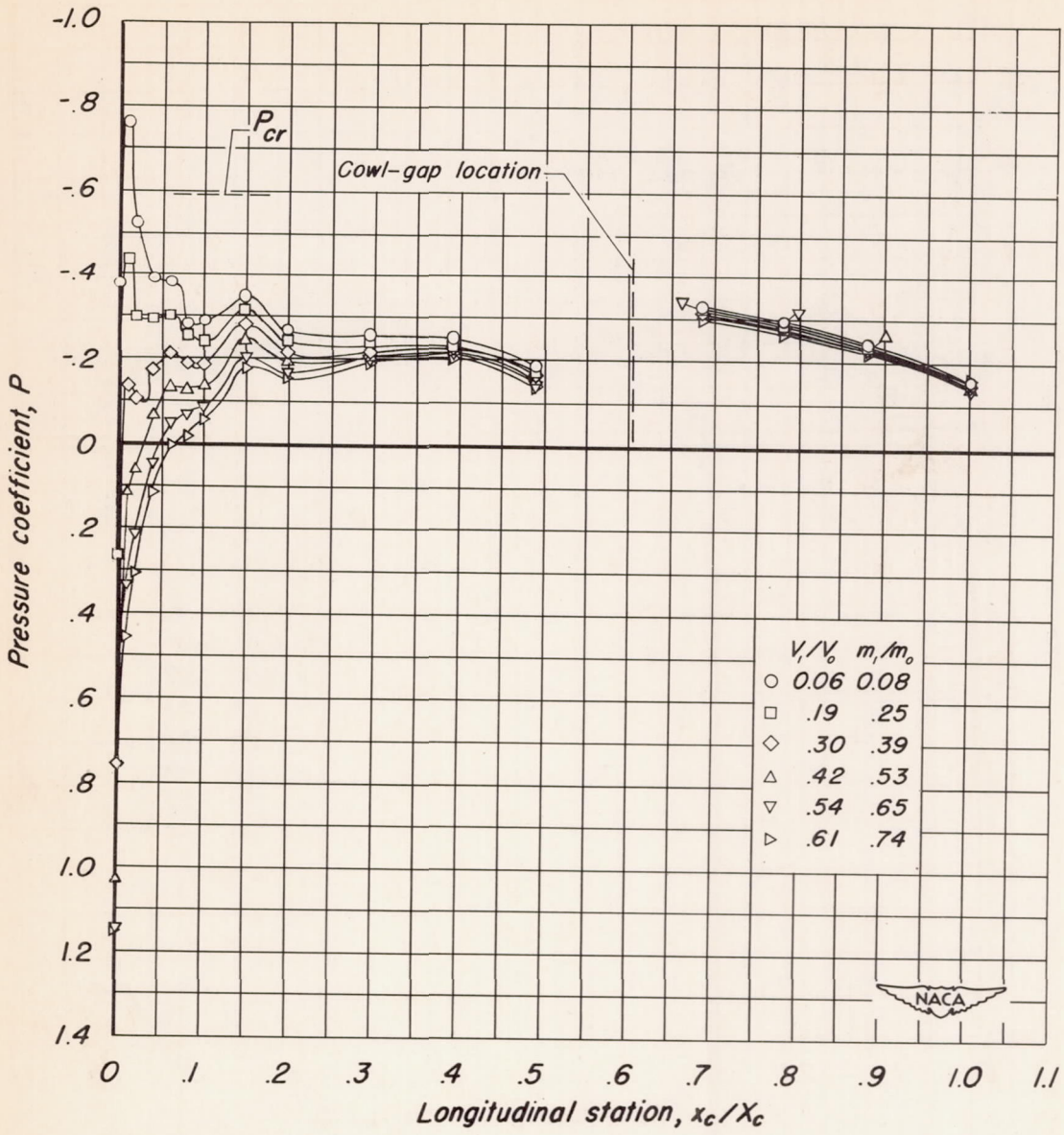

(f) M_o, 0.75

Figure 4.- Continued.

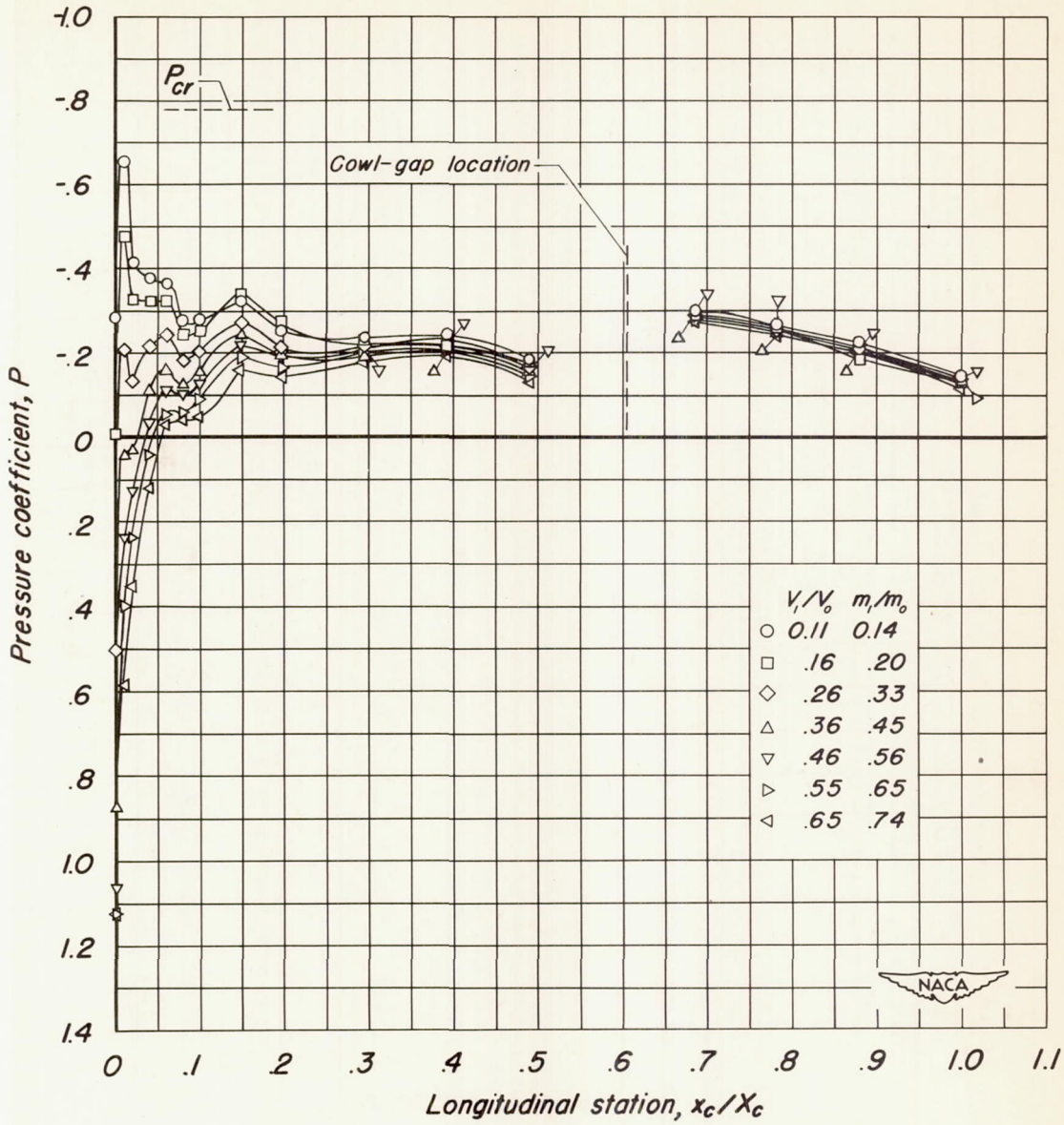

(g) M_o, 0.70

Figure 4.- Continued.

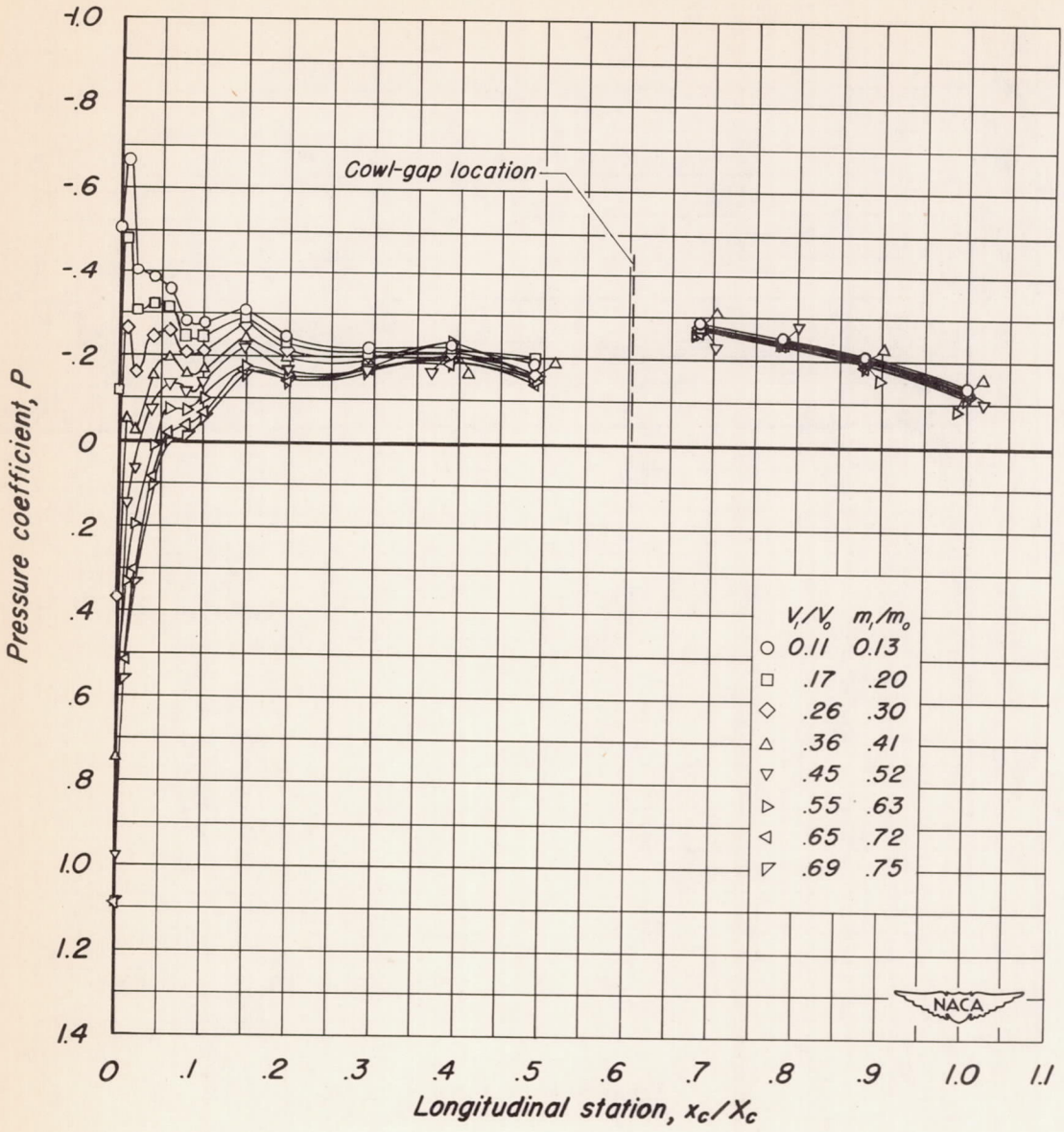

(h) M_o, 0.60

Figure 4.– Continued.

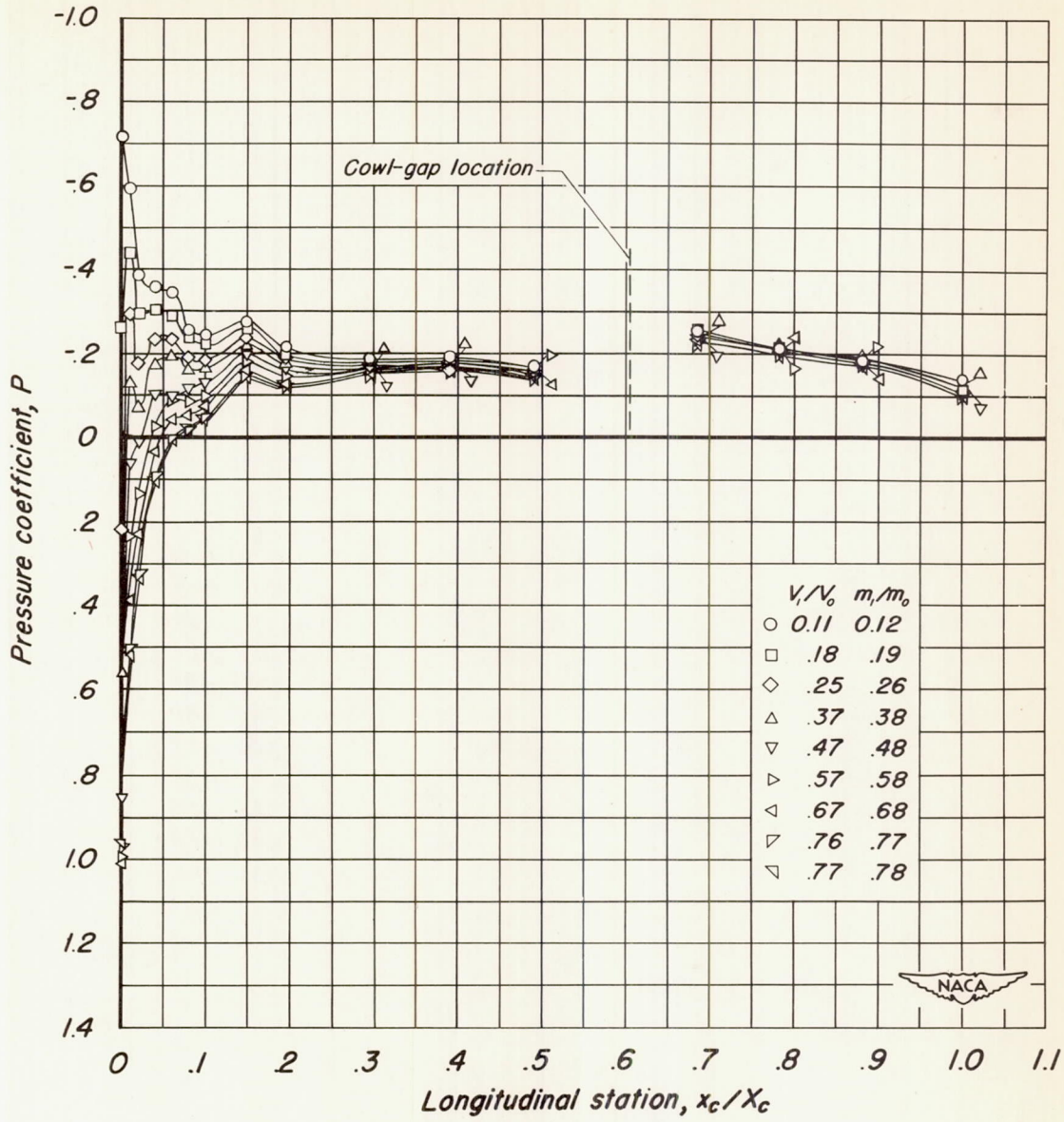

(i) M_o, 0.23

Figure 4.- Concluded.

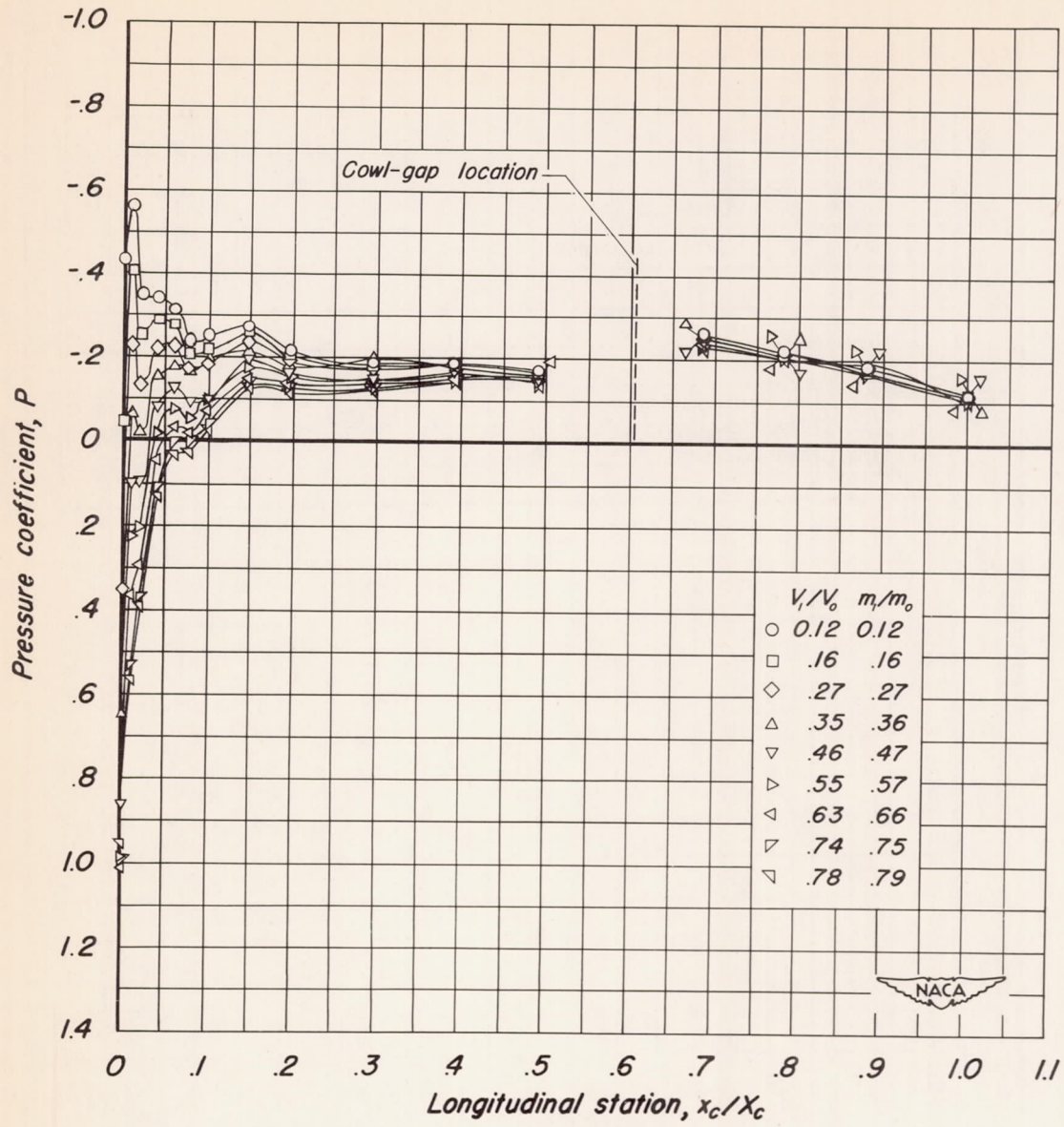

(a) R, 5,200,000

Figure 5.- Distribution of the pressure coefficient over the external surface of the cowl for Reynolds numbers of 5,200,000 and 8,100,000. M_o, 0.23.

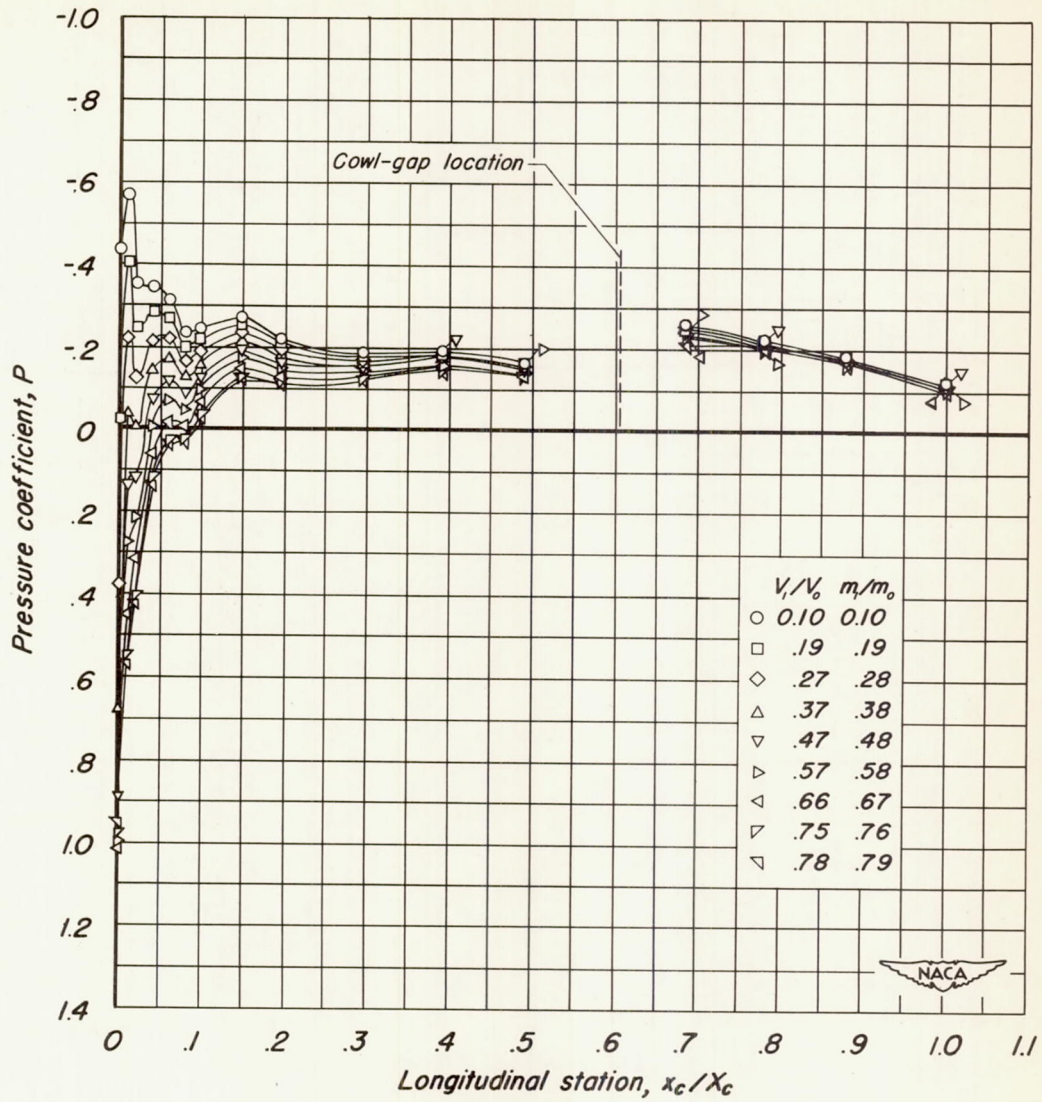

(b) R, 8,100,000

Figure 5.- Concluded.

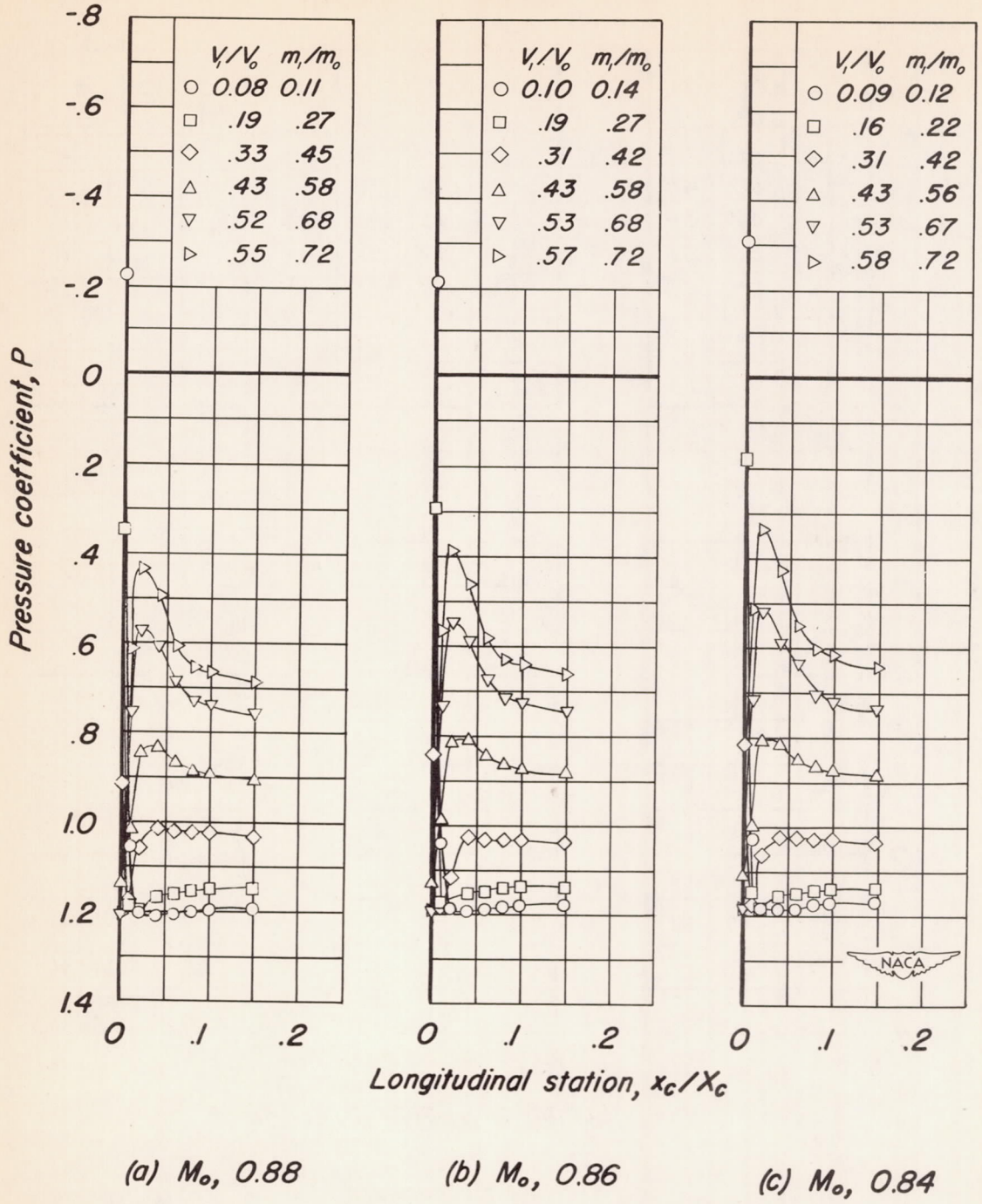

(a) M_o, 0.88 (b) M_o, 0.86 (c) M_o, 0.84

Figure 6.- Distribution of the pressure coefficient over the inner lip of the cowl for various Mach numbers. R, 1,800,000.

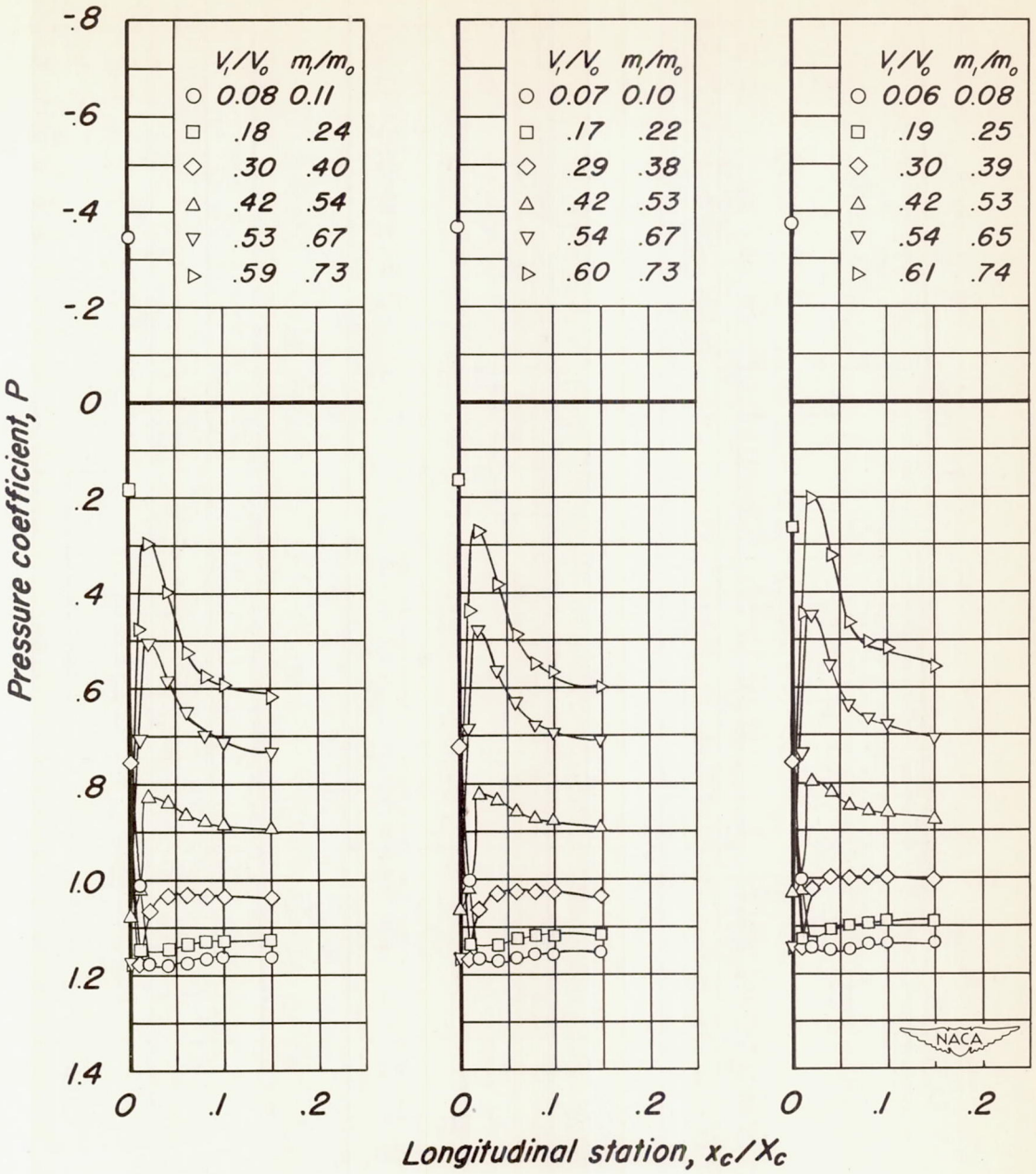

(d) M_o, 0.82 (e) M_o, 0.80 (f) M_o, 0.75

Figure 6.- Continued.

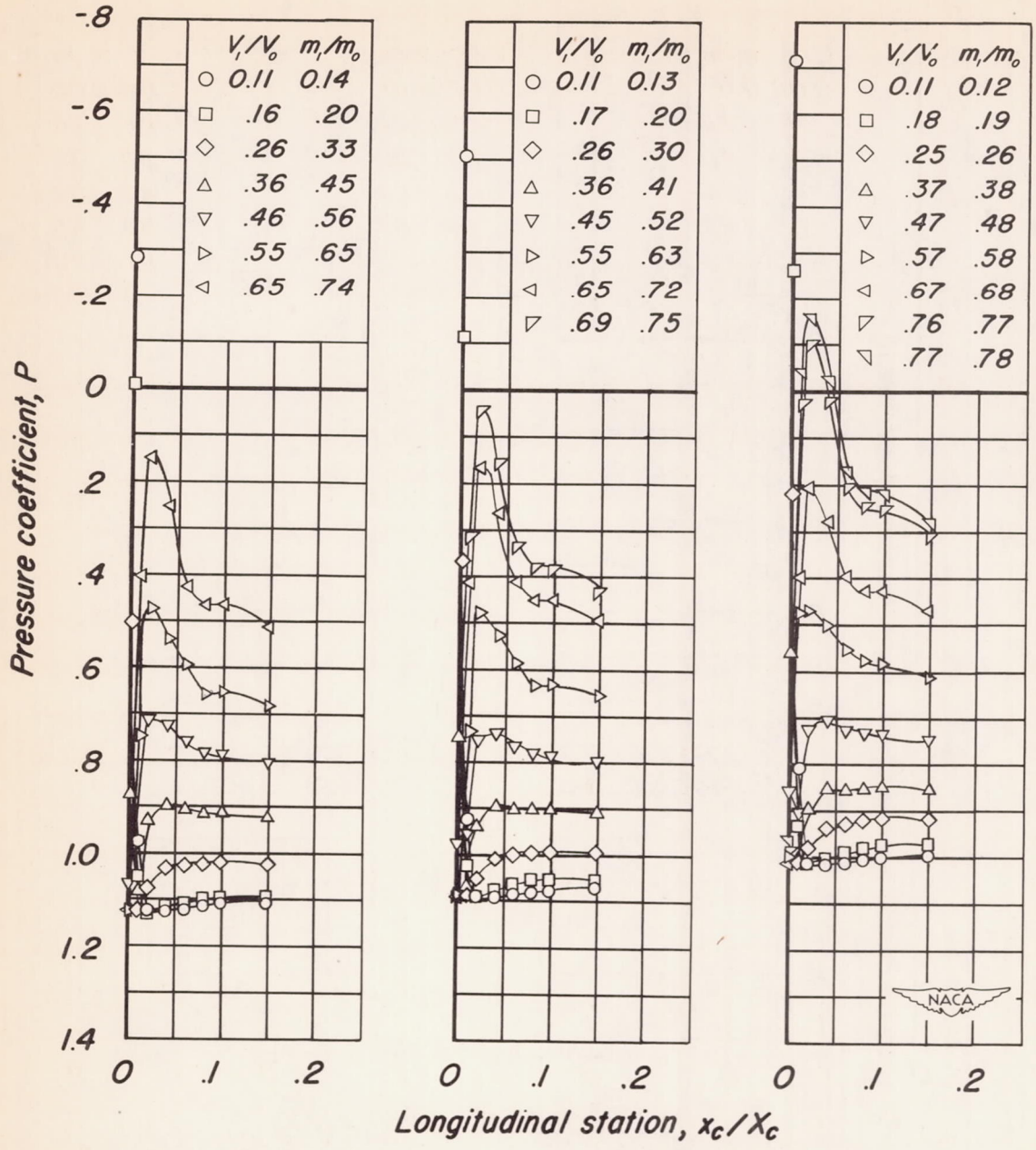

(g) M_o, 0.70 (h) M_o, 0.60 (i) M_o, 0.23

Figure 6.- Concluded.

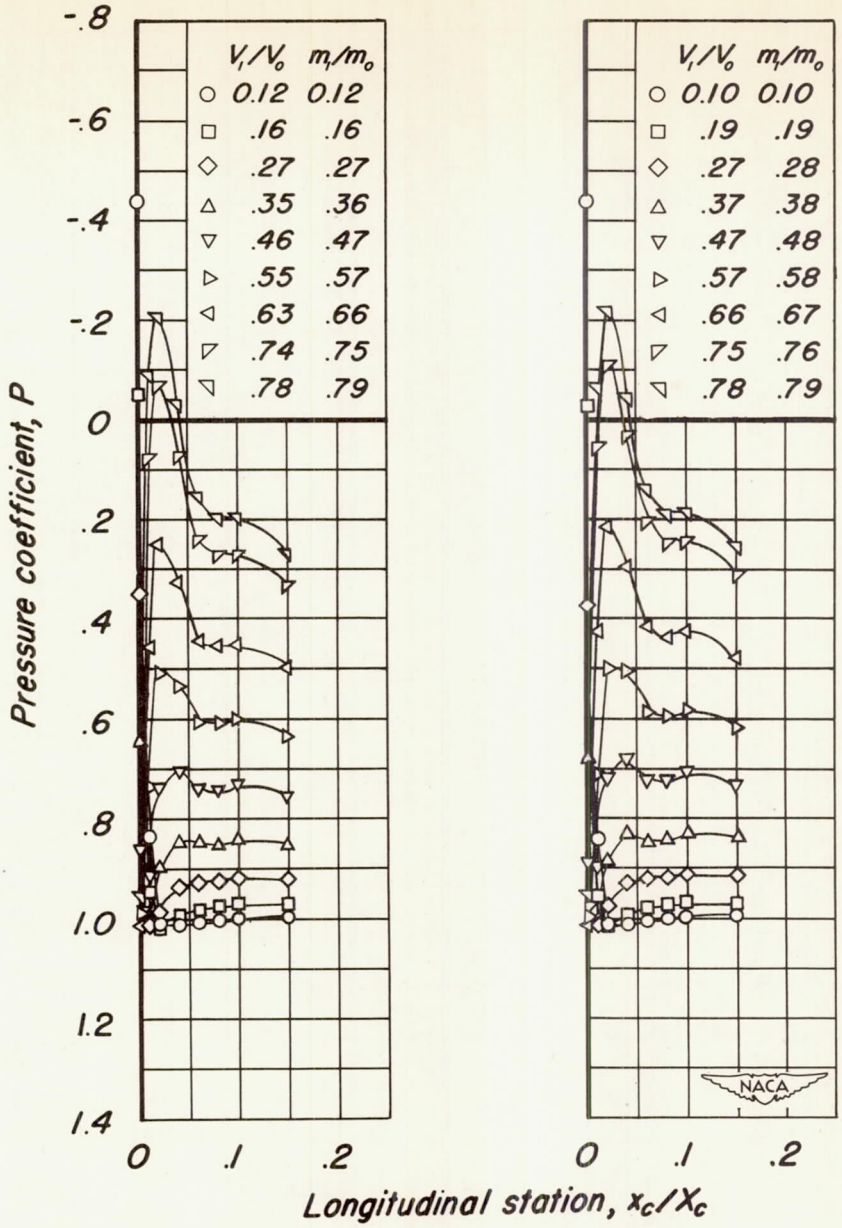

(a) R, 5,200,000 (b) R, 8,100,000

Figure 7.- Distribution of the pressure coefficient over the inner lip of the cowl for Reynolds numbers of 5,200,000 and 8,100,000. M_o, 0.23.

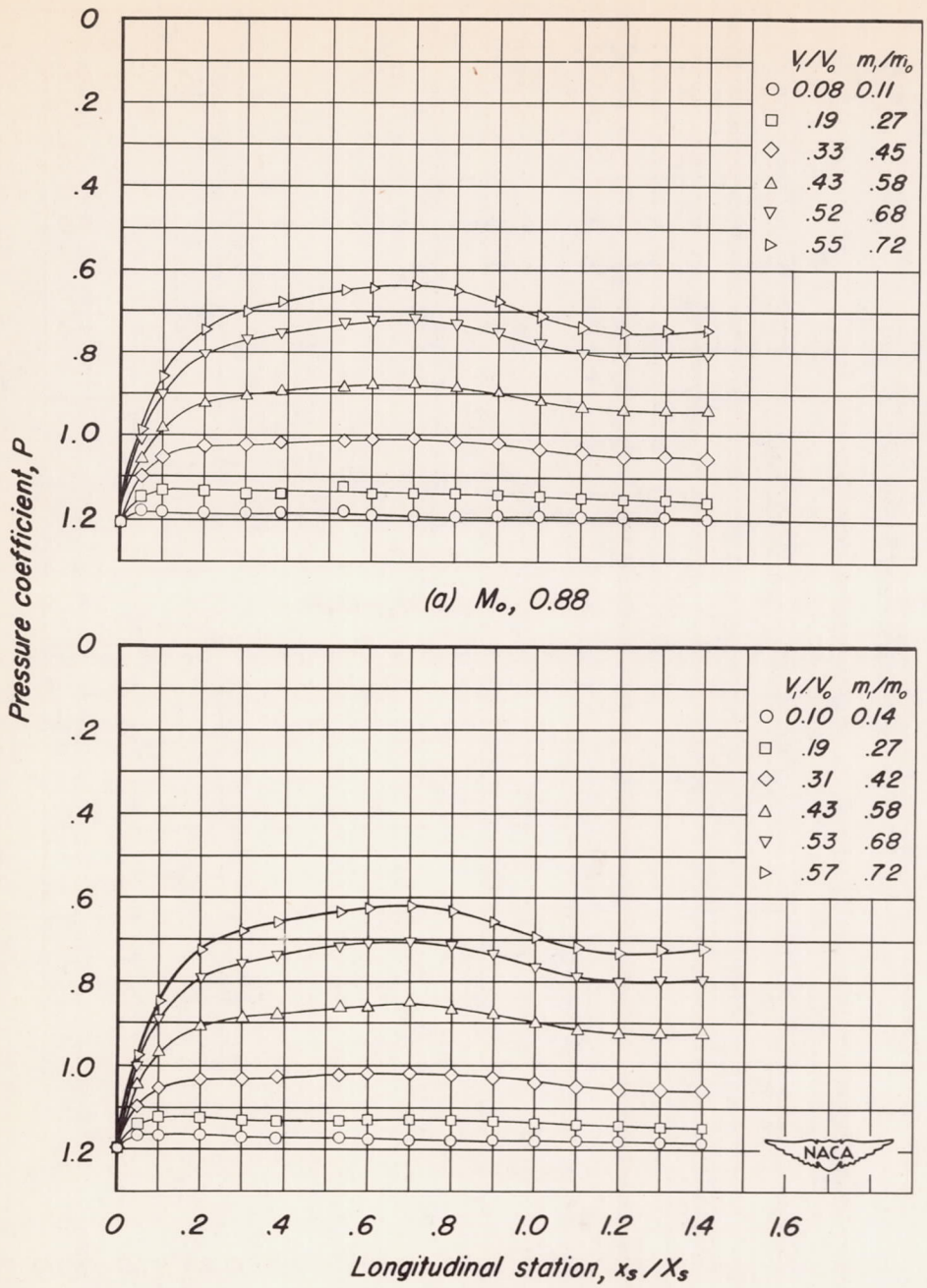

Figure 8.- Distribution of the pressure coefficient over the spinner for various Mach numbers. R, 1,800,000.

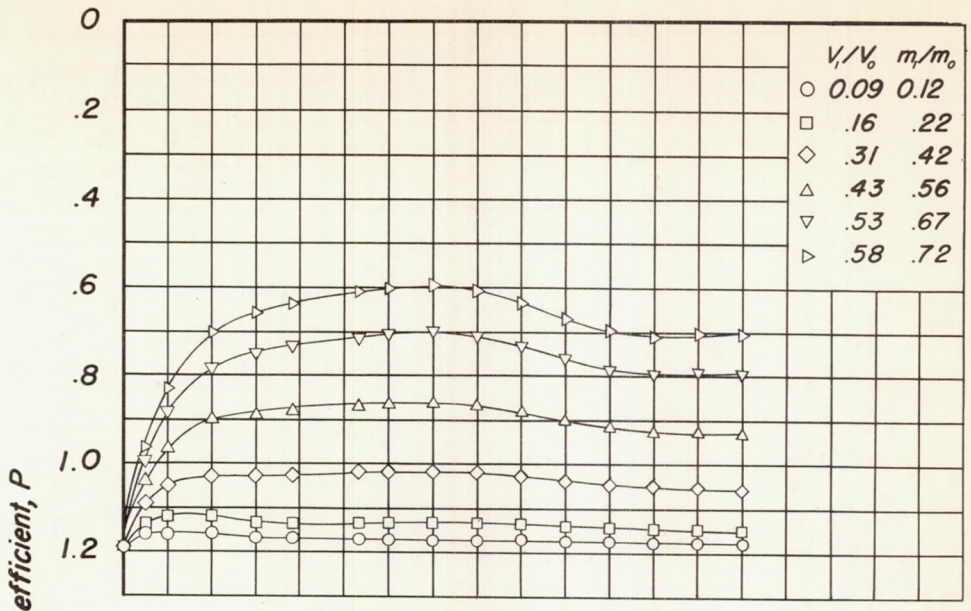

(c) M_o, 0.84

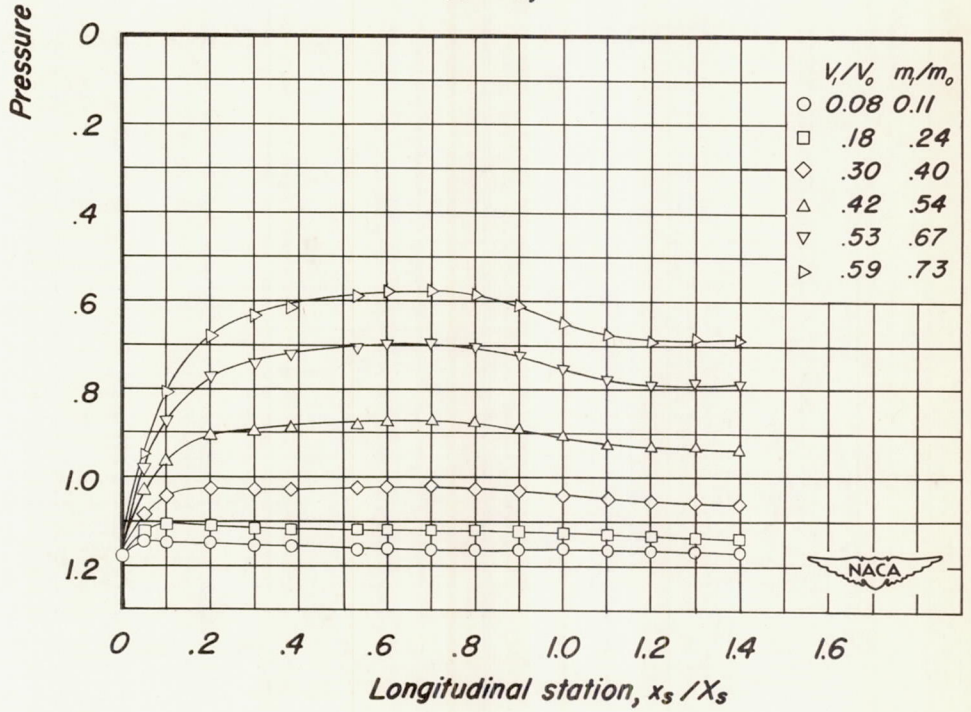

(d) M_o, 0.82

Figure 8.- Continued.

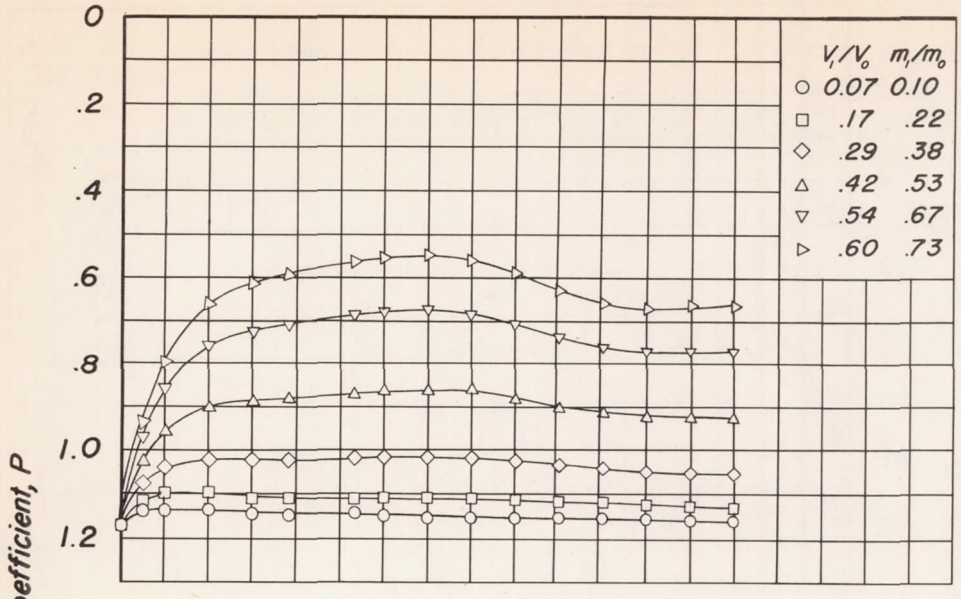

(e) M_o, 0.80

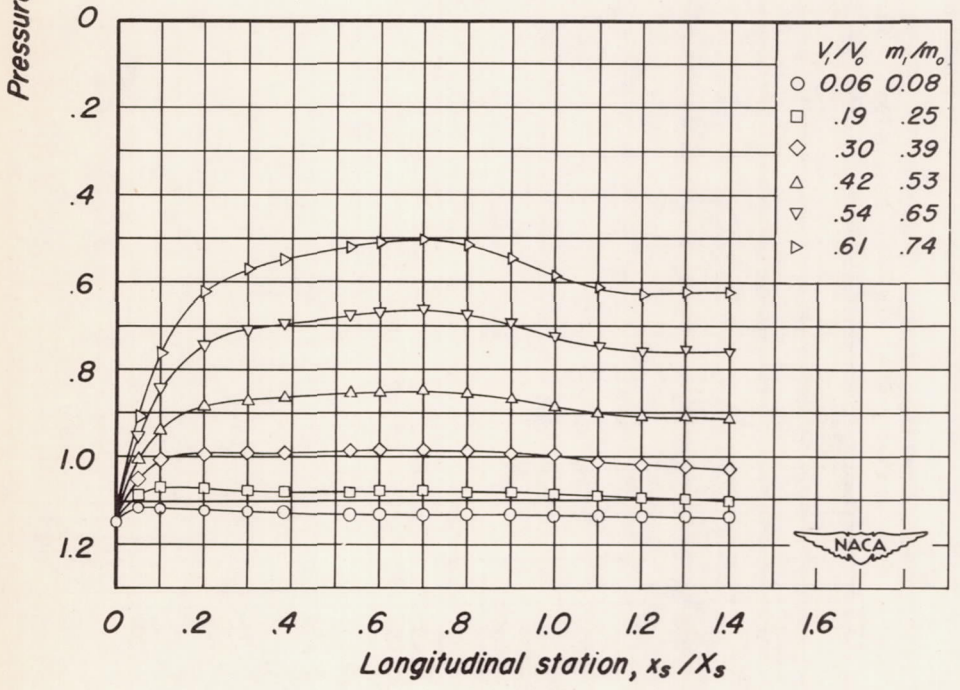

(f) M_o, 0.75

Figure 8.- Continued.

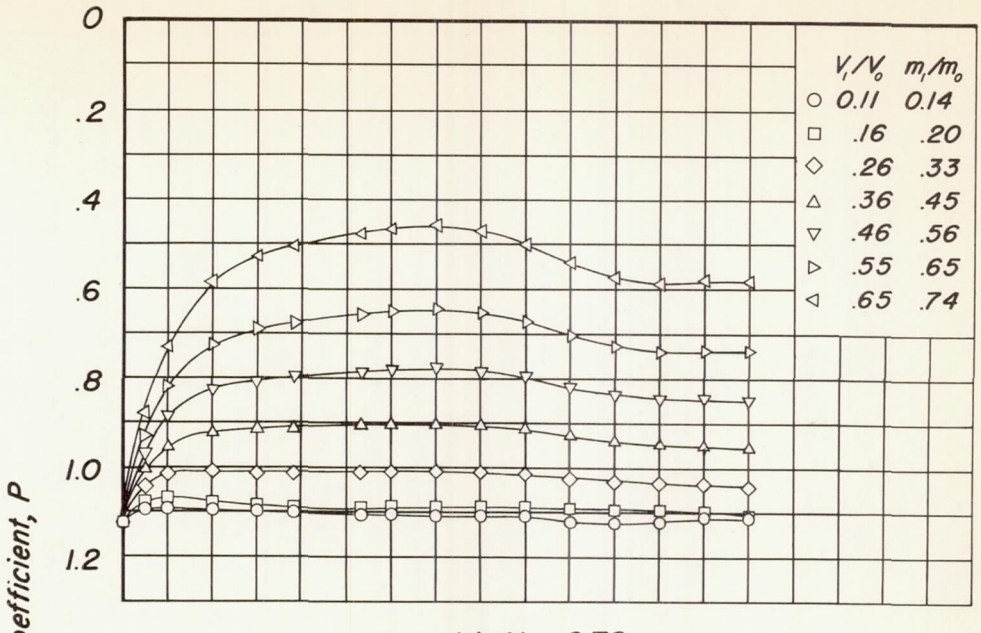

(g) M_o, 0.70

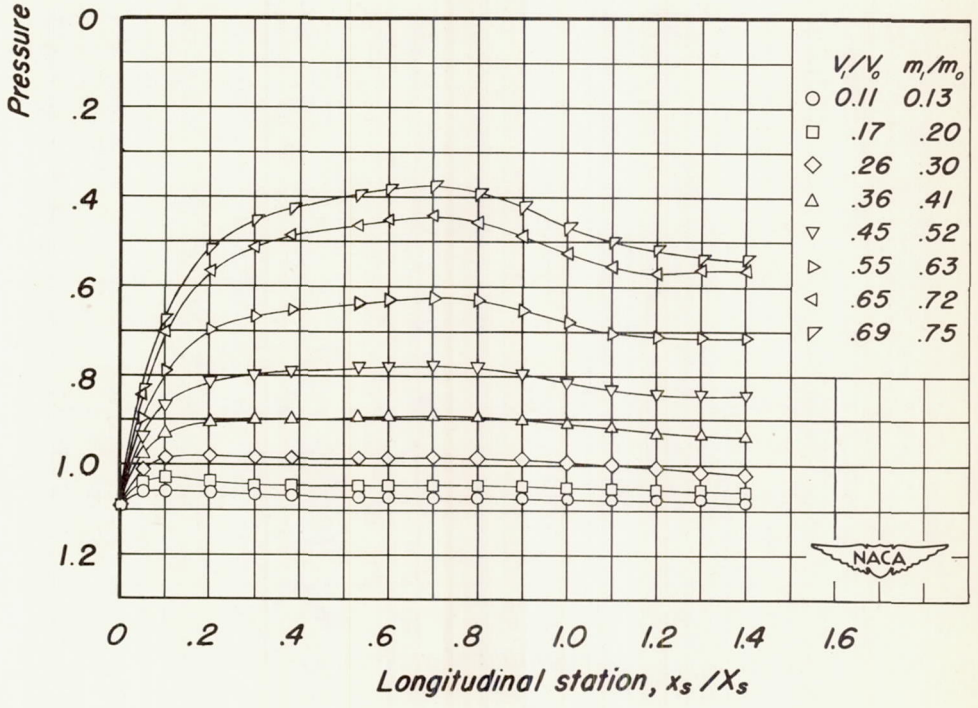

(h) M_o, 0.60

Figure 8.- Continued.

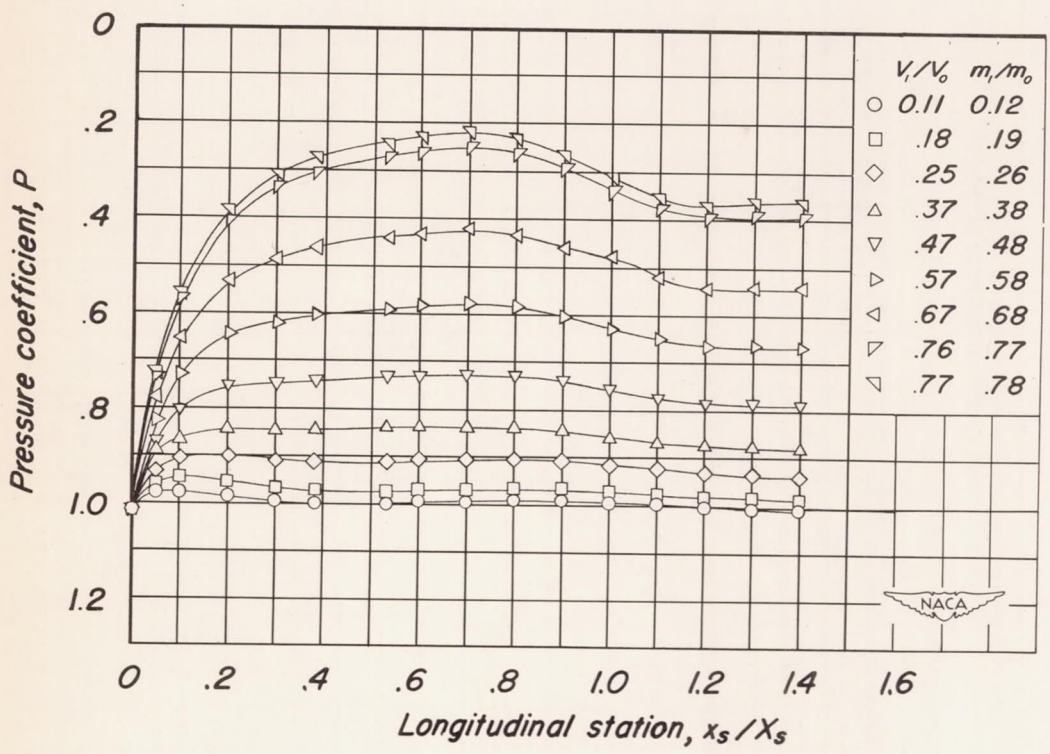

(i) M_o, 0.23

Figure 8.- Concluded.

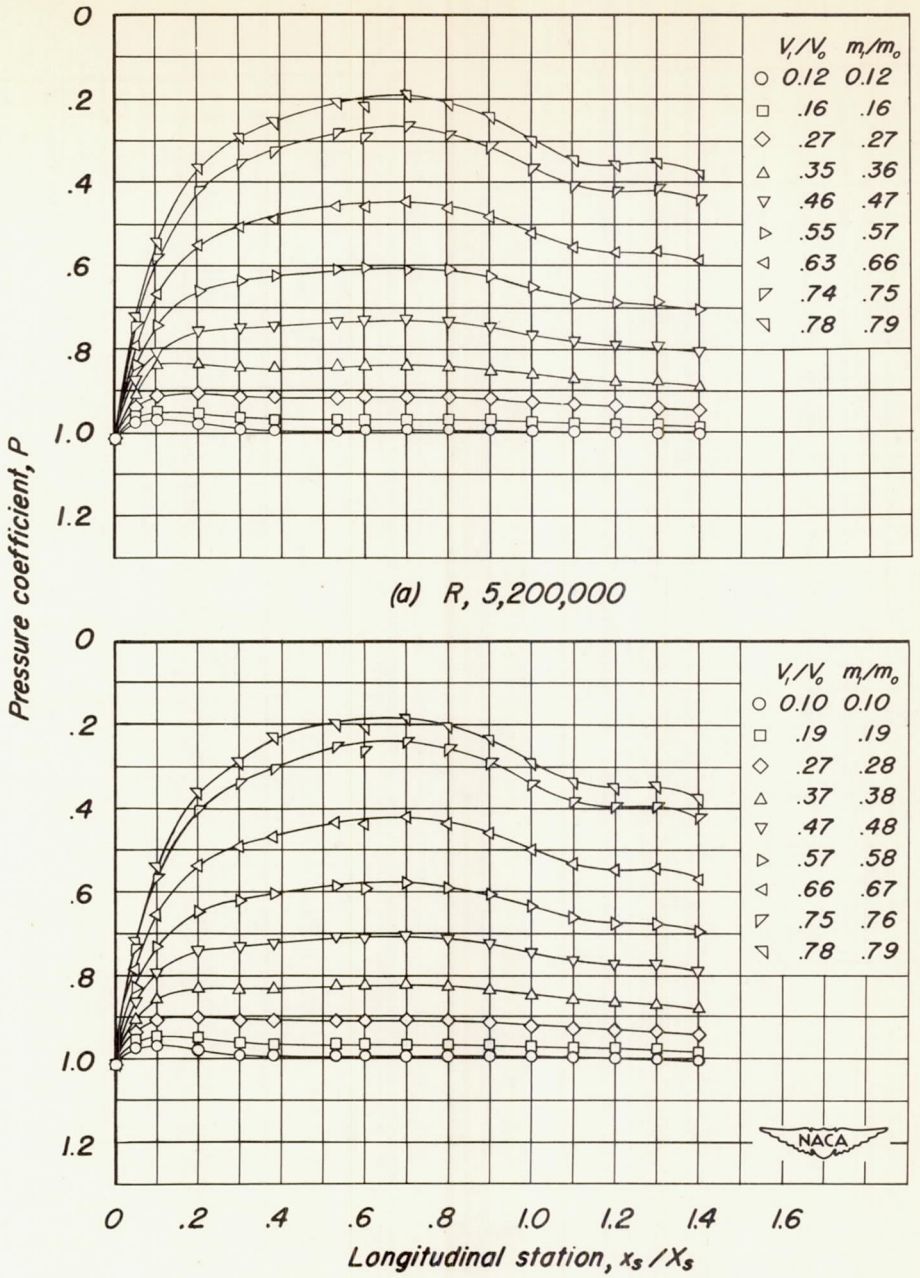

Figure 9.- Distribution of the pressure coefficient over the spinner for Reynolds numbers of 5,200,000 and 8,100,000. M_o, 0.23.

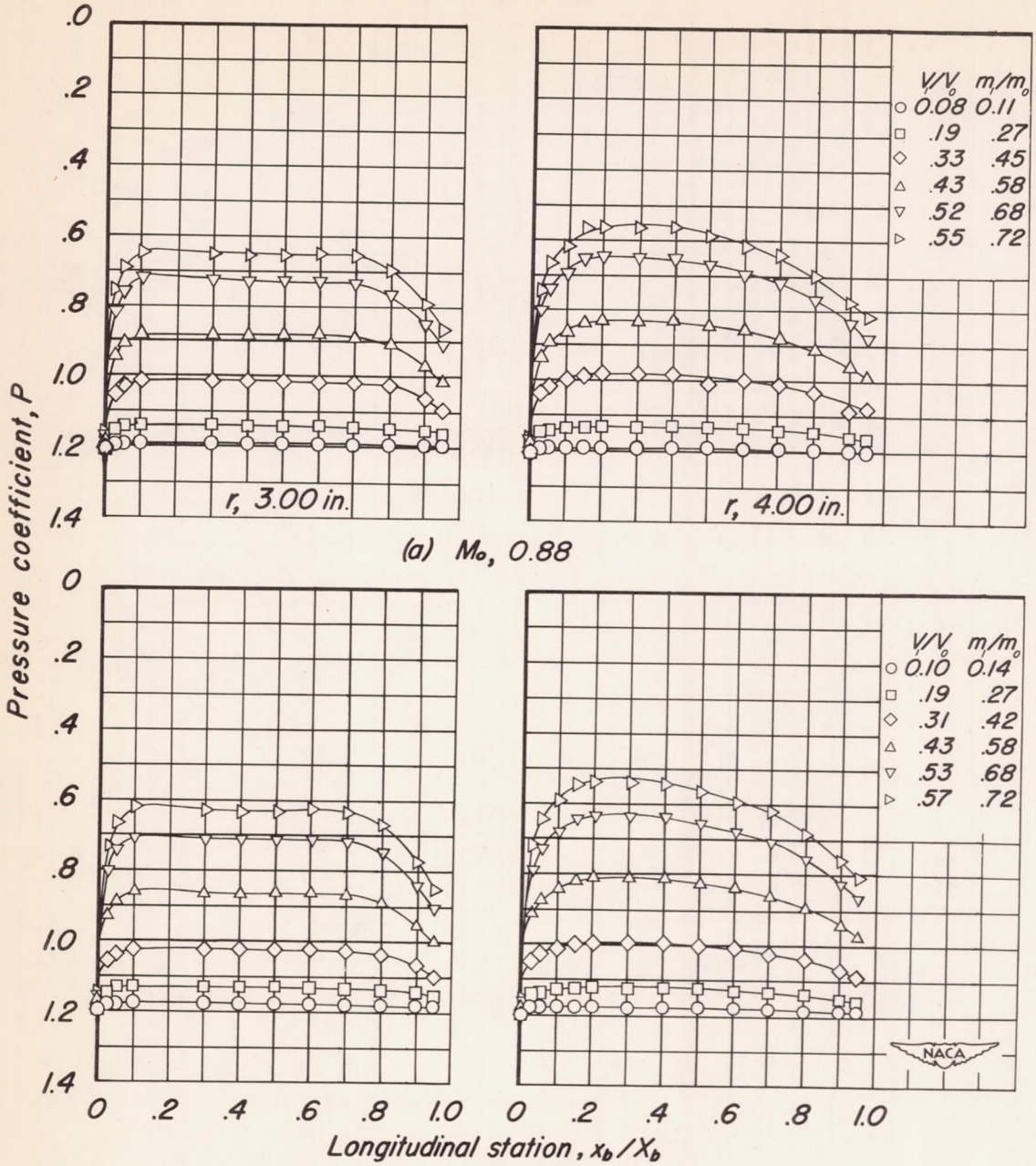

Figure 10.- Distribution of the pressure coefficient over the propeller-blade-shank fairings for various Mach numbers. R, 1,800,000.

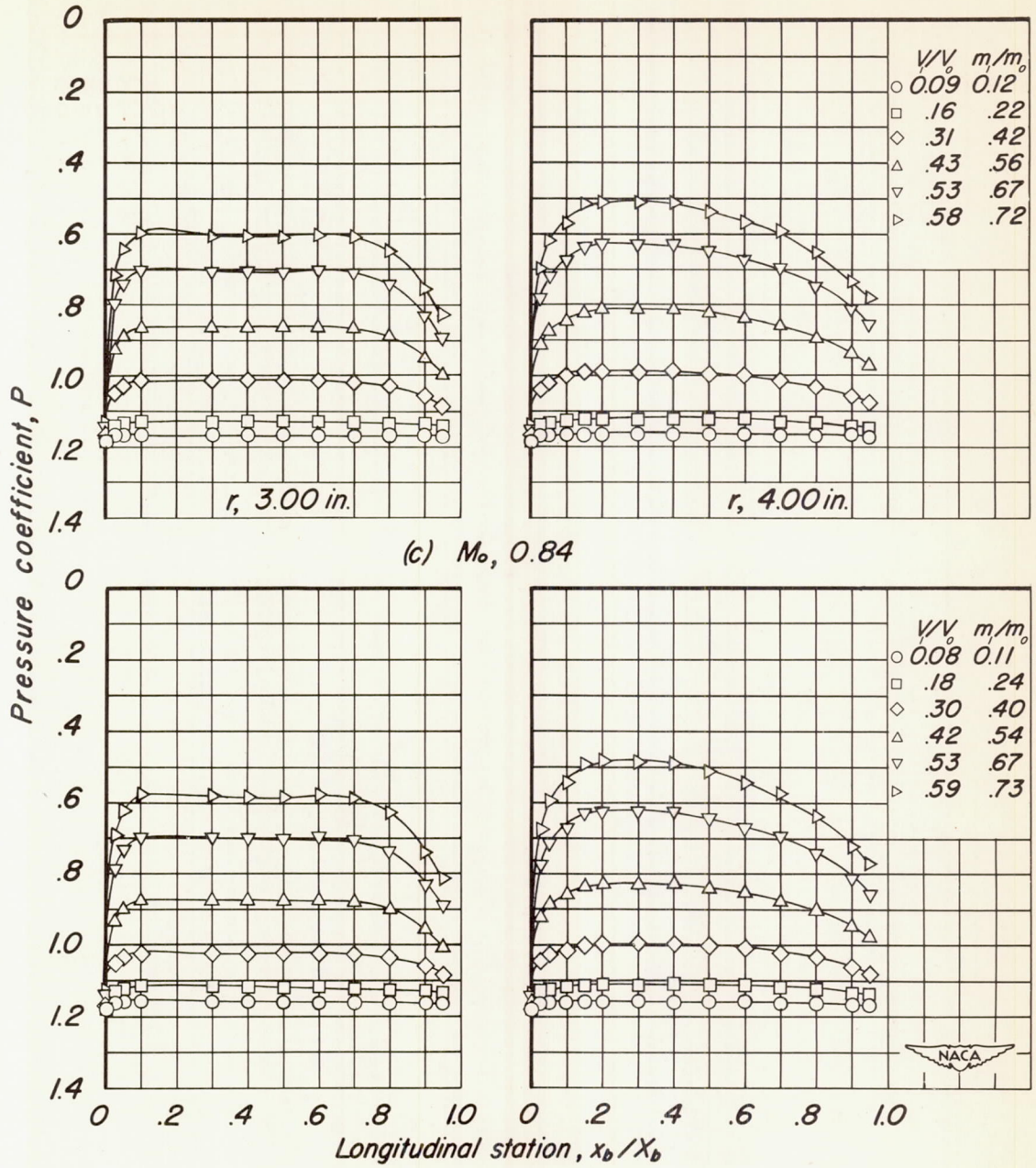

(c) M_o, 0.84

(d) M_o, 0.82

Figure 10.– Continued.

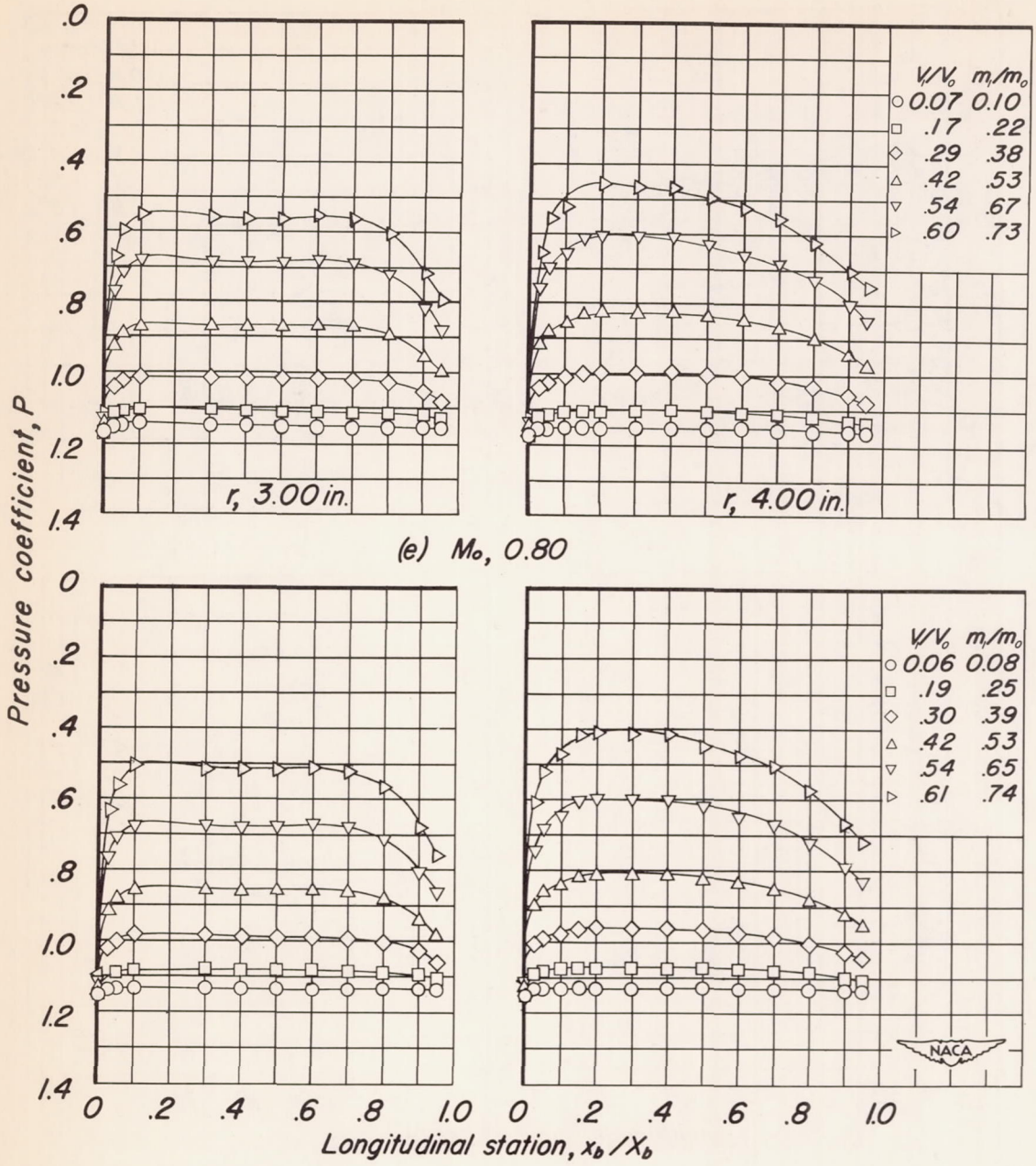

(e) M_0, 0.80

(f) M_0, 0.75

Figure 10.- Continued.

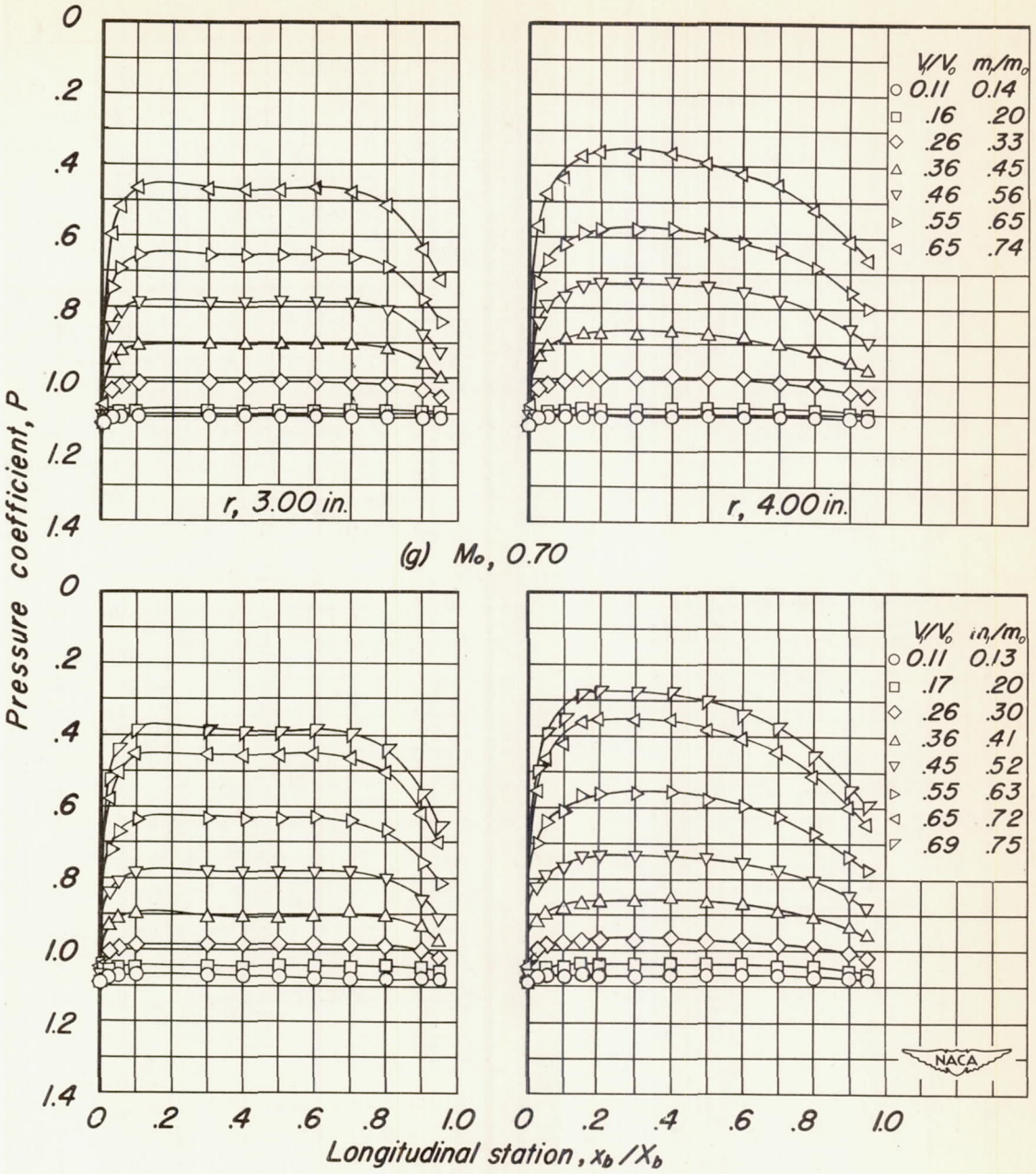

(g) M_0, 0.70

(h) M_0, 0.60

Figure 10.- Continued.

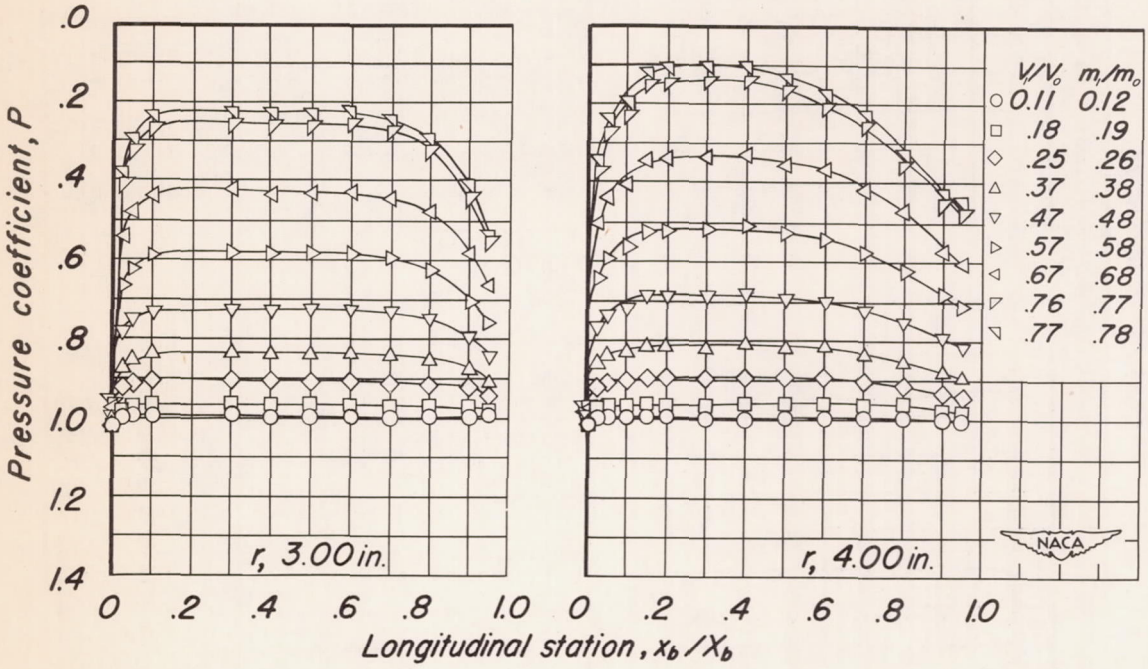

(i) M_0, 0.23

Figure 10.- Concluded.

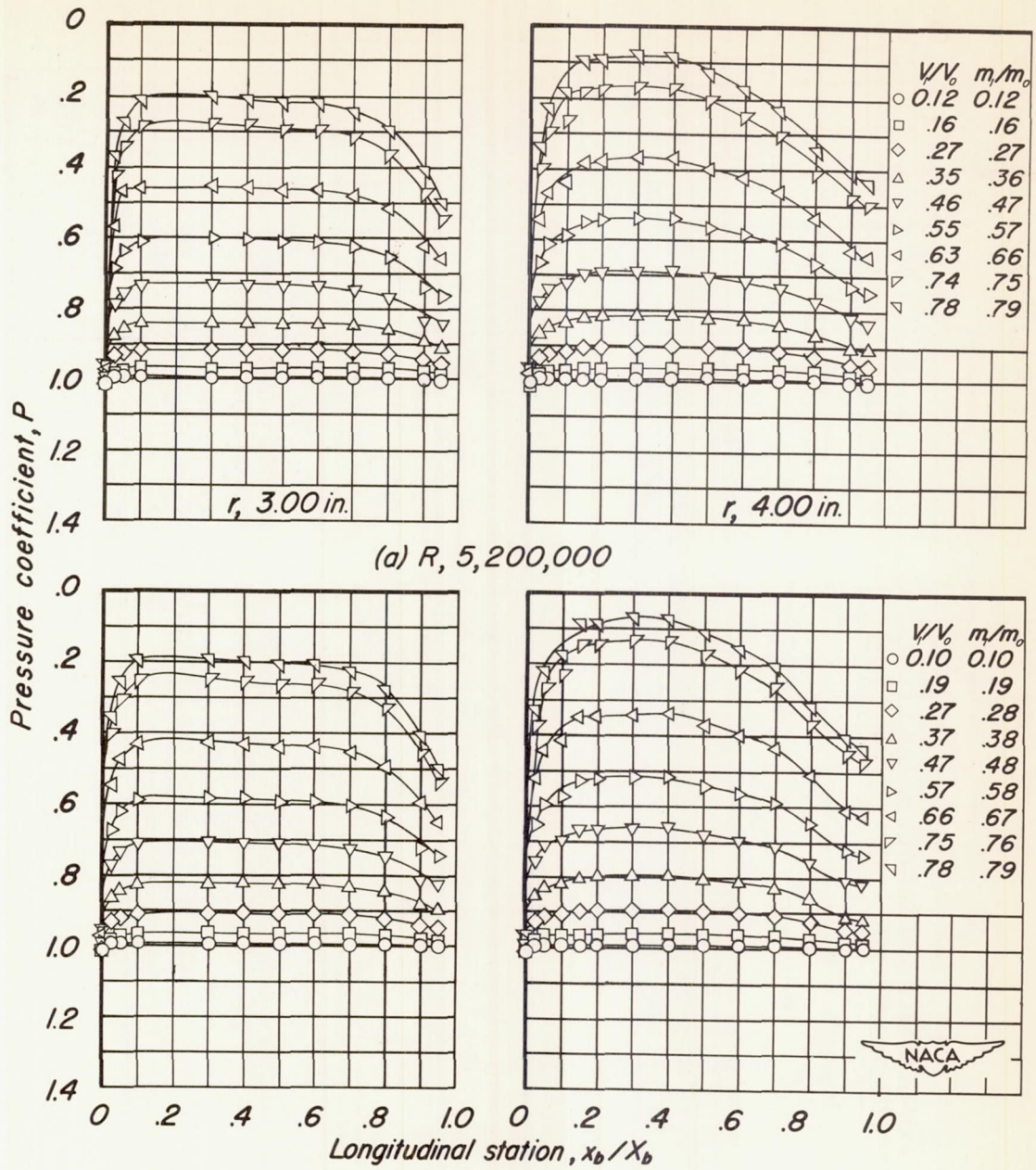

Figure 11.- Distribution of the pressure coefficient over the propeller-blade-shank fairings for Reynolds numbers of 5,200,000 and 8,100,000. M_o, 0.23.

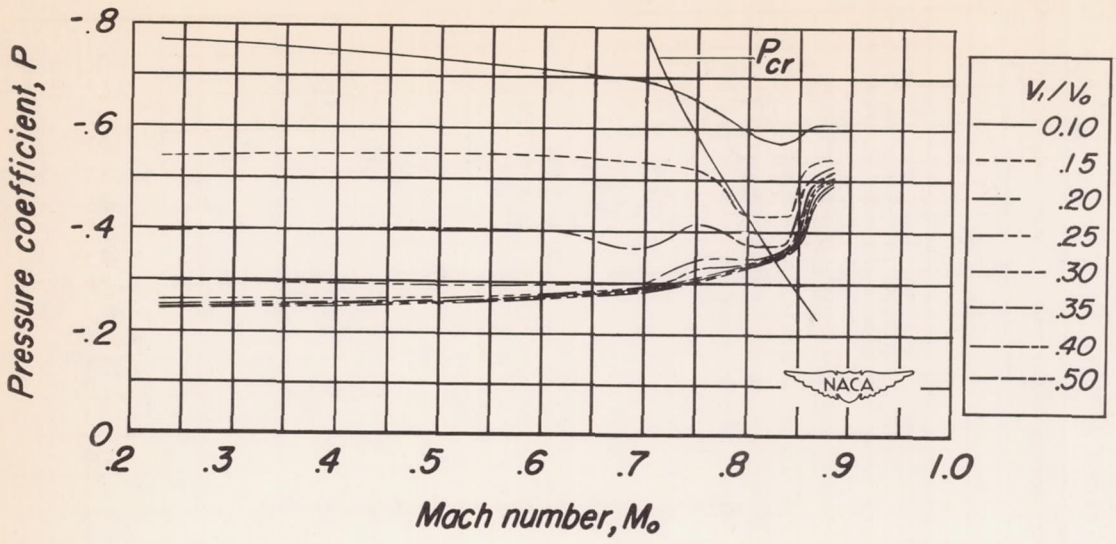

Figure 12.—The variation of minimum pressure coefficient with Mach number. R, 1,800,000.

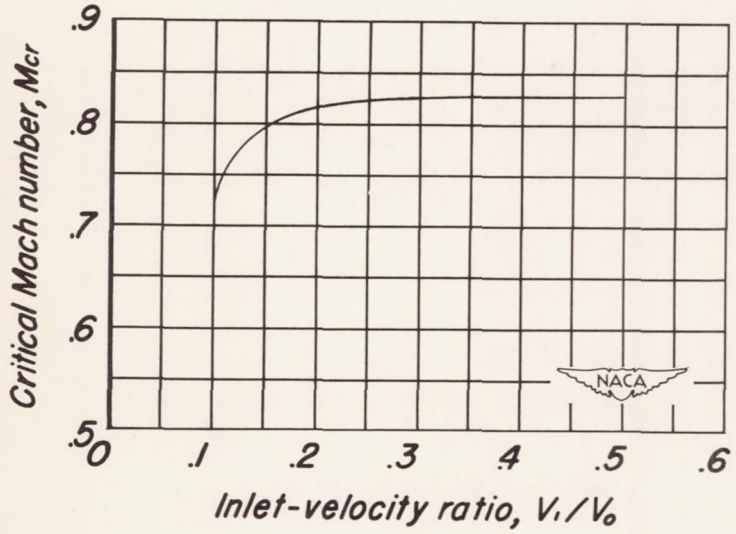

Figure 13.-The variation of critical Mach number with inlet-velocity ratio. R, 1,800,000.

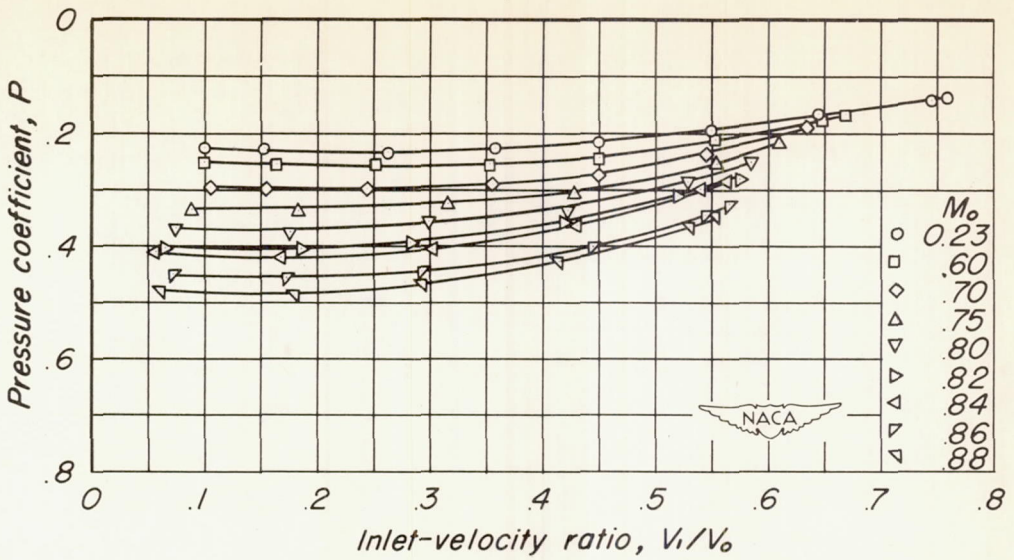

Figure 14.– The variation with inlet-velocity ratio of the average pressure coefficient in the cowl gap (station 2). R, 1,800,000.

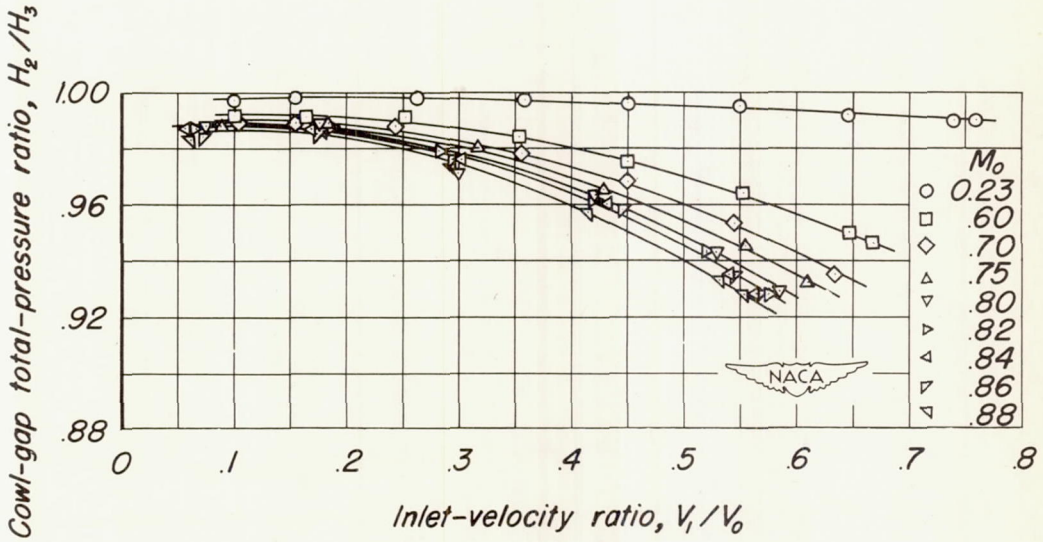

Figure 15 –The variation with inlet-velocity ratio of the cowl-gap total-pressure ratio for various Mach numbers. R, 1,800,000.

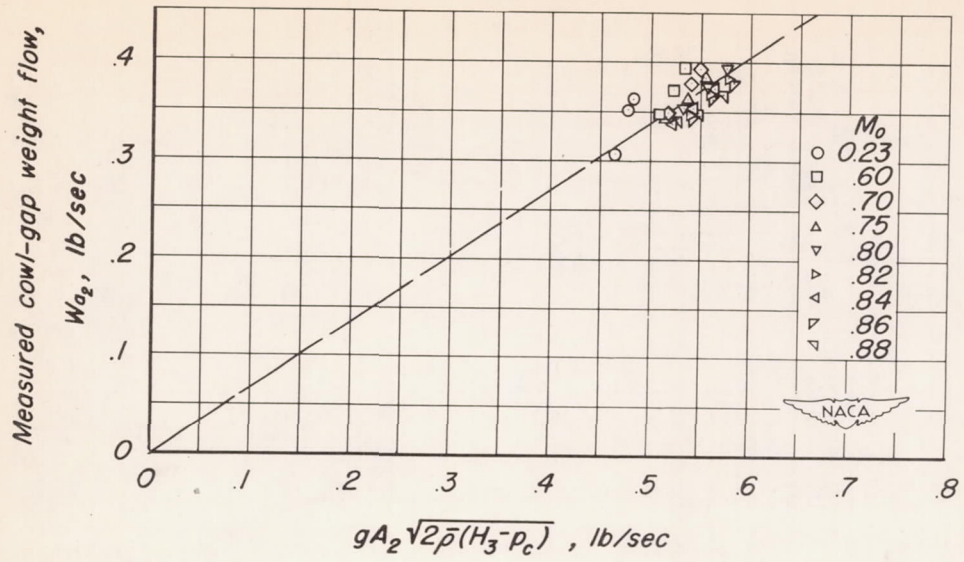

Figure 16.—The variation of the measured cowl-gap weight flow with the function $gA_2\sqrt{2\bar{\rho}(H_3-p_c)}$ for various Mach numbers. R, 1,800,000.

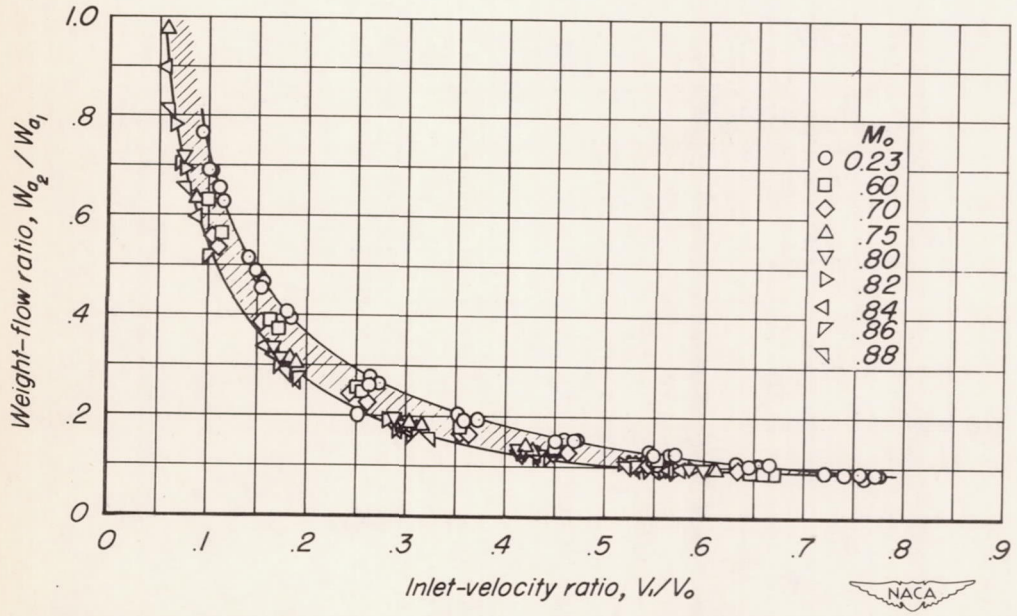

Figure 17.—The variation with inlet-velocity ratio of the ratio of cowl-gap weight flow to inlet weight flow for various Mach numbers. R, 1,800,000.

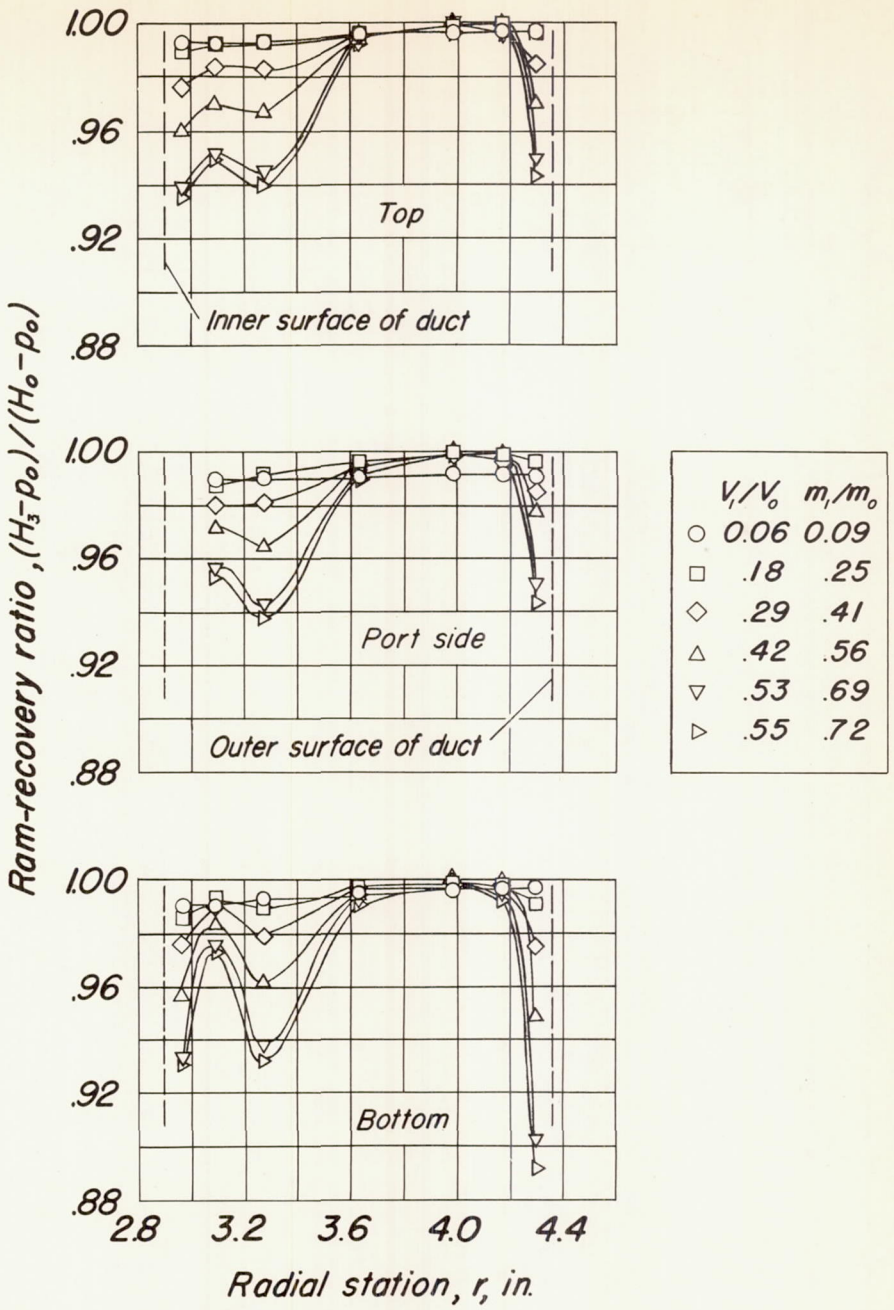

(a) M_o, 0.88

Figure 18.–The radial variation of ram-recovery ratio at station 3 for Mach numbers of 0.88, 0.80 and 0.23. R, 1,800,000.

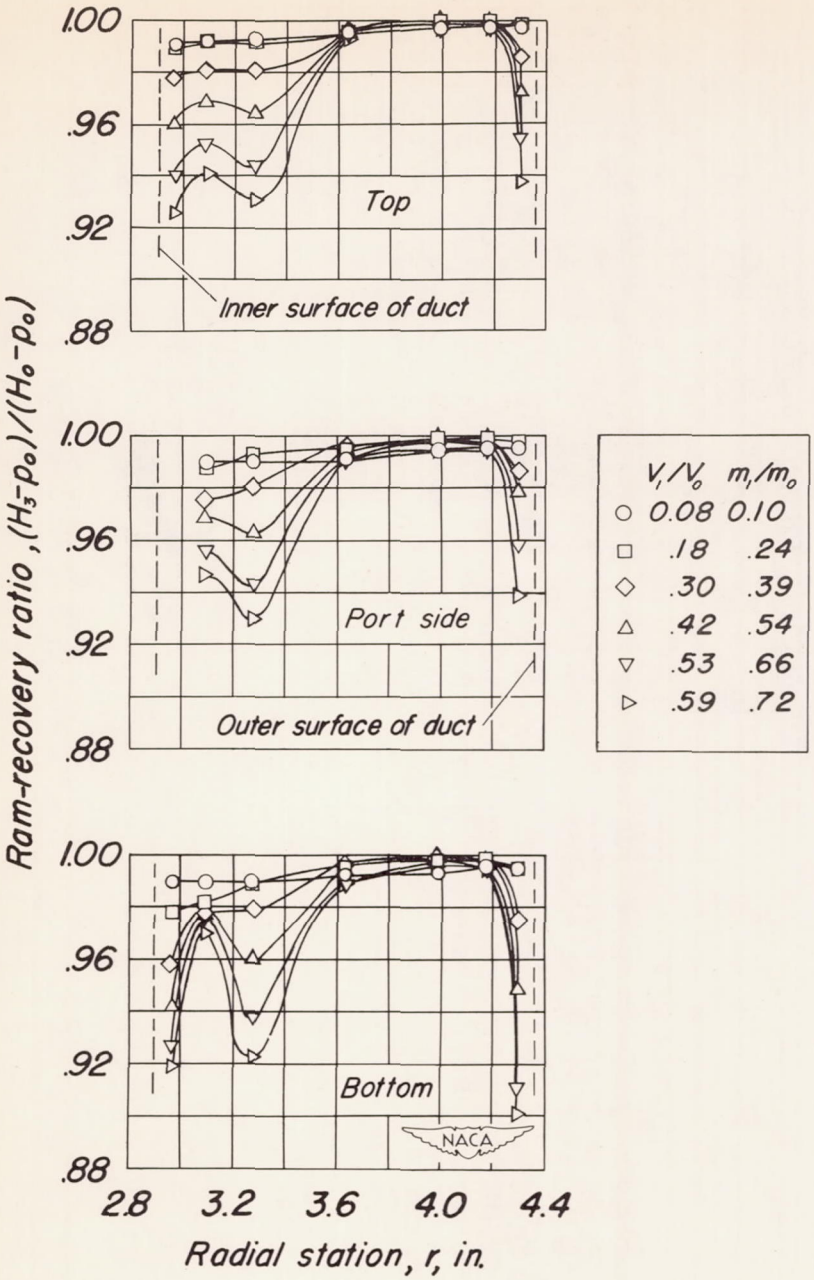

(b) M_o, 0.80

Figure 18.- Continued.

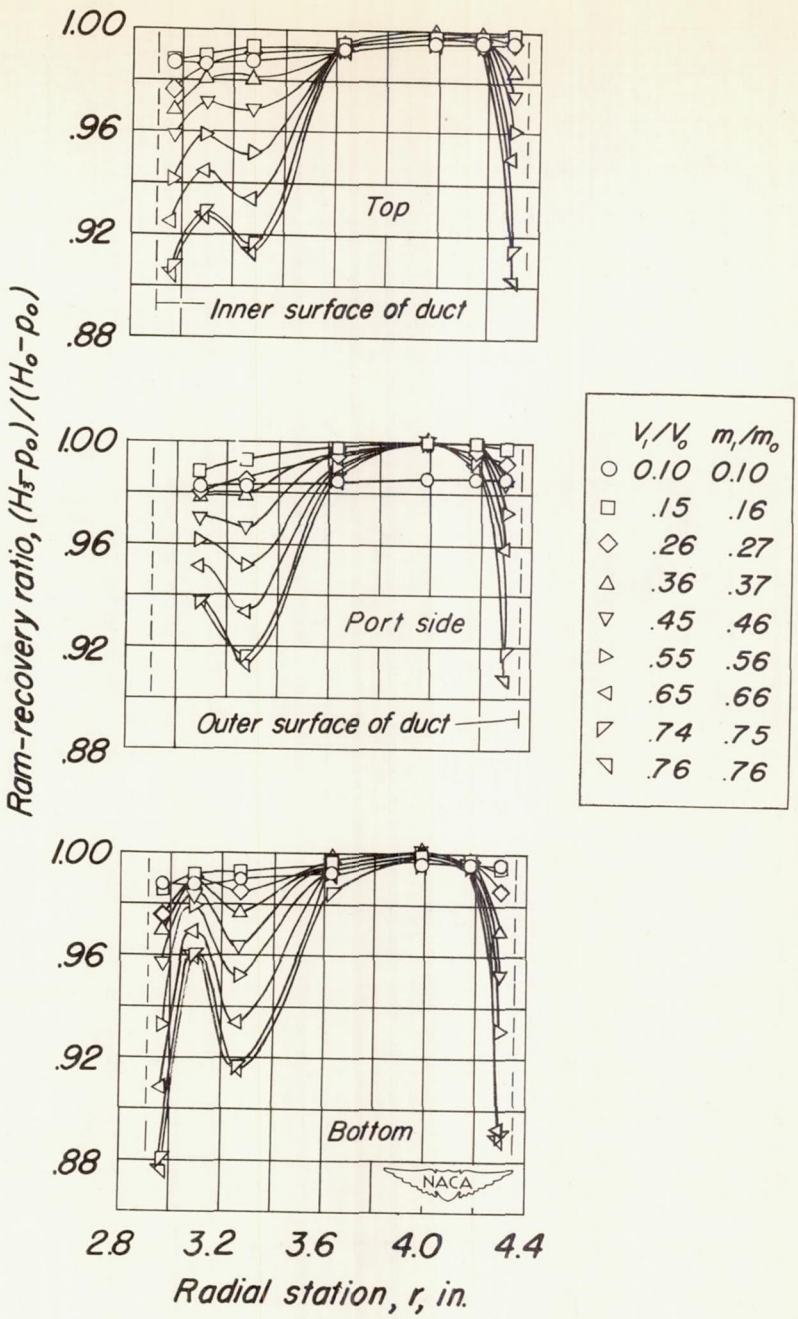

(c) M_o, 0.23

Figure 18.- Concluded.

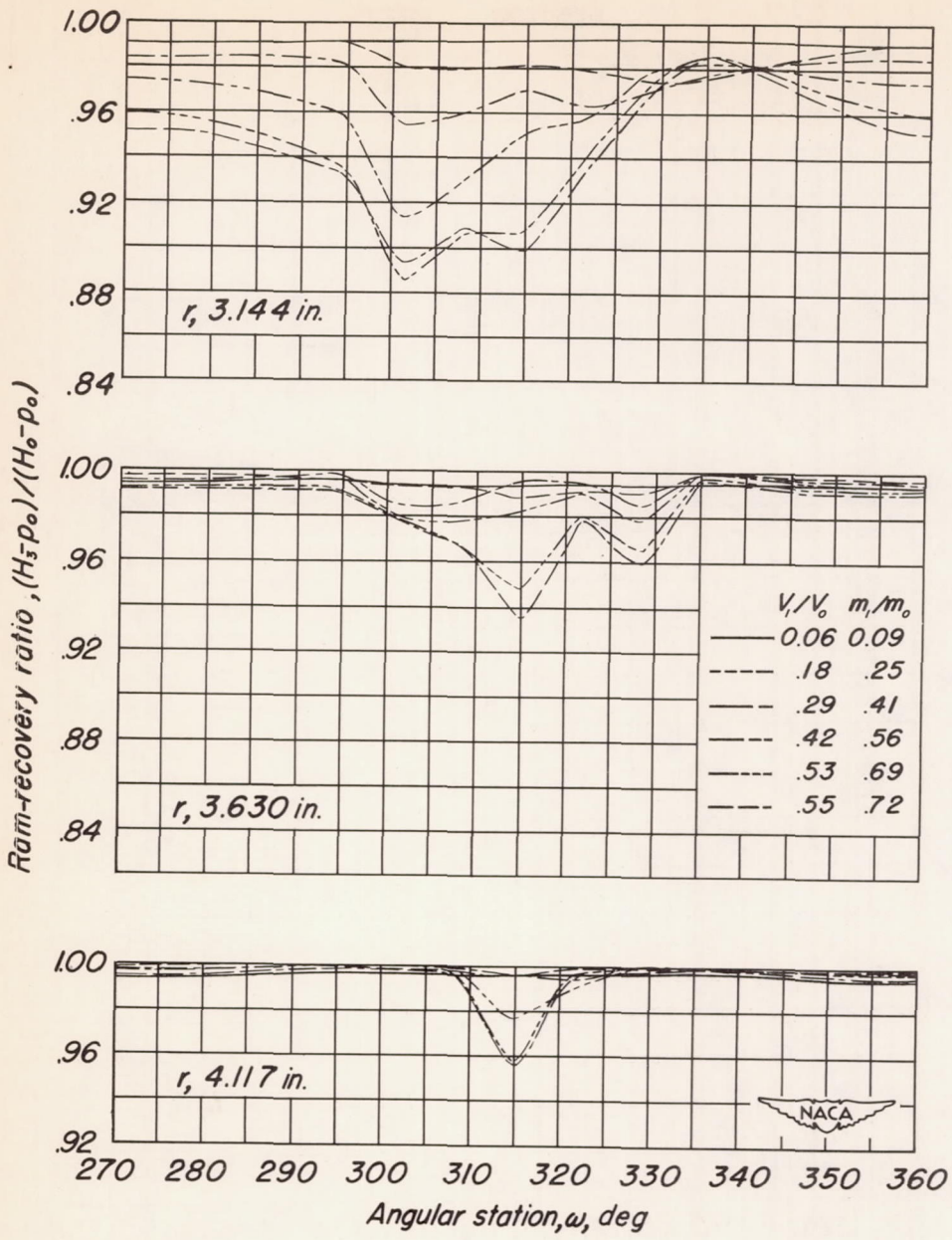

(a) M_0, 0.88

Figure 19.—The variation with angular station in one quadrant of the ram-recovery ratio at station 3 for Mach numbers of 0.88, 0.80 and 0.23. R, 1,800,000.

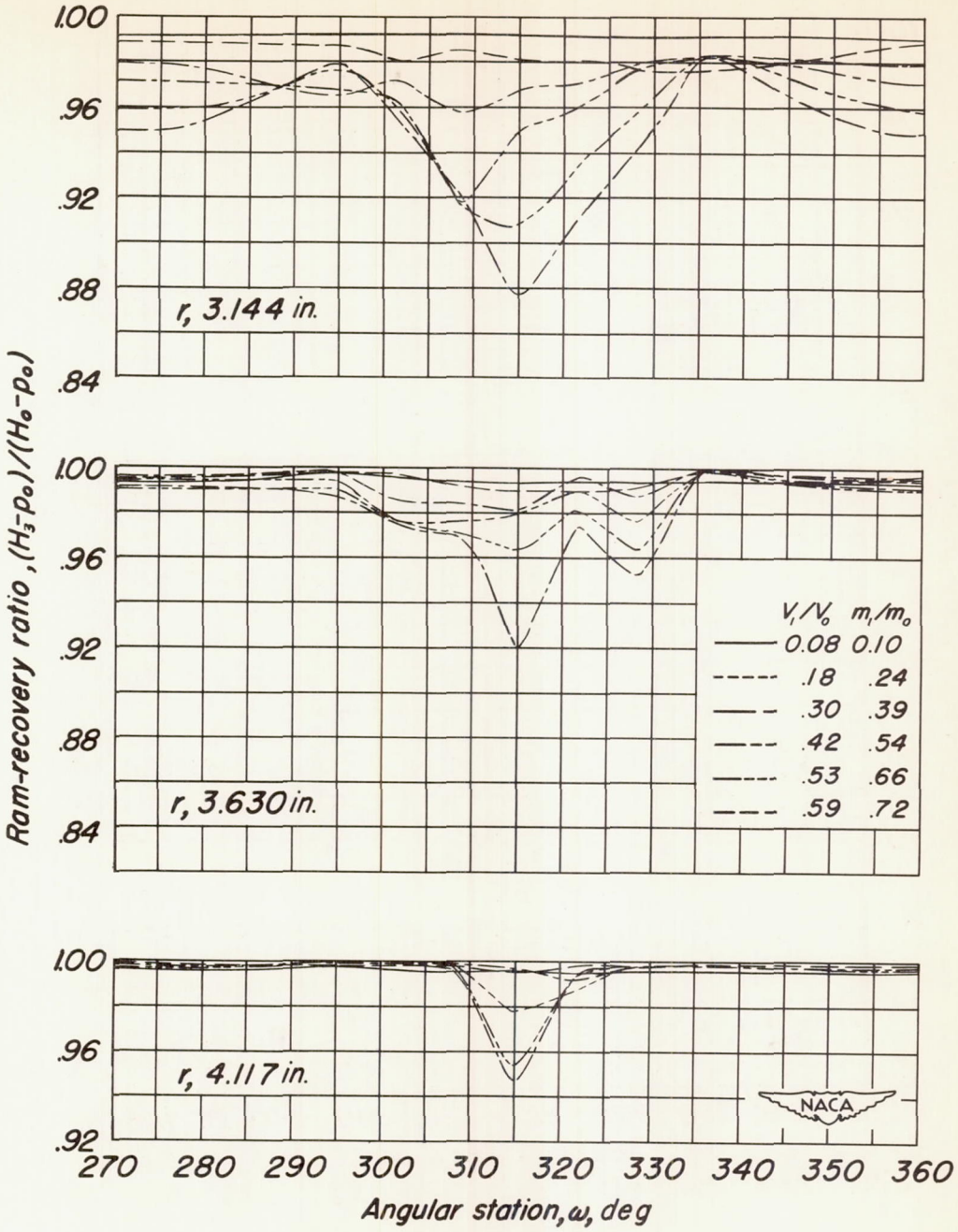

(b) M_o, 0.80

Figure 19.- Continued.

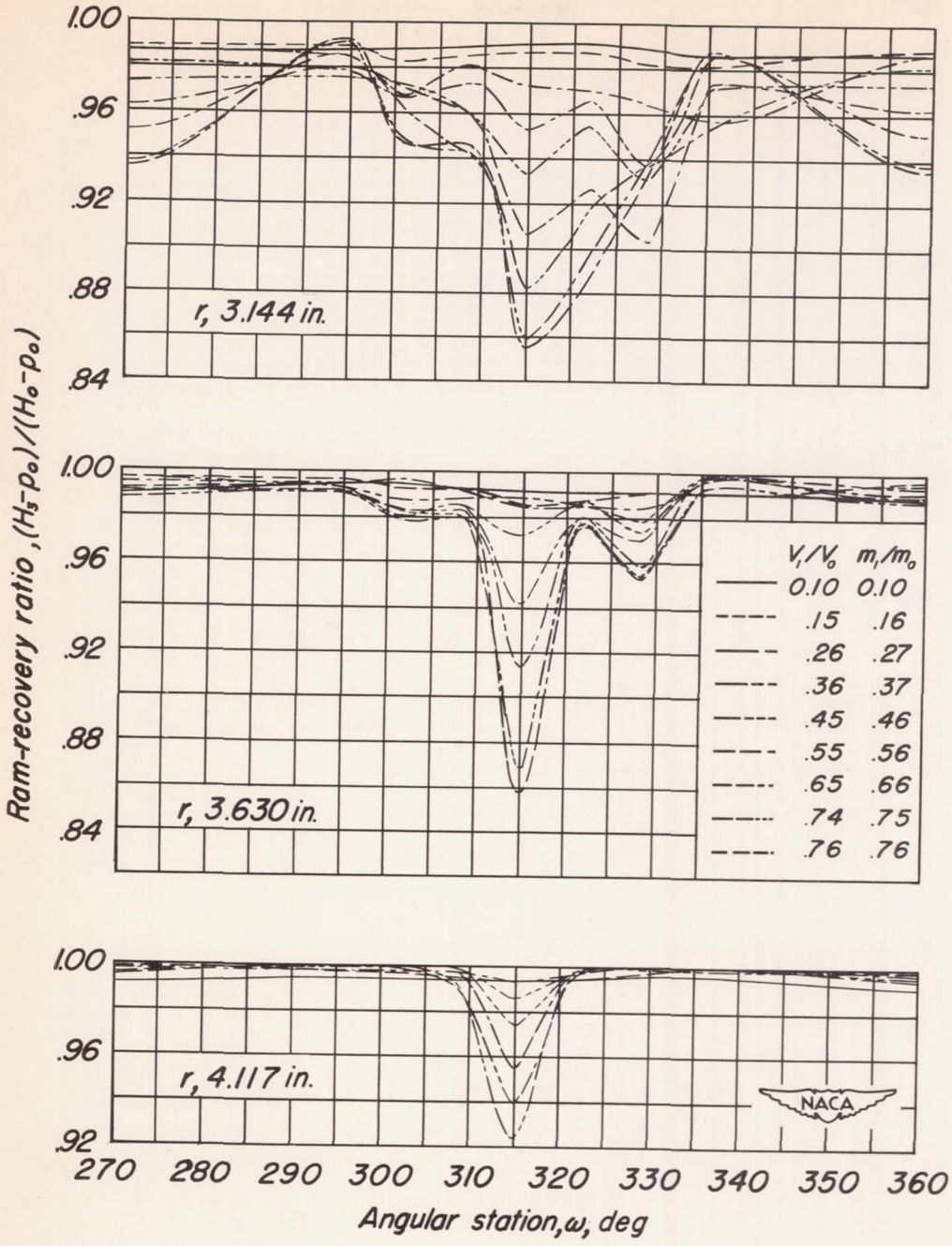

(c) M_o, 0.23.

Figure 19.- Concluded.

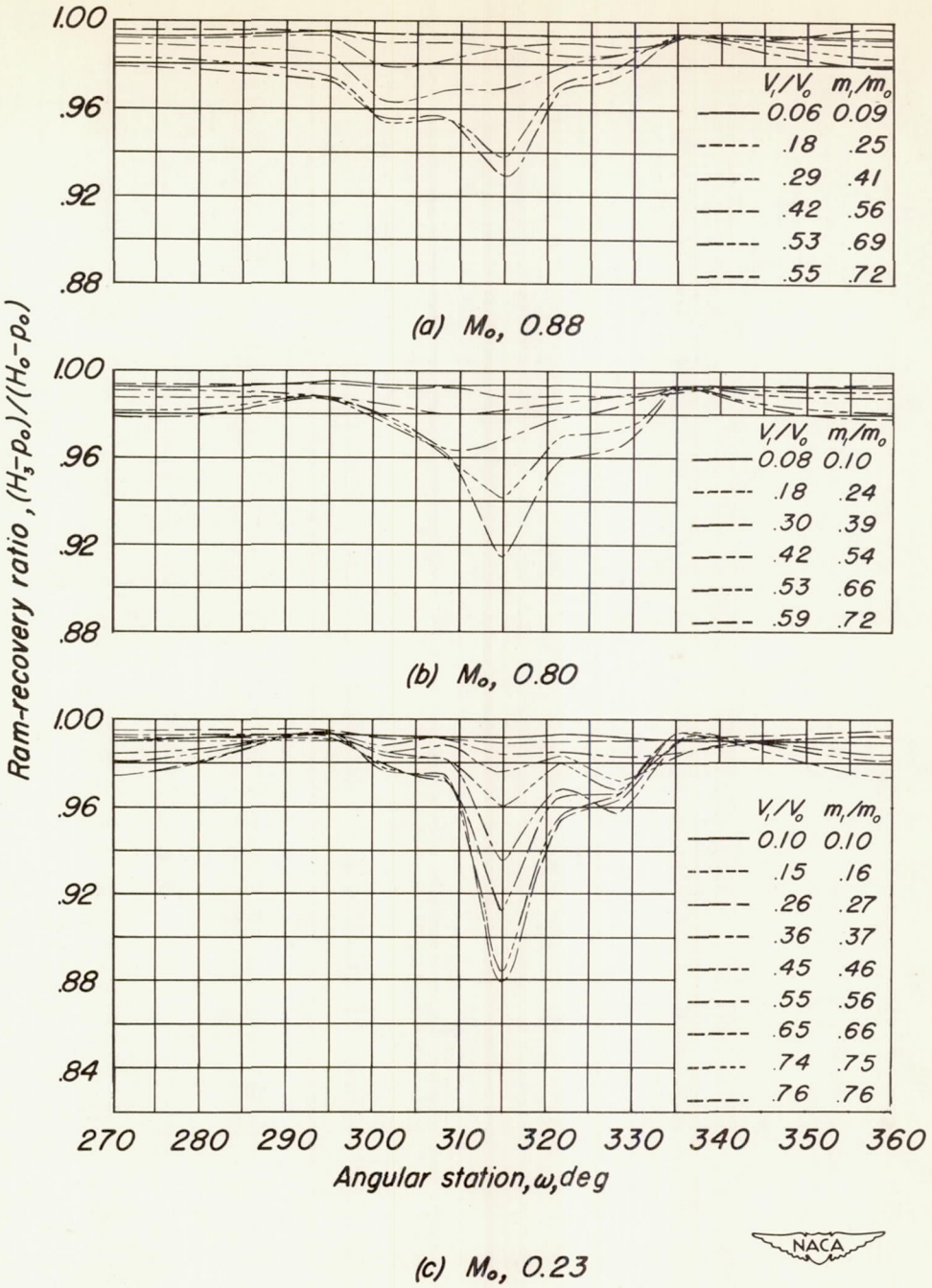

Figure 20.-The variation with angular station in one quadrant of the average ram-recovery ratio at station 3 for Mach numbers of 0.88, 0.80, and 0.23. R, 1,800,000.

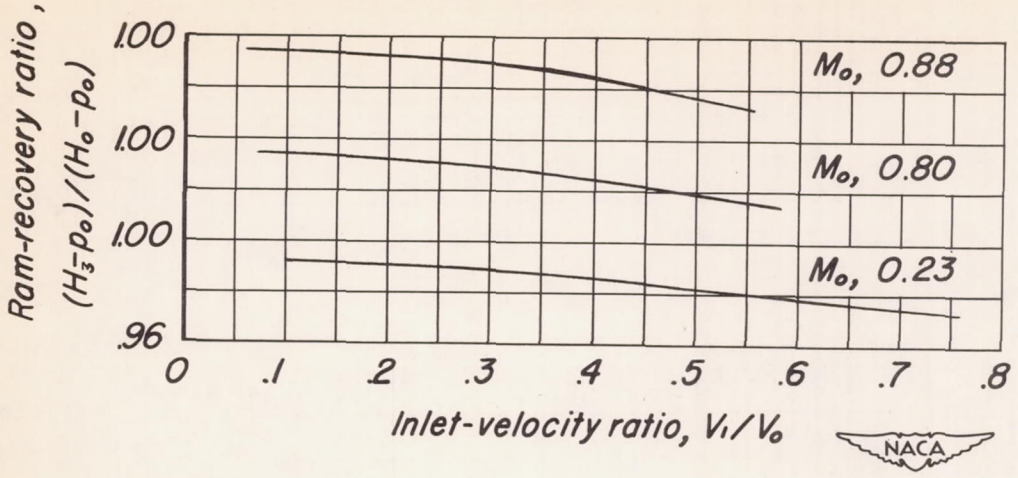

Figure 21.-The variation of the ram-recovery ratio at station 3 with inlet-velocity ratio for Mach numbers of 0.88, 0.80 and 0.23. R, 1,800,000.

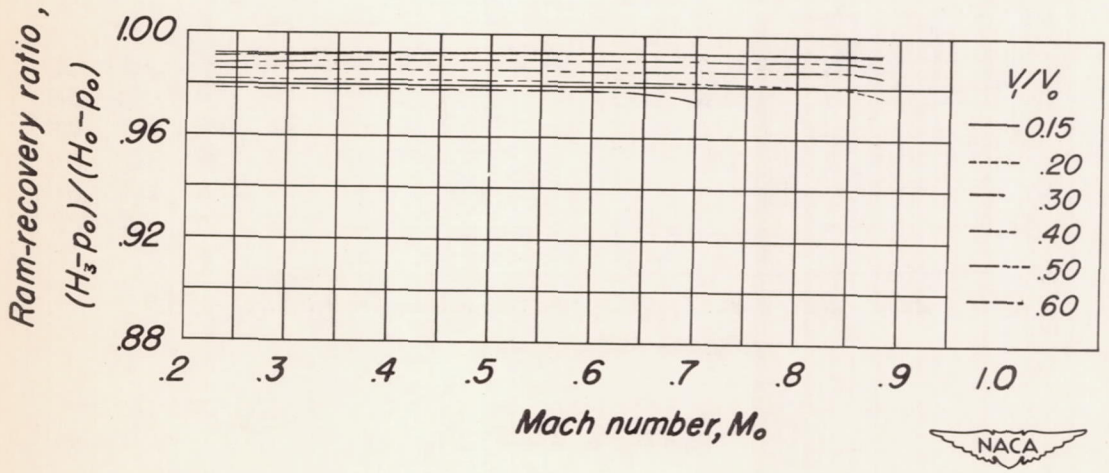

Figure 22.—The variation with Mach number of the ram-recovery ratio at station 3. R, 1,800,000.

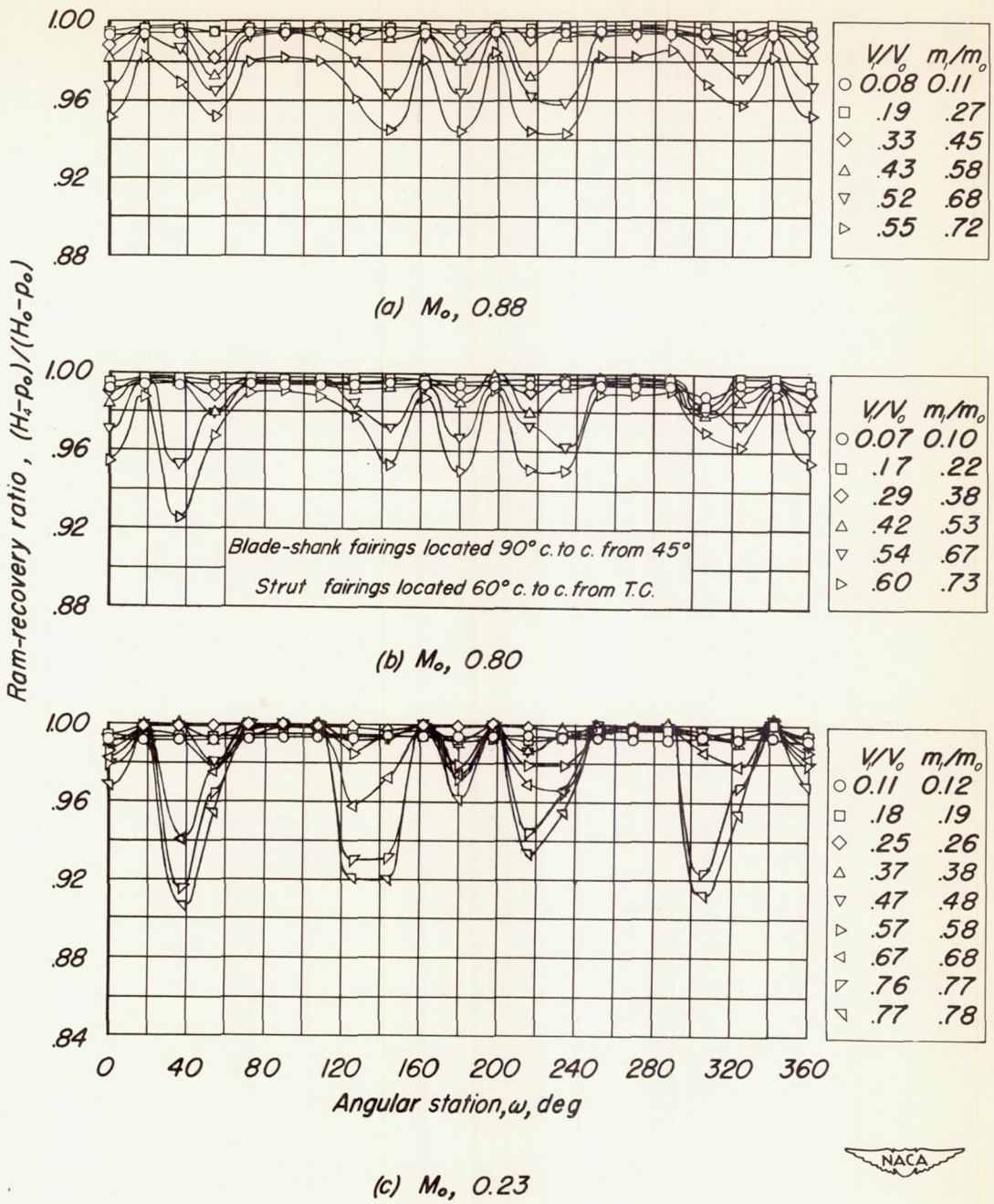

Figure 23.–The typical variation of ram-recovery ratio (r, 2.781) with angular station at the compressor inlet (station 4) for Mach numbers of 0.88, 0.80 and 0.23. R, 1,800,000.

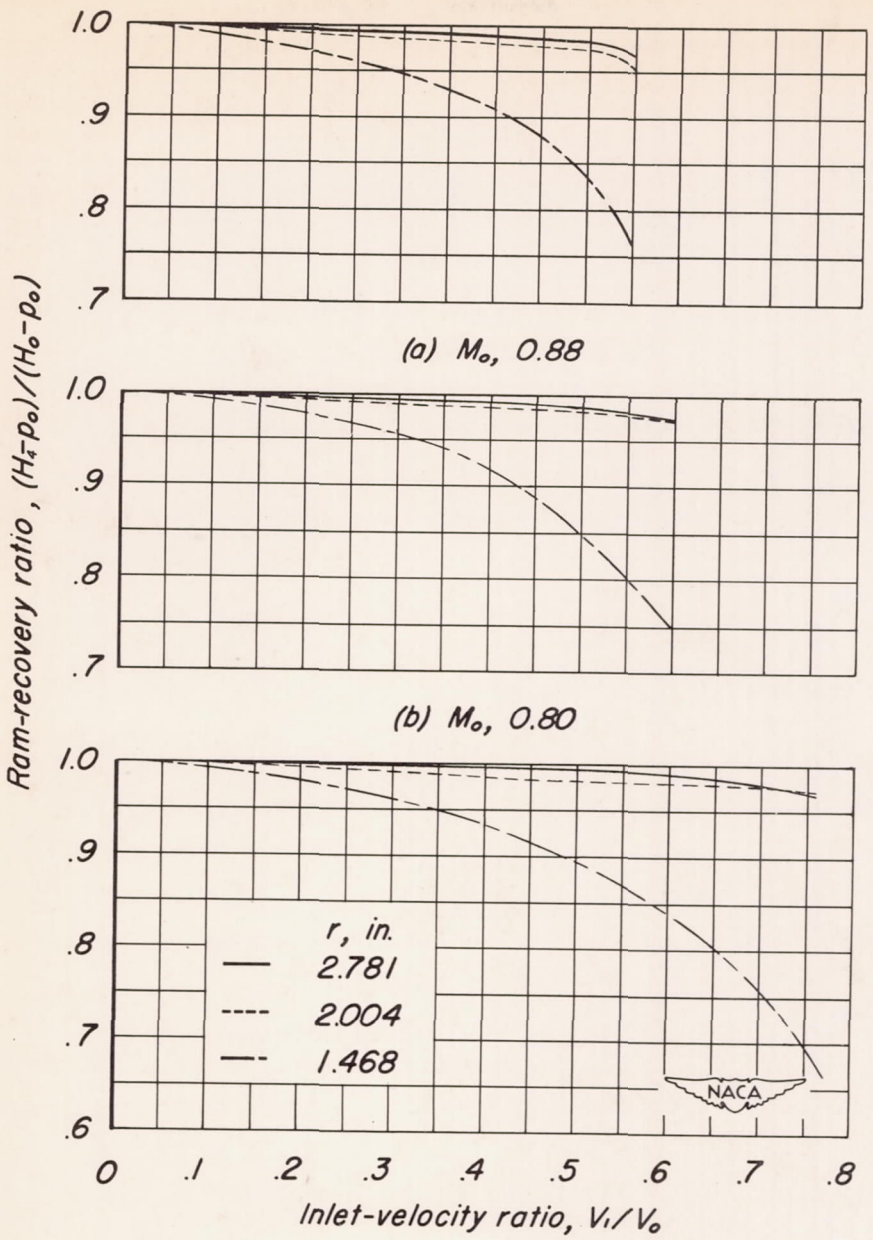

Figure 24.—The variation with inlet-velocity ratio of the ram-recovery ratio at the compressor inlet (station 4) for Mach numbers of 0.88, 0.80 and 0.23. R, 1,800,000.

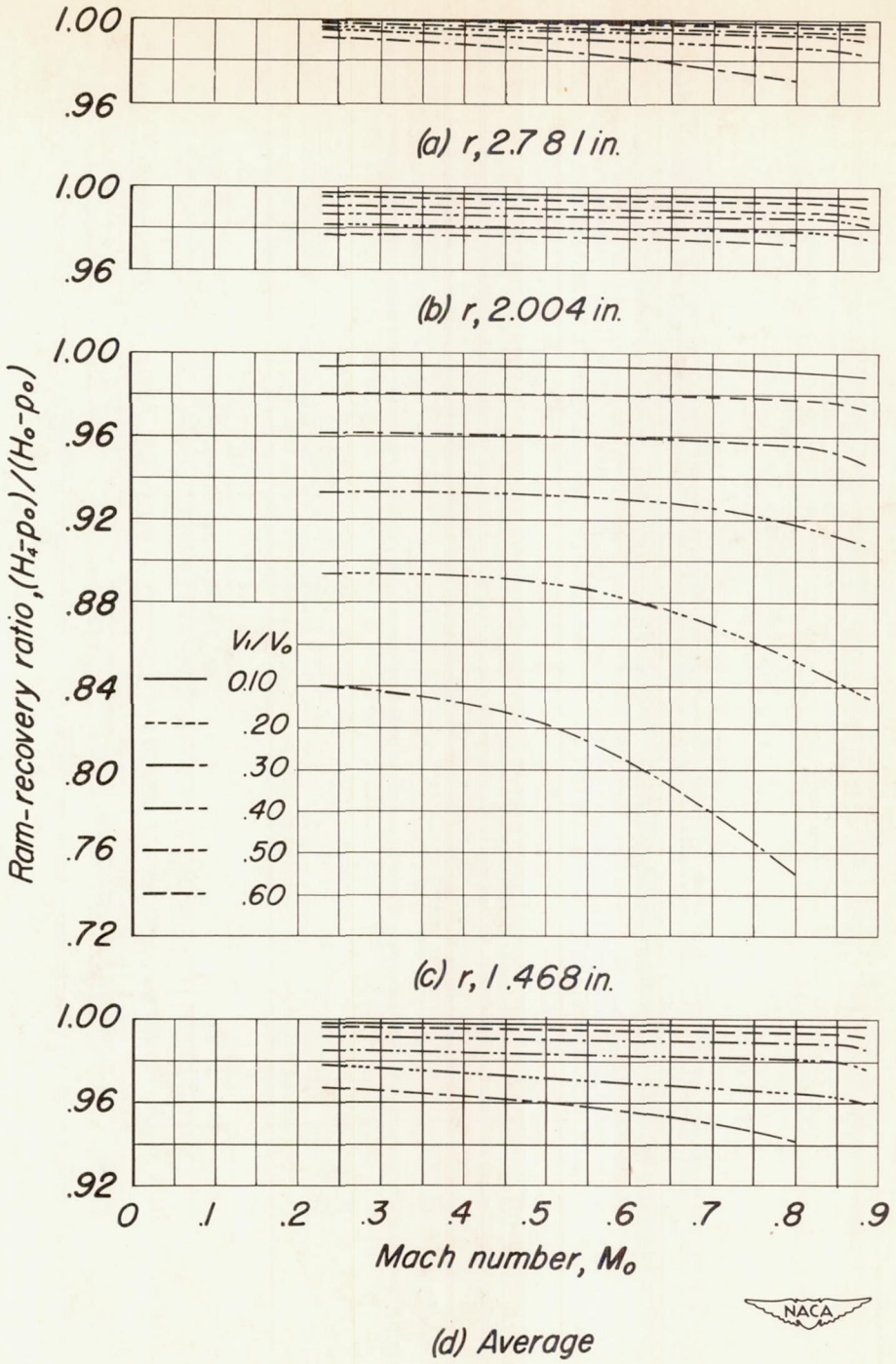

Figure 25.-The variation with Mach number of the ram-recovery ratio at the compressor inlet (station 4). R, 1,800,000.

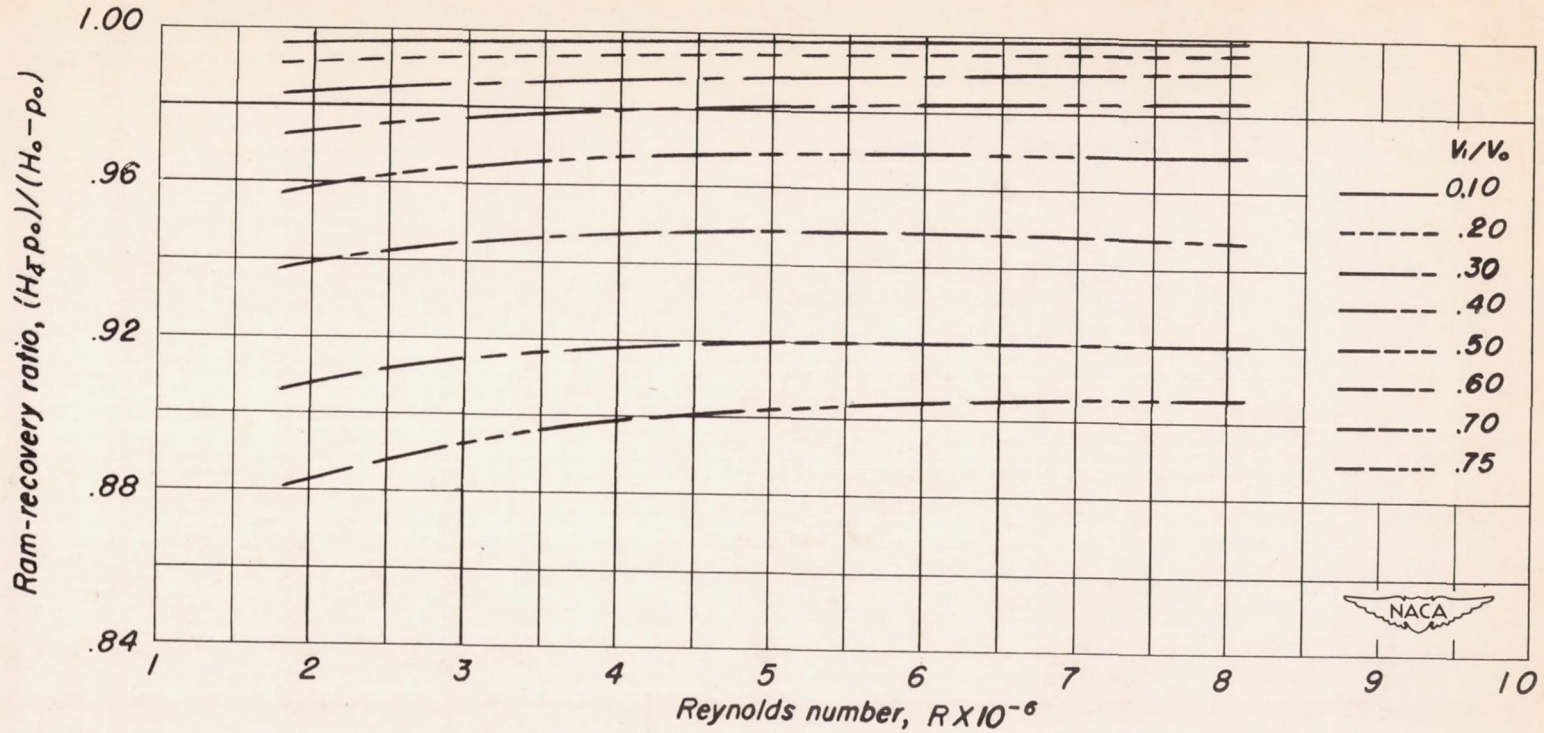

Figure 26.- The variation with Reynolds number of the average ram-recovery ratio at the compressor inlet (station 4). M_0, 0.23.

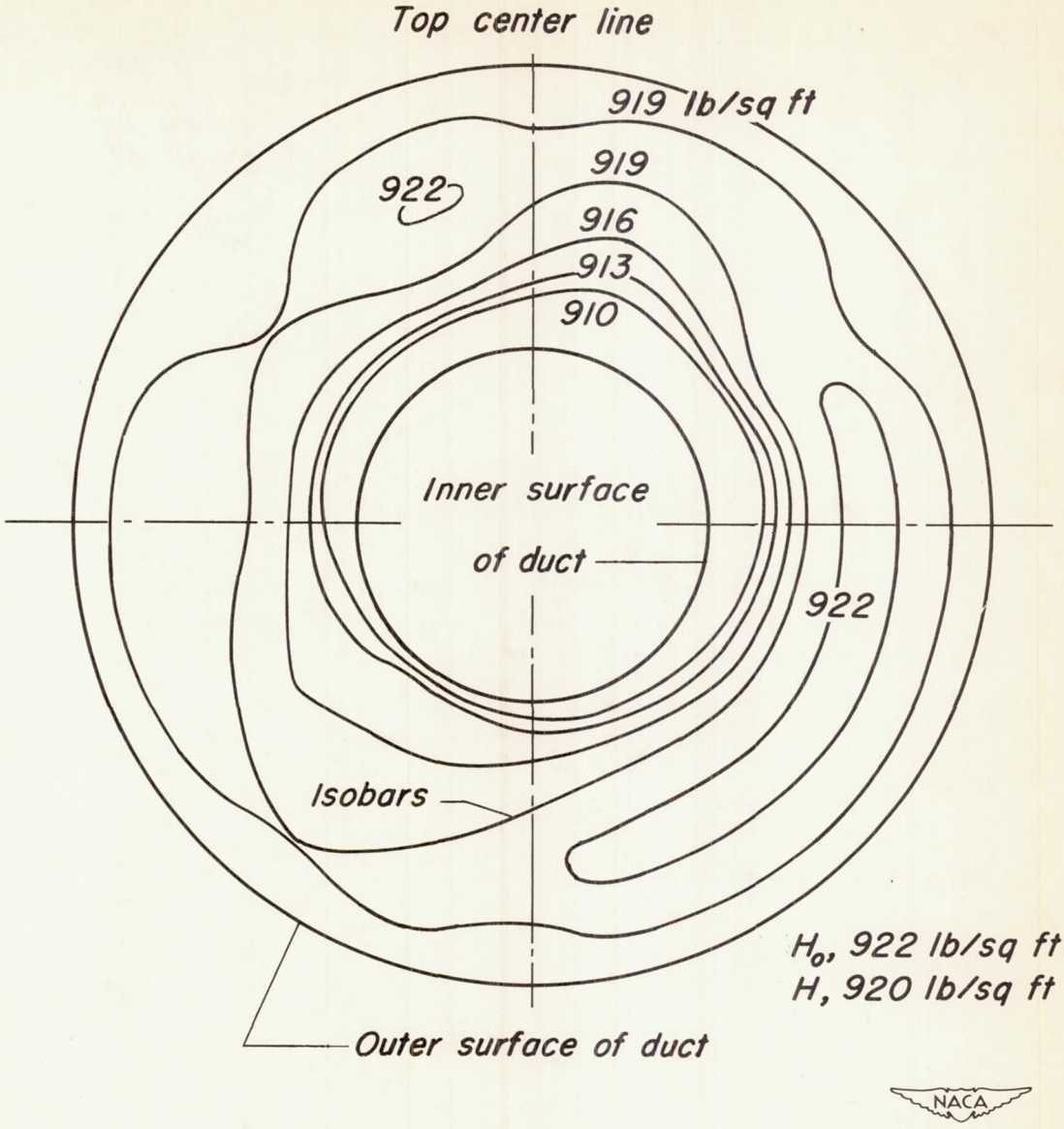

Figure 27.-The variation of the total pressure at the compressor inlet (station 4) for a Mach number of 0.80 and an inlet-velocity ratio of 0.29. R, 1,800,000.

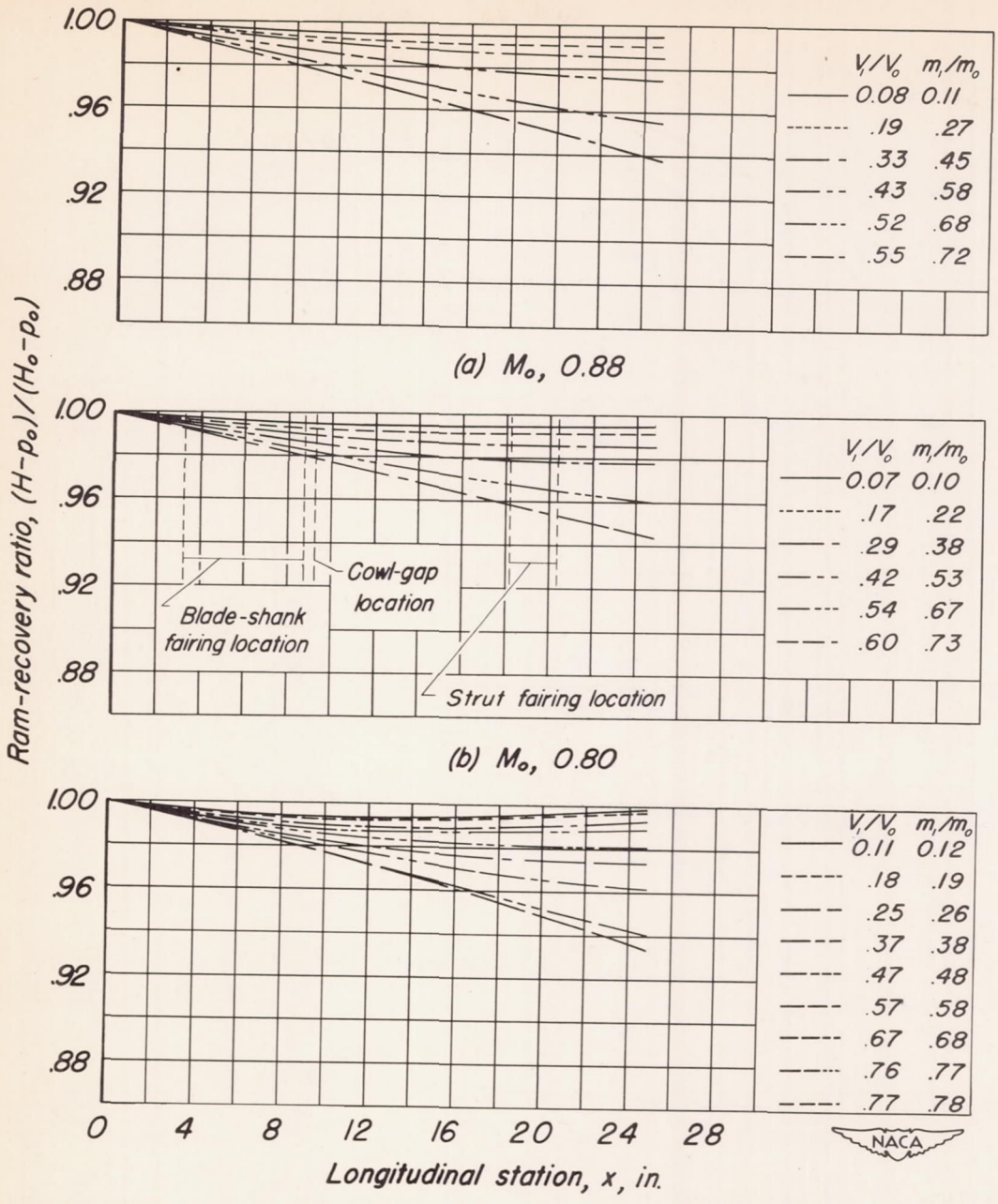

Figure 28.—The trend of the average ram-recovery ratio with longitudinal station for Mach numbers of 0.88, 0.80 and 0.23. R, 1,800,000.

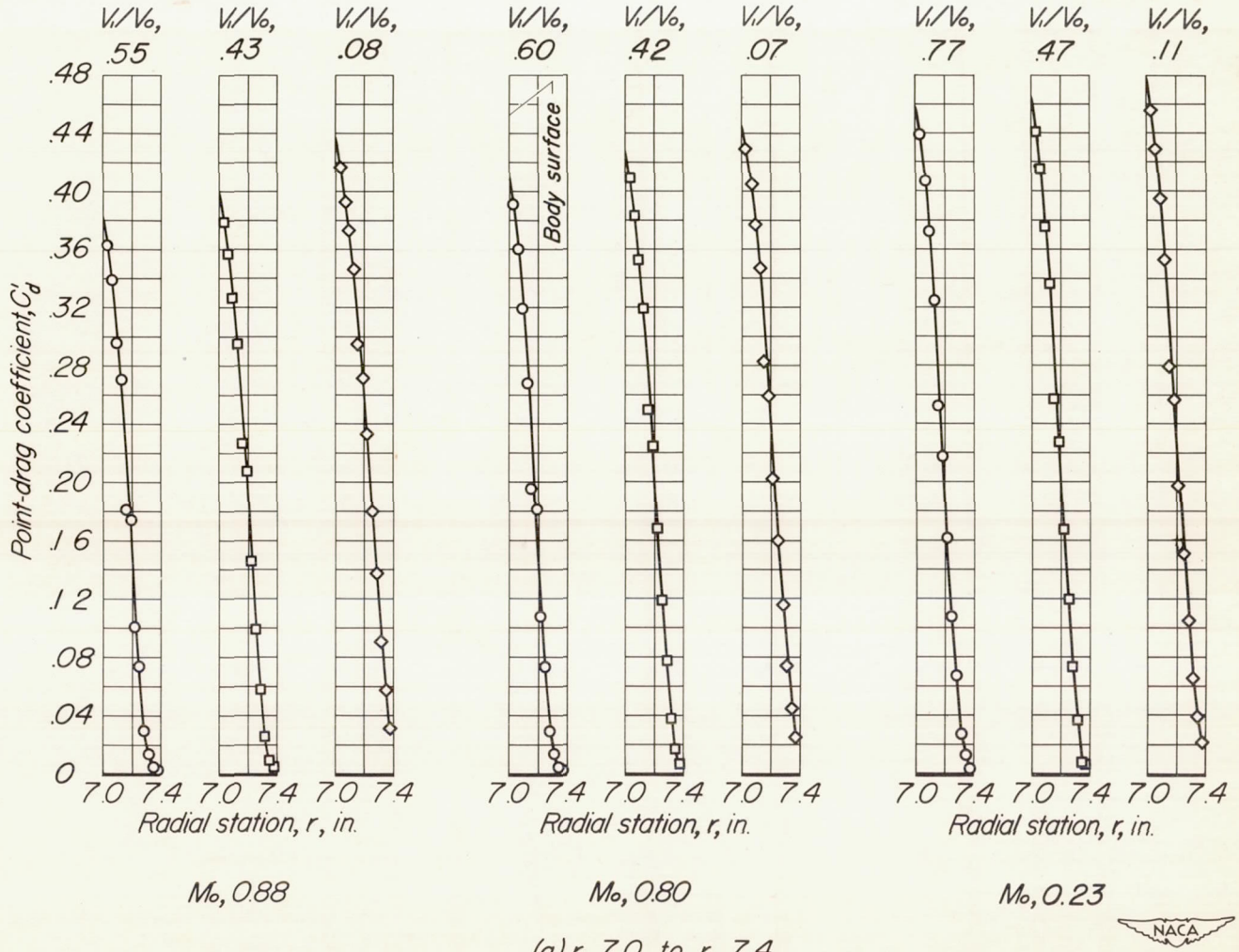

(a) r, 7.0 to r, 7.4

Figure 29.-The typical radial variation of the point-drag coefficient in the wake of the cowl for Mach numbers of 0.88, 0.80 and 0.23. R, 1,800,000.

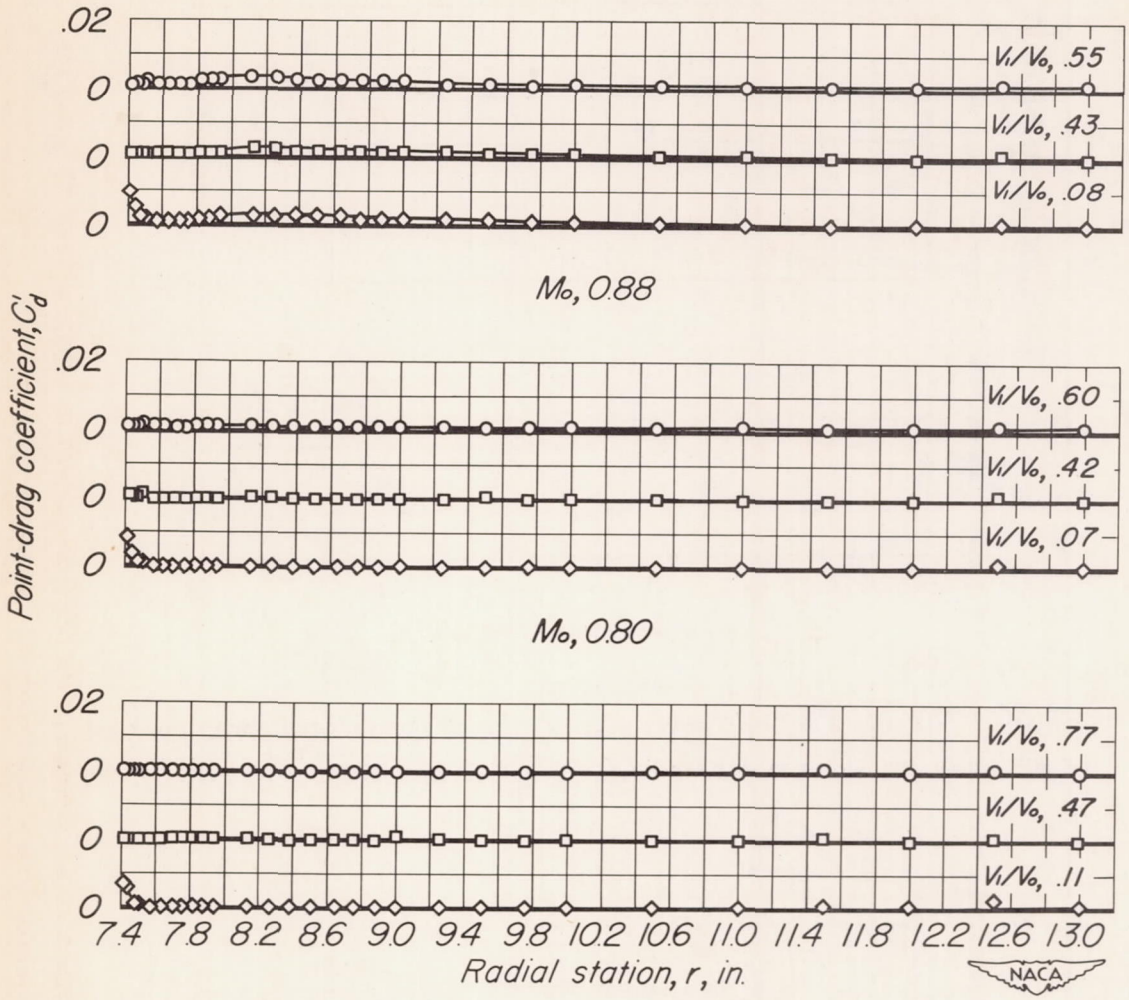

(b) r, 7.4 to r, 13.0

Figure 29. - Concluded.

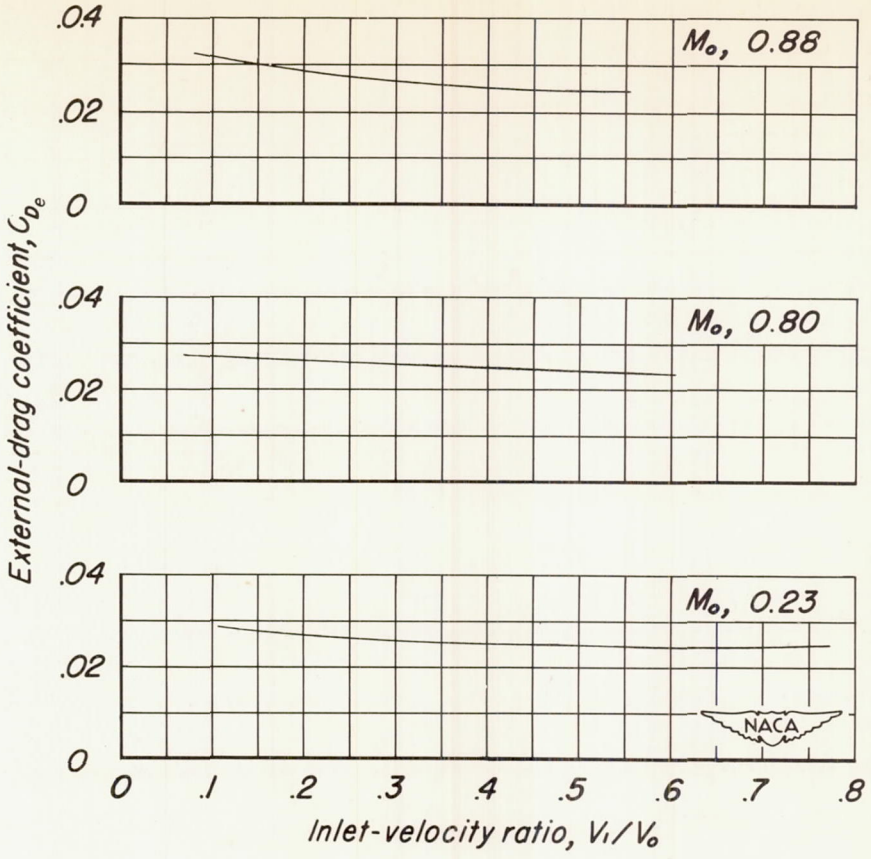

Figure 30.—The variation with inlet-velocity ratio of the external-drag coefficient of the cowl for Mach numbers of 0.88, 0.80, and 0.23. R, 1,800,000.

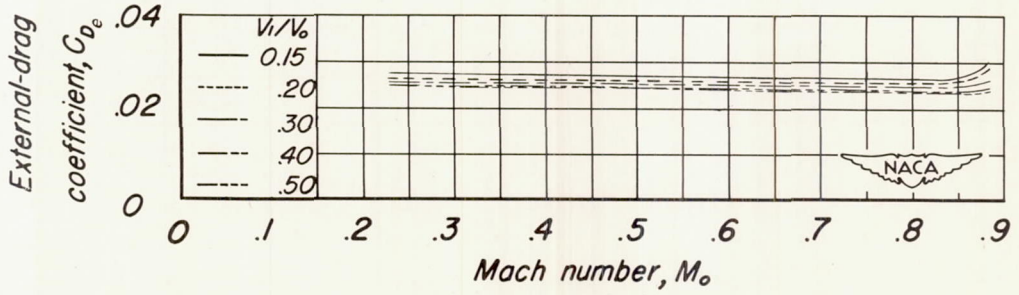

Figure 31.—The variation with Mach number of the external-drag coefficient of the cowl. R, 1,800,000.

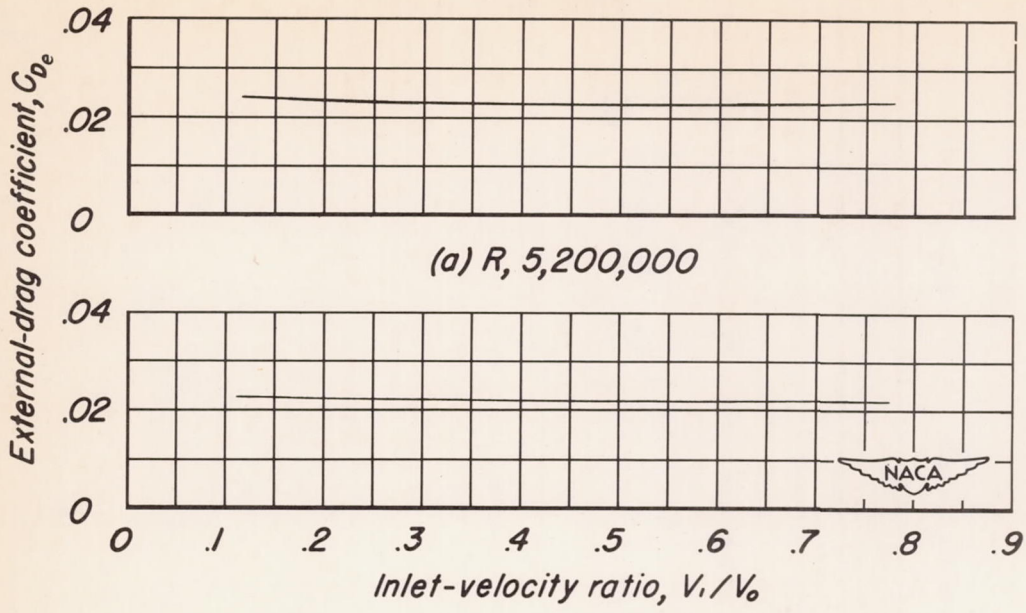

Figure 32.–The variation with inlet-velocity ratio of the external-drag coefficient of the cowl for Reynolds numbers of 5,200,000 and 8,100,000. M_o, 0.23.

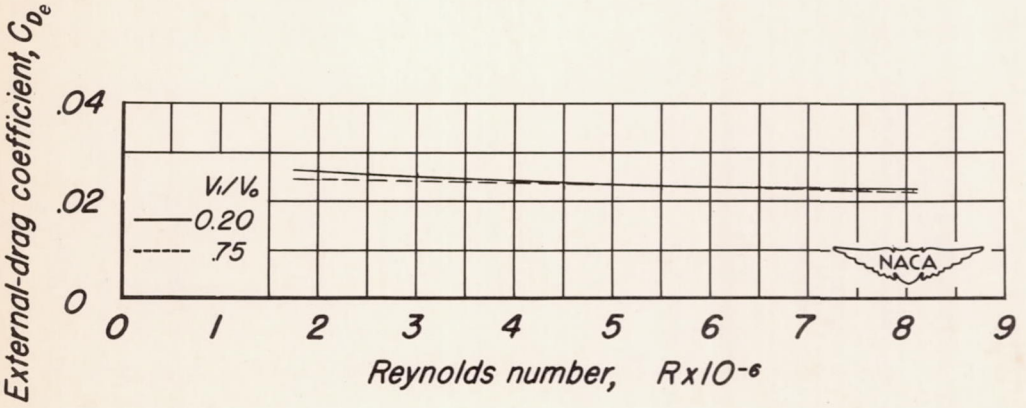

Figure 33.–The variation with Reynolds number of the external-drag coefficient of the cowl. M_o, 0.23.